Rijkswaterstaat
Ministerie van Infrastructuur en Milieu

Rijkswaterstaat Technisch Document (RTD)

Validation of the Guidelines for Nonlinear Finite Element Analysis of Concrete Structures

Part: Reinforced beams

Doc.nr.: RTD 1016-3A:2017
Versie: 1.0
Status: Final
Datum: 15 June 2017

Water. Wegen. Werken. Rijkswaterstaat

Preface

At an international workshop on shear force capacities of concrete structural element, held in Rotterdam, the Netherlands in 2007, predictions of the ultimate limit state of three different girder experiments were presented. This workshop was initiated by the Dutch Ministry of Infrastructure and organized by TNO (Vervuurt & Leeghwater, 2008). The ultimate capacities, predicted by six teams using different nonlinear software packages, showed a large scatter. Also the predicted crack patterns showed a large scatter.

With this in mind, research on the development of a "guideline for nonlinear analysis of concrete girders" was started. The *fib* Model Code 1990 was the background document when Peter Feenstra started with the development of the guideline. Also, Joop den Uijl was involved in validating the guidelines. From 2010 the draft version of the *fib* Model Code 2010 was used as background document. Today, both the MC2010 and the Eurocode2 allow the use of nonlinear analysis to verify the design capacity of concrete objects.

The validation of the guidelines is done by simulating old and new experiments. To verify human and software factors, several people were involved in this project and two commercially available software packages were used. Finally the first version of the guideline was published in May 2012. It is used by the Dutch Ministry of Infrastructure and the Environment when commissioning engineering work for re-examinations of existing concrete structures in the Netherlands to reveal extra remaining structural capacity.

To verify whether the guideline is also valid for a larger group of international end-users and for other software packages, a prediction contest of T-shaped prestressed girders was set up in 2014. The tests were performed by Sebastiaan Ensink in the Stevin Laboratory of the Delft University of Technology. The participants of the contest gathered in a workshop in Parma. The outcome of this contest showed that the guidelines are indeed helpful for reducing model and human factors when predicting the behaviour of concrete structures by means of nonlinear finite element analysis.

As a result of additional validation studies and making use of the experiences of the workshop in Parma a new version of the guidelines has been published in 2016. The present document gives an overview of validations studies for this version of the guideline. Maciej Kraczla has contributed to this document.

This document is one from a series of documents. At the time of writing, the following documents have been drafted:

RTD 1016-1:	Guidelines for Nonlinear Finite Element Analysis of Concrete Structures
RTD 1016-2:	Validation of the Guidelines for Nonlinear Finite Element Analysis of Concrete Structures - Part: Overview of results
RTD 1016-3A:	Validation of the Guidelines for Nonlinear Finite Element Analysis of Concrete Structures - Part: Reinforced beams
RTD 1016-3B:	Validation of the Guidelines for Nonlinear Finite Element Analysis of Concrete Structures - Part: Prestressed beams
RTD 1016-3C:	Validation of the Guidelines for Nonlinear Finite Element Analysis of Concrete Structures - Part: Slabs

Beatrice Belletti, Cecilia Damoni, Max A.N. Hendriks, Ane de Boer
March 2017

Contents

1 Introduction

In the period 2008-2015 the Dutch Ministry of Infrastructure and the Environment has financed a project leading to a set of guidelines for the nonlinear finite element analysis of concrete structures (RWS, 2016). Apart from the guidelines document itself, the project resulted in the present publication: a document that describes the validation of the guidelines.

This introductory chapter begins with describing the background of the project. It continues with presenting the objectives and the outline of the present validation report.

1.1 Background

Modern codes of practice for civil engineering projects offer so-called levels-of-approximations (Muttoni & Ruiz, 2012). Depending on the stage of the project, e.g. preliminary design, executive design or a reassessment study, a modern code distinguishes several levels of design expressions and design methods. The *fib* Model Code for concrete structures 2010 (fib, 2013) is a good example. The idea is: the higher the level-of-approximation, the more sophisticated the analysis, the more realistic the estimation of the safety, the more possibilities of finding "hidden" structural capacities, the higher is the likelihood of avoiding over-conservative designs and reassessments, the more probable is that unnecessary costs can be avoided. The highest level-of-approximation, sometimes denoted as level IV, is a design or a reassessment method based on nonlinear finite element analysis.

Whereas the lower levels-of-approximations are usually well-described using clear-cut expressions, applicability statements and examples, the situation is remarkably different when it comes to using nonlinear finite element analysis for design or reassessment studies. The *fib* Model Code has made an important step by providing safety formats to be used in connection with nonlinear finite element analysis. These safety formats define safety factors for the material properties and the global structural resistance. However the development of specifications on *how to perform* the analyses has not kept pace with the development of safety formats. It is beyond doubt that the results of nonlinear finite element analysis can be substantially influenced by model and human factors.

1.2 Scope and objectives

The development of the guidelines for the nonlinear finite element analysis of concrete structures (RWS, 2016) has the primary goal to advice the analysts and consequently to reduce the model and human factors. The development of the guidelines went hand in hand with the performance of numerical benchmark studies. The guidelines were tuned and, in the end, validated by comparing the results of numerical analyses with experimental results. It is believed that by this process a coherent set of advices was obtained. This document gives an overview of the main case studies that were used during the development of the guidelines.

The case studies include numerical examples with reinforced concrete beams, prestressed beams and slabs. The main objective is to compare the results of the numerical analyses with the experimental results for these cases and, in this way, to validate the set of advices.

Next to the main objective, the case studies reported in this document are used to demonstrate sensitivities of modelling choices, to compare the applications of different safety formats and to show examples of documenting finite element analysis results.

1.3 Outline

After this introductory chapter, Chapter 2 summarizes the used methods. Each subsequent chapter addresses a single case study of a reinforced concrete beam. These chapters use a similar structure of sections, describing respectively: the experimental setup and results, the finite element model adopting the advices of the guidelines, analytical verifications, the nonlinear finite element results using mean or "measured" material properties and the application of safety formats. Additional sections are e.g. used to show sensitivity studies.

2 Methods used for modelling reinforced concrete members

This chapter summarizes the methods that are used in the subsequent chapters.

2.1 Analytical code provisions

The analytical methods used in this report are based on the CEN Eurocode 2 (EC, 2005) and the *fib* Model Code 2010 (fib, 2013).

2.2 Nonlinear finite element modelling approach

There is a great variety of modelling options for modelling the nonlinear behaviour of concrete structures. The guidelines for the nonlinear finite element analysis of concrete structures (RWS, 2016) comprise specific modelling choices. It is important to consider these modelling choices as a coherent set of advices. For the details about these advises the reader is referred to the guidelines document itself. This section includes a summary of the main advices.

Units. The preferred units are the base units of the International System of Units (SI). Possibly, the length unit might be replaced by millimetres.

Constitutive models for concrete. Smeared cracking models are considered. A total strain-based rotating or fixed crack model is preferred. Adequate tensile softening and compressive hardening-softening relations should be considered, based on the specification of tensile and compressive fracture energies and the definition of equivalent lengths to define "crack-band" widths. For the fixed crack models variable shear retention models are recommended. Tension-compression interaction needs to be addressed in structures subjected to multi-axial stress states. These include the reduction of the compressive strength due to lateral cracking and a diminishing Poisson effect upon cracking.

Constitutive models for reinforcement. Elasto-plastic material models with hardening should be used.

Constitutive models for concrete-reinforcement interaction. At the macro-level, simplified models can be used, taking into account tension stiffening effects. Limited attention is devoted to modelling slip and dowel action. These aspects should not be significant in the global behaviour of a structure and are more related to details near the USL load level.

Finite elements for concrete. Elements with quadratic interpolation of the displacement field should be used. Typically, at least 6 elements over the height of a structural element should be used.

Finite elements for reinforcement. Embedded reinforcement elements are preferred; both embedded bars and grids can be used.

Prestressing. Prestressing should be applied taking into account prestress losses.

Existing cracks. Existing cracks in the structure should be taken into account whenever detailed information about the location and crack widths is available.

Loads. The design codes and national guidelines in force should be applied.

Boundary conditions. Unless the objective of the analysis is to study the detailed behaviour of the loading and support points, the supports and loading platens should be modelled such that local stress concentrations are reduced.

Loading. The loading sequence will contain an initial phase where dead weight, permanent loads and, if appropriate, prestressing is applied to the structure. Following the initial phase, the variable loads are increased until a clear failure mode is present or a significant load reduction was achieved.
Note that in the current report, for all cases, we are referring to experimental tests. For this reason, when safety formats are applied to obtain the design resistance, we are considering a load combination of action with a partial safety factor related to self-weight of 1.0.

Equilibrium iterations. Equilibrium between internal and external forces should be achieved iteratively using a Newton-Raphson method with arc-length procedure. Preferably an energy-norm together with a force-norm should be used.

All analyses have been performed with Diana 9.4.4.

2.3 Nonlinear finite element limit state verifications

Serviceability limit states. As requested by current codes (EC2, MC2010) serviceability limit states verifications must be performed as post-analysis checks. For the crack opening calculation, the average strain values are obtained from the analysis, whereas crack spacings are obtained from codes.

Ultimate limit states. Three alternative methods to obtain the design resistance from the non-linear finite element analysis: the Global Resistance Factor method (GRF), the Partial Factor method (PF) and the Estimate of Coefficient of Variation or resistance method (ECOV).

3 Case RB1: Vecchio & Shim (2004)

The experimental program of Vecchio & Shim (2004) is a re-examination of the classical experiments of Bresler & Scordelis (1963). The complete experimental program consisted of twelve beams with different ratios of shear and longitudinal reinforcement. Beam C3 is selected, as this beam has the longest span (6400 mm) and featured a flexure-compressive failure mechanism.

3.1 Experimental setup and results

Geometry

The geometry of the beam and reinforcement is shown in Figure 3-1 and Figure 3-2. The beam has a total length of 6.840 m, a depth of 0.552 m, and a width of 0.152 m.

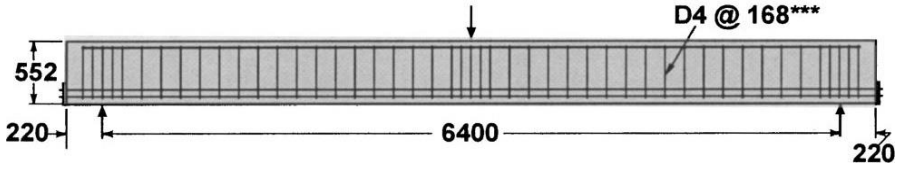

Figure 3-1: Case RB1. Dimensions (in mm), reinforcements and loading (Vecchio & Shim 2004)

The bottom longitudinal reinforcement is extended outside the beam and welded to one-inch thick plates. It is assumed that the dimensions of these plates are $0.192 \times 0.350 \times 0.025$ m^3.

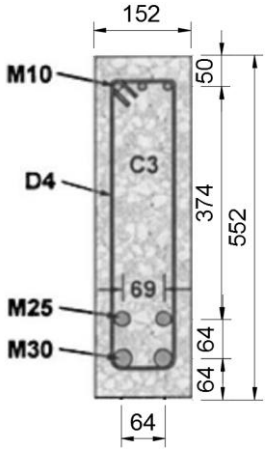

Figure 3-2: Case RB1. Cross section details (in mm), (Vecchio & Shim 2004)

Material Properties

Concrete and reinforcement properties, given in Vecchio & Shim (2004) are listed in Table 3-1

Table 3-1: Case RB1. Concrete and reinforcement properties

Concrete properties					
	f_{cm} (N/mm^2)			d_{max} (mm)	
	43.5			20	
Reinforcement properties					
Bar	Φ (mm)	A_s (mm^2)	E_s (N/mm^2)	f_{ym} (N/mm^2)	f_{tm} (N/mm^2)
M10	11.3	100	200000	315	460
M25	25.2	500	220000	445	680
M30	29.9	700	200000	436	700
D4	3.7	25.7	200000	600	651

Loading and Boundary Conditions

The loading and boundary conditions in the experimental setup are shown in Figure 3-3.

The out-of-plane dimensions of the loading and support plates are larger than the out-of-plane thickness of the beam.

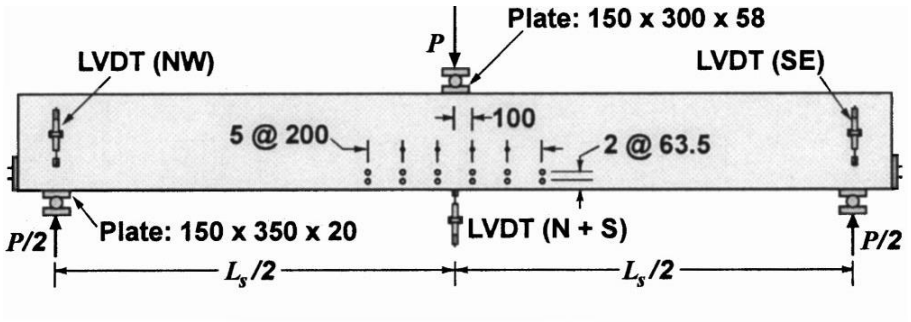

Figure 3-3: Case RB1. Loading and boundary conditions (Vecchio & Shim 2004)

Experimental Results

The beam exhibited a flexural-compressive failure mode with a clear maximum in the load-deflection response, Figure 3-4 and Figure 3-5. The experimental ultimate value of applied load was equal to $P_{Exp} = 265kN$ at the deflection of 44.3 mm.

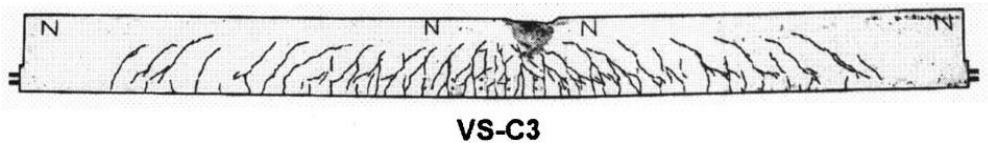

Figure 3-4: Case RB1. Failure mechanisms at experimental ultimate value of applied load (Vecchio & Shim 2004)

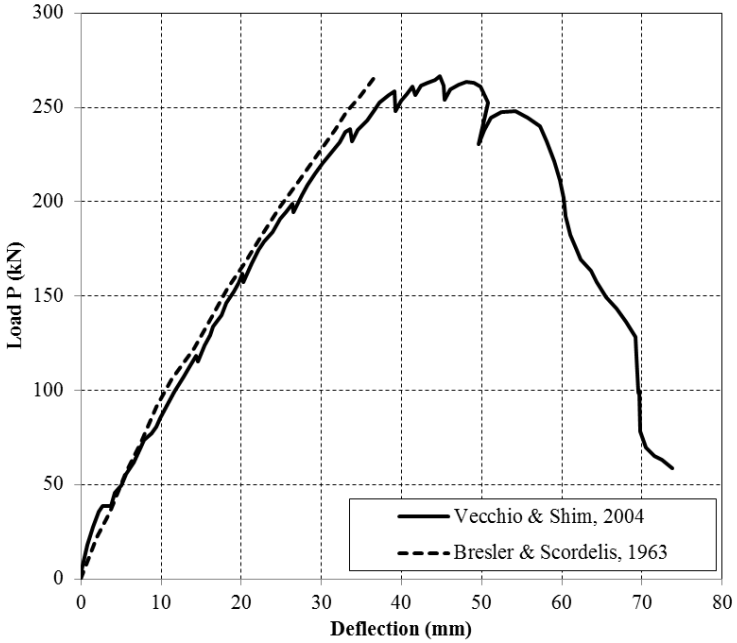

Figure 3-5: Case RB1. Experimental load-deflection at midspan

3.2 Analytical analysis

In Figure 3-6 the load configuration at failure is reported. The distributed load representing the beam weight is equal to $q = 0.152m \times 0.552m \times 25\,kN/m^3 = 2.098\,kN/m$.

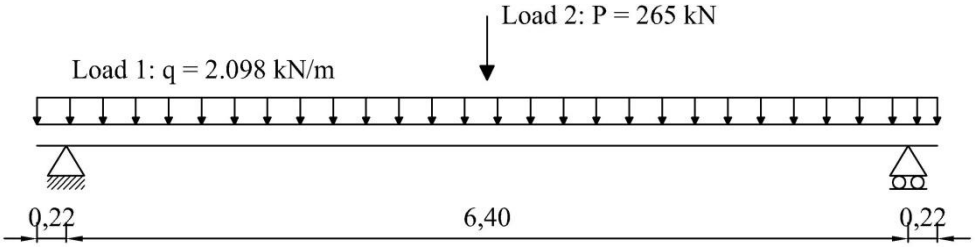

Figure 3-6: Case RB1. Load configurations (dimensions in m)

Load case 1

Figure 3-7 shows that the maximum value of applied moment at the midspan is equal to $M_{E,\max} = 2.098kN/m \times \frac{(6.4m)^2}{8} - 2.098kN/m \times \frac{(0.22m)^2}{2} = 10.69\,kNm$

and the maximum value of applied shear force at the supports is equal to

$V_{E,\max} = 2.098\,kN/m \times \frac{6.4m}{2} = 6.71kN$.

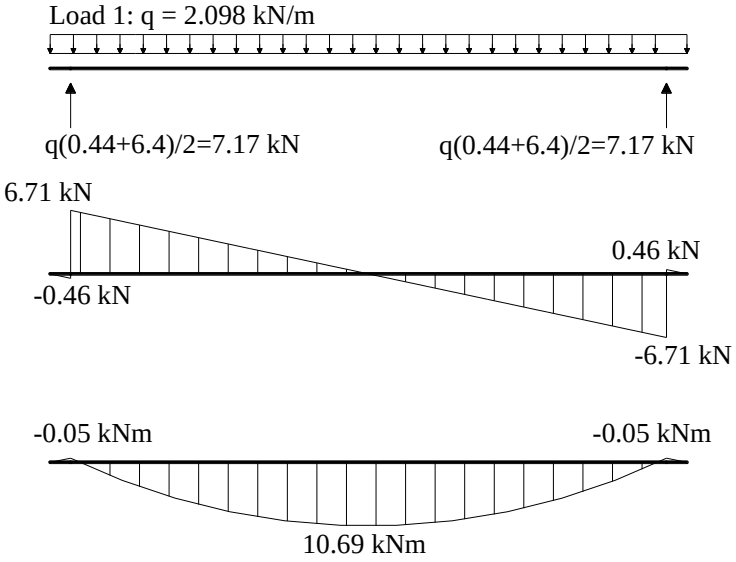

Figure 3-7: Case RB1. Load 1: Internal forces

Load case 2

The experimental ultimate value of the applied load is equal to $P_{E,\max} = 265kN$.

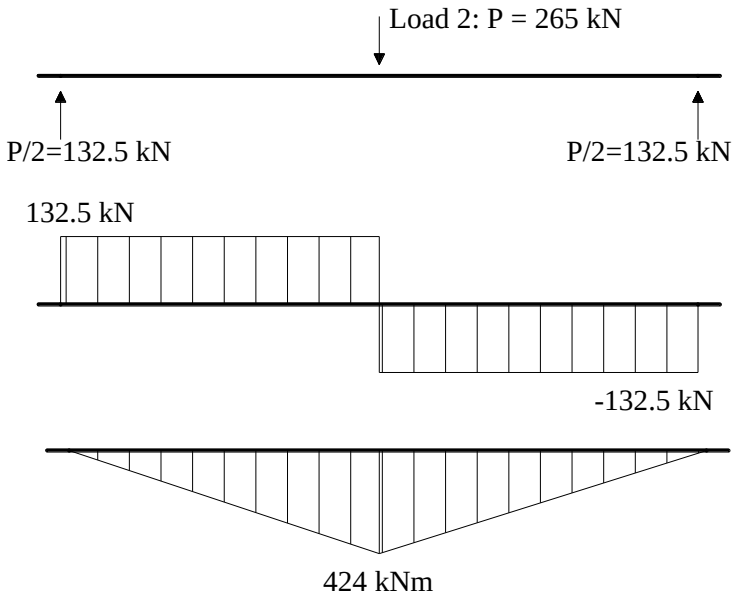

Figure 3-8: Case RB1. Load 2: Internal forces

Figure 3-8 shows that the maximum value of applied moment at midspan is equal to $M_{E,\max} = 265kN \times \frac{6.4m}{4} = 424\,kNm$ and the value of applied shear force is equal to $V_{E,\max} = 1325\,kN$.

Load case 1 + Load case 2

At failure the maximum value of applied moment is $M_{E,\max} = 10.69kNm + 424kNm = 434.69\,kNm$ and the value of applied shear force is equal to $V_{E,\max} = 6.71kN + 132.5kN = 139.21\,kN$.

The design value of resistance moment is evaluated with sectional analysis by assuming:

- the tensile strength of concrete is ignored,
- the compressive stresses in concrete are derived from a parabola-rectangle relation,
- the stresses in the reinforcing steel are derived from an elastic–plastic stress-strain relation with hardening,
- the partial safety factor for the mechanical properties of reinforcing steel equals γ_s=1.15, the factor for concrete material properties equals γ_c=1.5.

The failure mechanism of the specimen is caused due to crushing of concrete after yielding of reinforcing steel. The design bending moment resistance is calculated below.

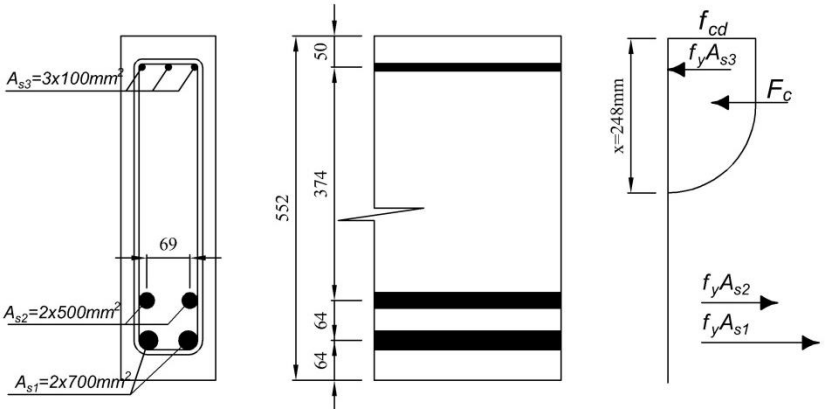

Figure 3-9: Case RB1. Stress block for determination of the design moment resistance

Assuming that reinforcement yields at strains: $\varepsilon_s = \frac{f_{yd}}{E_s} = 1.72 \cdot 10^{-3}$

$A_{s1} f_{yd} + A_{s2} f_{yd} - A_{s3} f_{yd} - 0.8095 x b f_{cd} = 0 \rightarrow x = 248mm$

which is smaller than $x_{\lim} = 327mm$.

Verification of the assumptions for the calculated value of x:

$$\varepsilon_{s1} = \frac{\varepsilon_{cu2}(d_1 - x)}{x} = \frac{0.0035(488mm - 248mm)}{248mm} = 3.387 \cdot 10^{-3} \rightarrow steel\ yields$$

$$\varepsilon_{s2} = \frac{\varepsilon_{cu2}(d_2 - x)}{x} = \frac{0.0035(424mm - 248mm)}{248mm} = 2.484 \cdot 10^{-3} \rightarrow steel\ yields$$

$$\varepsilon_{s3} = \frac{x - a_1}{x}\varepsilon_{cu2} = \frac{248mm - 50mm}{248mm} 0.0035 = 2.794 \cdot 10^{-3} \rightarrow steel\ \ yields$$

thus the assumptions that reinforcement yields is fulfilled.

The design value of the moment resistance in calculated around the centre of the compression zone $0.416x$:

$M_{Rd} = A_{s1} f_{yd}(d_1 - 0.416x) + A_{s2} f_{yd}(d_2 - 0.416x) + A_{s3} f_{yd}(0.416x - a_1) = 300.7kNm$

The value of applied moment equals to

$$M_{E,\max} = -q\frac{(0.22m)^2}{2} + q\frac{(6.4m)^2}{8} + P\frac{6.4m}{4} = 300.7\ kNm$$

which results in the value of the applied load

$$P_{Rd} = \frac{4}{6.4m}\left(300.7kNm + q\frac{(0.22m)^2}{2} - q\frac{(6.4m)^2}{8}\right) = 181.232kN$$

The design value of shear resistance is $V_{Rd} = \min(V_{Rd,c}, V_{Rd,s}) = 149.96\ kN$. The design shear resistance attributed to concrete is evaluated with:

$$V_{Rd,c} = 0.9 d b_w \alpha_{cw} v_1 f_{cd} \frac{(\cot\alpha + \cot\theta)}{1 + \cot^2\theta} =$$

$$= 0.9 \times 152mm \times 461mm \times 1 \times 0.6 \times \left(1 - \frac{35.5}{250}\right) \times 23.67 \frac{N}{mm^2} \times \frac{(0 + 2.5)}{1 + 2.5^2} = 264.95kN$$

whereas the design shear resistance provided by stirrups is calculated as:

$$V_{Rd,s} = 0.9d \frac{A_{sw}}{s} f_{ywd} \cot\theta = 0.9 \times 461mm \times \frac{51.4mm^2}{168mm} \times 472.56 \frac{N}{mm^2} \times 2.5 = 149.96kN$$

The value of shear resistance equals to $V_{Rd} = 6.71kN + \frac{P_{Ed}}{2} = 149.96\ kN$ which solved for unknown P_{Ed} yields the value of the applied load of 286.5kN.
From the comparison of the calculated values of the applied load related to the design moment resistance – 181.23kN and dictated by the shear resistance – 286.5kN, it can be concluded that because the former force is lower – thus governing, the beam fails in bending.

Table 3-2: Case RB1. Design value of beam resistance expressed in terms of applied load P_{Rd}

P_{Rd} **(EC2 – MC2010)** **(kN)**
181.232

In Table 3-2 the design value of beam resistance expressed in terms of applied load P_{Rd} obtained with Eurocode 2 (CEN, 2005) and Model Code 2010 (fib, 2013) is summarized.

3.3 Finite element model

Units

Units are N, m.

Material models and parameters

The concrete model is based on a total strain rotating crack model with

- exponential softening in tension and parabolic behavior in compression,
- variable Poisson's ratio of concrete dependent on crack strain values,
- reduction of compressive strength of concrete due to lateral cracking with a lower limit of 0.6 according to (Vecchio, 1986),
- increase in compressive strength due to lateral confinement according to the model proposed by Selby and Vecchio (Selby and Vecchio, 1993).

The mechanical properties for concrete are summarized inTable 3-3. The uniaxial stress-strain curve is shown in Figure 3-10. In the input file of the analysis, the G_F value has been decreased with a factor $\sqrt{2}$ in order to compensate for an underestimation of the crack band width for cracks with an inclination angle of 45 degrees, $G_{F,reduced} = 0.144/\sqrt{2} = 0.102$.

Table 3-3: Case RB1. Constitutive model parameters for concrete

	f_{cm} (N/mm^2)	f_{ctm} (N/mm^2)	E_c (N/mm^2)	ν	G_F (Nmm/mm^2)	G_C (Nmm/mm^2)
Mean measured values	43.5	3.24*	34925*	0.15	0.144*	35.99*

* Not specified in reference; estimated according to MC2010 (fib, 2013).

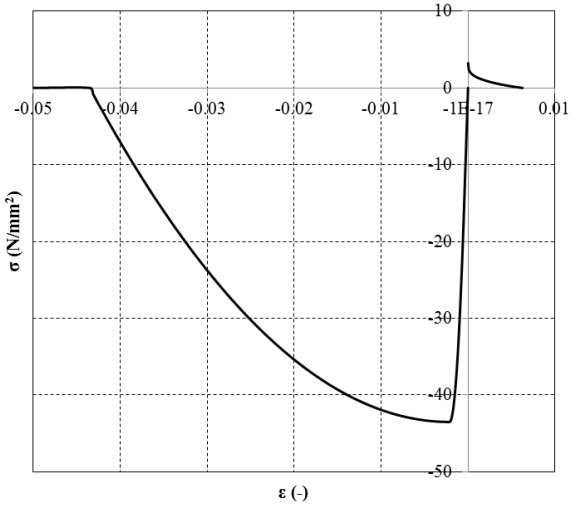

Figure 3-10: Case RB1. Stress-strain curve for concrete

The model for the reinforcement bars and stirrups is based on hardening plasticity. Geometrical and mechanical features of reinforcing bars are summarized in Table 3-1. The stress- strain curve of the M30 reinforcing bars is plotted in Figure 3-11.

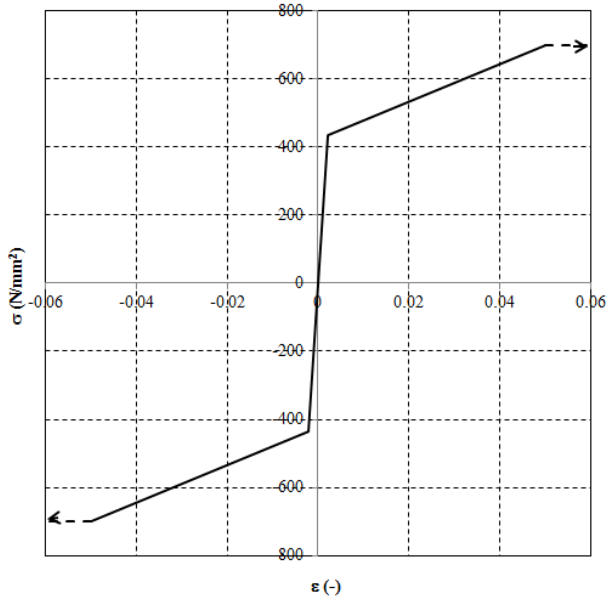

Figure 3-11: Case RB1. Stress-strain curve for M30 reinforcing bars

For the steel plates a linear elastic behavior is assumed, see Table 3-4.

Table 3-4: Case RB1. Steel plates properties

E (N/mm^2)	ν
200000	0.3

Interface elements were used between the steel plates and the concrete beam at the supports and loading positions. The thickness of interface elements equals 10 mm. Stress-strain relation in compression was derived by assuming a stiffness equivalent to the stiffness of a layer of mortar 1 mm thick having a Young's modulus derived from the mean measured of compressive strength of concrete as reported in Table 3-3.
A bilinear behavior is assumed in normal direction (see Figure 3-12) and a linear elastic relation is assumed in shear direction. The normal stiffness in tension and the stiffness in shear direction were assumed almost equal to zero. For stableness of the analysis horizontal displacements of one pair of nodes across the interface elements of support plates and loading plate were tied. The mechanical features of the interface elements are summarized in Table 3-5.

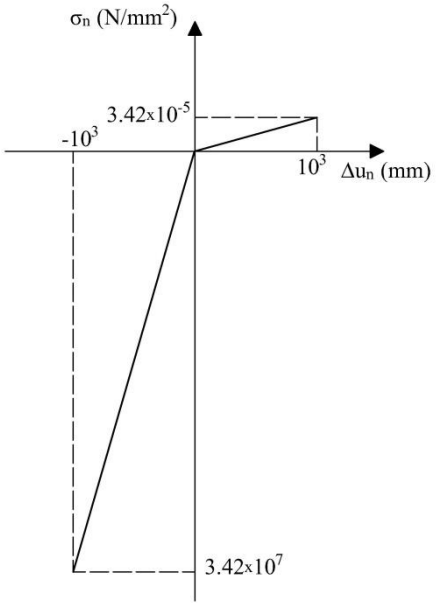

Figure 3-12: Case RB1. Traction-displacement diagram in normal direction for interfaces (not to scale)

Table 3-5: Case RB1. Interface properties

$K_{nn\ in\ tension}$ (N/mm^3)	$K_{nn\ in\ compression}$ (N/mm^3)	K_t (N/mm^3)
3.42×10^{-8}	$3.42\times10^{+4}$	3.42×10^{-8}

Element types and finite element mesh

For meshing the concrete, 8-node membrane elements (CQ16M) with a full Gauss integration scheme (3×3) are used. The average element size is 44×36 mm^2. The reinforcement bars and stirrups are modelled with embedded truss elements with two Gauss integration points along the axis of the element. A perfect bond is assumed. For the steel plates 8-node membrane elements (CQ16M) with a full Gauss integration scheme (3×3) are used.
The 6-node interfaces element have three Lobatto integration points.

The adopted dimensions for the beam and for the transversal cross section of the beam are given in Figure 3-13 and Figure 3-14, respectively.

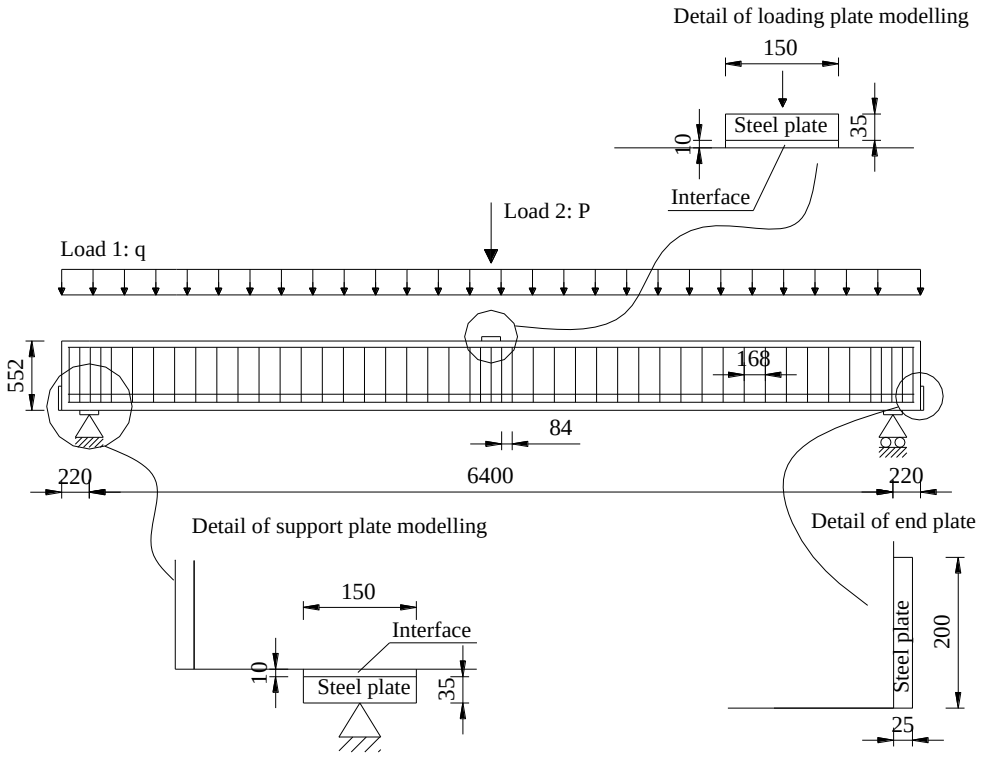

Figure 3-13: Case RB1. Dimensions adopted for the beam (in mm)

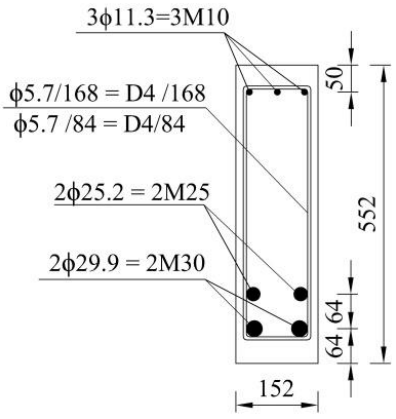

Figure 3-14: Case RB1. Dimensions adopted for the transversal cross section of the beam (in mm)

The mesh of the beam is presented in Figure 3-15(a). The different materials are indicated with different colors in Figure 3-15(b).
Different groups of elements were defined to distinguish the concrete elements that can be subjected to crushing or cracking during the analyses and the steel elements that can yield during the analysis. These groups will be used in section 3.4 to monitor the failure mode during the analysis. For monitoring steel yielding the groups RETOPM10 (red), REBOTM25 (blue), REBOTM30 (green) and STIRRUPS (black) refer to reinforcing bars and stirrups of the beam, see Figure 3-16

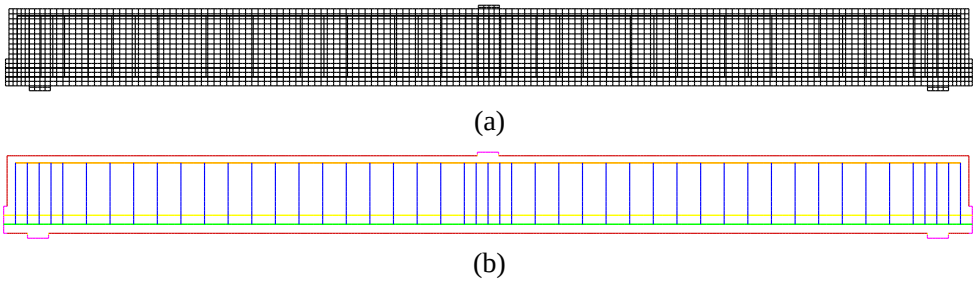

(a)

(b)

Figure 3-15: Case RB1. (a) Mesh and (b) material sets.

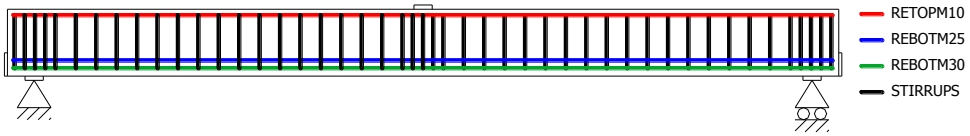

Figure 3-16: Case RB1. Groups of steel elements monitoring yielding

Figure 3-17 shows the group of elements named CRUSHING, used for monitoring the inelastic behavior of concrete in compression. This group of elements has a length equal to 5 times the length of the loading steel plate and a depth equal to the length of the loading steel plate, Figure 3-17.

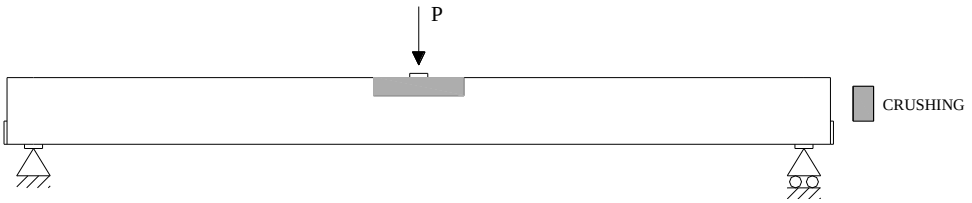

Figure 3-17: Case RB1. Group of concrete elements monitoring crushing due to bending

Figure 3-18 shows the group of elements named SHEAR, where the inelastic behavior of concrete due to shear was monitored. The group SHEAR has a length equal to the space between the end of the loading plate and the end of the support plate and a depth equal to the space between upper and lower reinforcement.
Group shear is lying between the RETOPM10 and the group REBOTM25 and between the edges of the load and support steel plate.

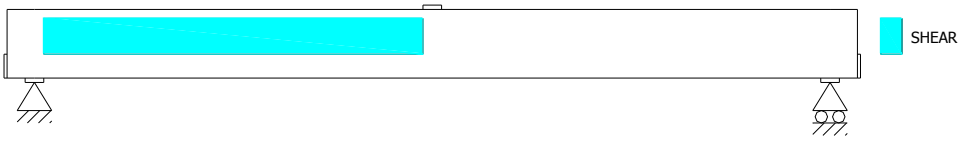

Figure 3-18: Case RB1. Group of concrete elements monitoring inelastic behavior due to shear

Boundary conditions and loading

The translations along *x* and *y* axes at a single node of the left steel plate (support 1) are constrained as well as the translation along *y* axis at a single node of the right steel plate (support 2), Figure 3-19.

Dead load is applied in load case 1; load *P* as a unit load of $1\times10^{-3}N$ is added at the load case 2 as a concentrated load applied at the mid node of the loading plate, Figure 3-19.

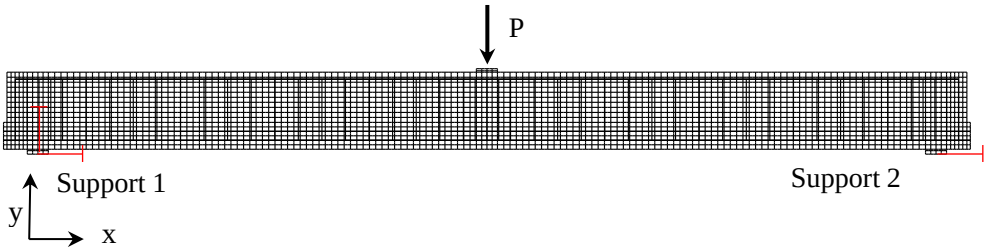

Figure 3-19: Case RB1. Boundary conditions and load case 2

Load increments and convergence criteria

Load case 1 is applied in a single step. The regular Newton-Raphson method with a maximum of 25 iterations is used. The selected convergence norms are according to both force and energy norms. The analysis continues even if the convergence criteria are not satisfied. The convergence tolerance is equal to 5×10^{-2} for the force norm and 1×10^{-2} for the energy norm. A Line Search algorithm is used to improve the convergence performance.

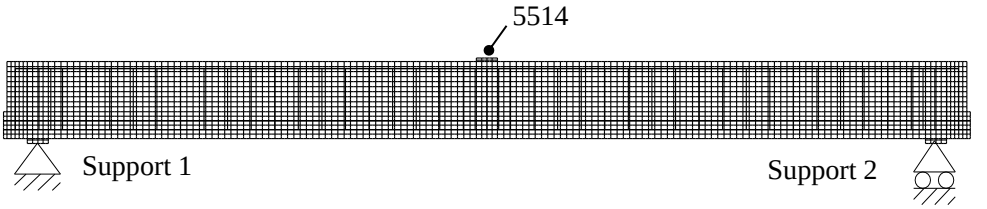

Figure 3-20: Case RB1. `Indirect Displacement control' technique applied referring to node 5514

Load case 2 is applied with automatic adaptive load increments based on energy. The initial load factor equals 5, the upper limit of the incremental load factor equals 10 and the lower limit of the incremental load factor equals 5. The maximum number of steps is 150. Arc-length control was applied based on translation along y axis of node 5514 at mid-span ("indirect displacement control"), Figure 3-20. The analysis continues even if the convergence criteria are not satisfied. The convergence tolerances are equal to 1×10^{-3} and 1×10^{-2} for energy and forces, respectively. A maximum of 25 iterations is used. A line search algorithm is used to improve the convergence performance.

3.4 Nonlinear finite element analysis

Load deflection

The load-deflection curve is presented in Figure 3-21 where the applied load values corresponding to the onset of yielding of the M30 and M25 longitudinal bars, yielding of the M10 longitudinal bars, yielding of the stirrups D4 are indicated. The step in which the first integration point reaches a minimum principal strain value lower than -3.5×10^{-3} is defined crushing of concrete.

Convergence behavior

For most steps convergence is achieved on the basis of the energy criterion, Figure 3-22 and Figure 3-23.

For load case 2 the peak load is defined as the highest load step for which the energy norm ratio satisfies the fixed tolerance of 1×10^{-3} and it is marked in Figure 3-22 and Figure 3-23 with a red dot.

The convergence behavior is quite poor after reaching the peak load. After step 82, the analysis continues even if the energy convergence criteria are not satisfied within the

maximum number of iterations equal to 25. The post peak branch of the load - deflection curve is for this reason plotted with a dot line.
The force norm ratio is higher than the fixed tolerance of 1×10^{-2} for most of the steps.

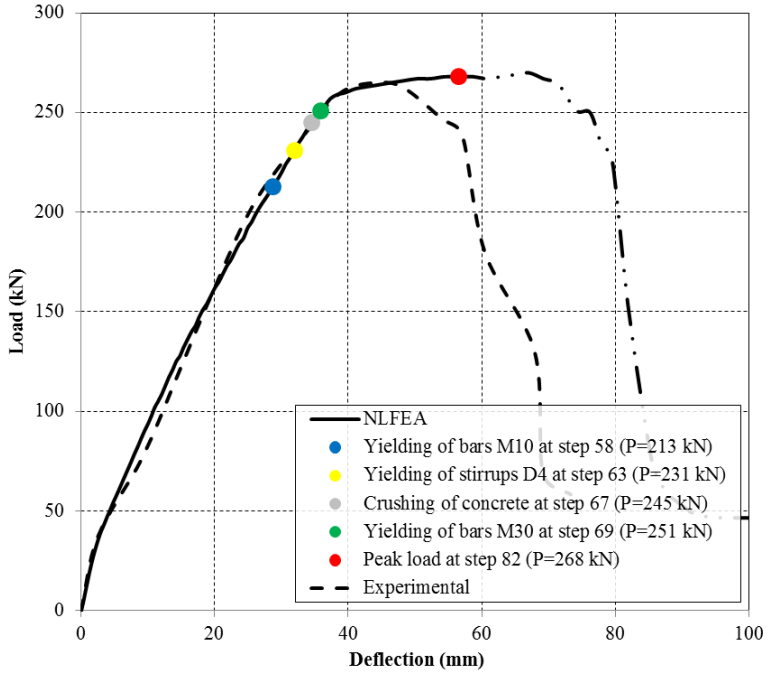

Figure 3-21: Case RB1. Load-deflection curves

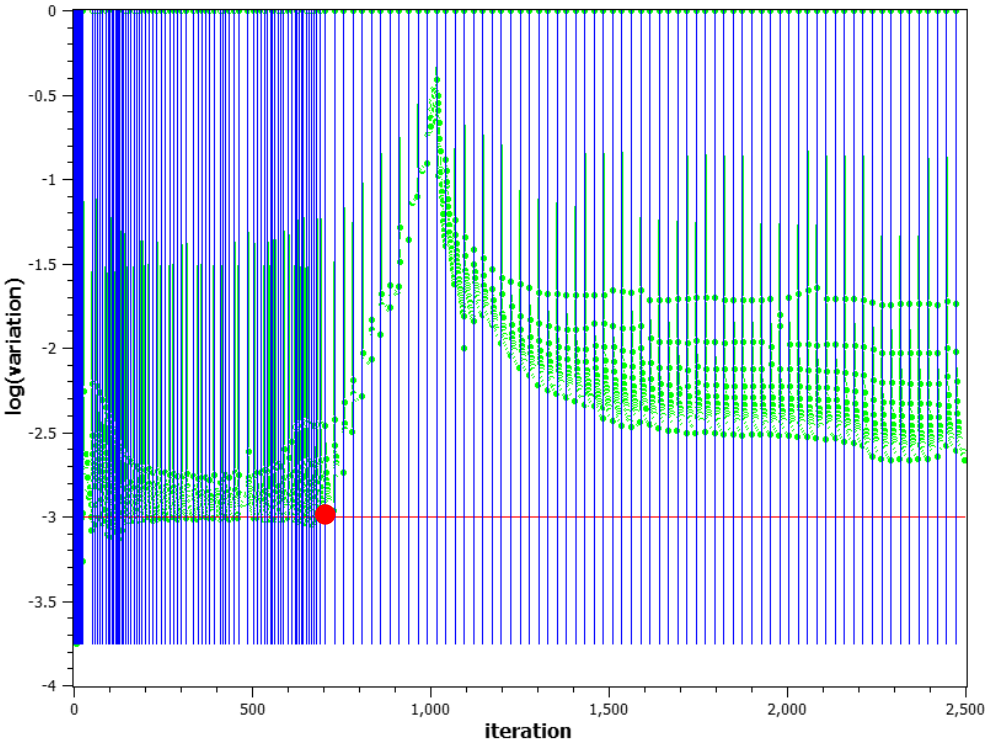

Figure 3-22: Case RB1. Evolution of the energy norm (blue lines indicate steps, red line indicates tolerance, green points indicate iterative results)

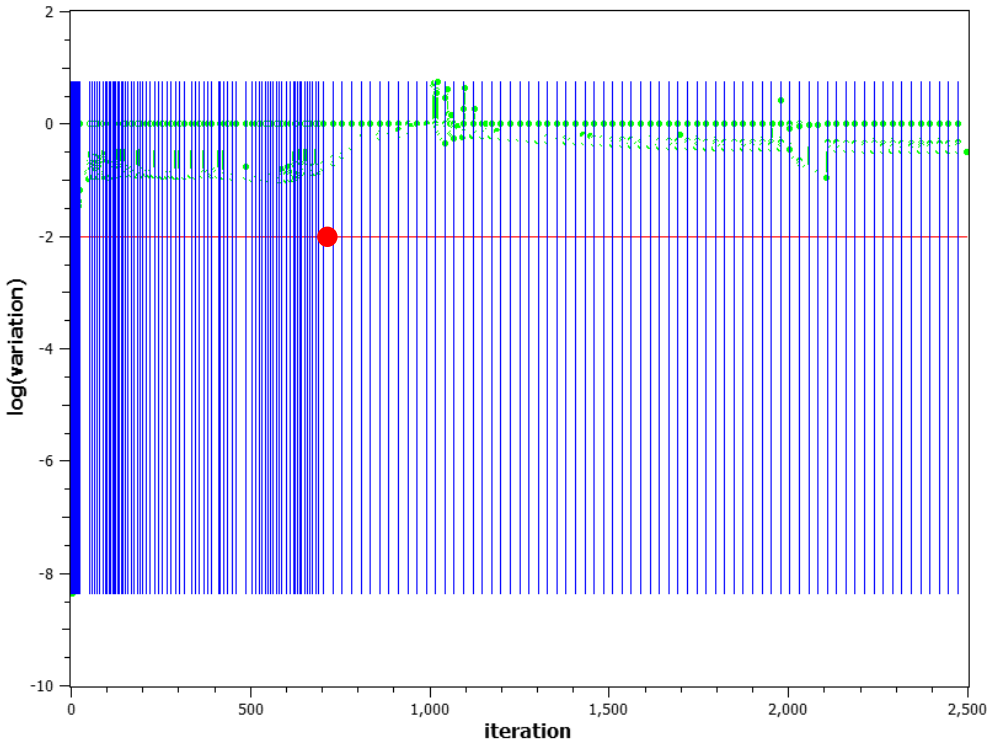

Figure 3-23: Case RB1. Evolution of the force norm (blue lines indicate steps, red line indicates tolerance, green points indicate iterative results)

Strains

Figure 3-24 shows the crack strain values (which are the plastic part of the maximum principal strain values) at step 65 (load $P = 238kN$). The first crack strain value plotted in Figure 3-24, equal to 7.86×10^{-4}, corresponds to the ultimate crack strain value calculated as $\varepsilon_{t,u} = \frac{G_F}{h \cdot f_{ctm}}$, while the third crack strain value, equal to 3.62×10^{-3}, is the crack strain value corresponding to a stress value equal to 1% of f_{ctm}. An intermediate crack strain value was added in the contour plot.

The crack pattern, which can be derived from the contour of the principal strain value, shows that the failure is mainly due to bending.

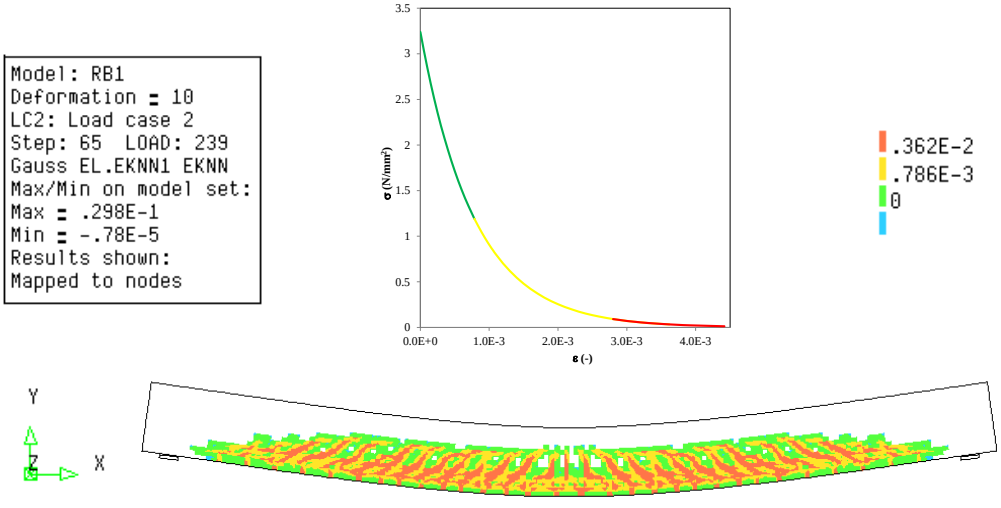

Figure 3-24: Case RB1. Crack strain values at step 65 ($P = 238kN$)

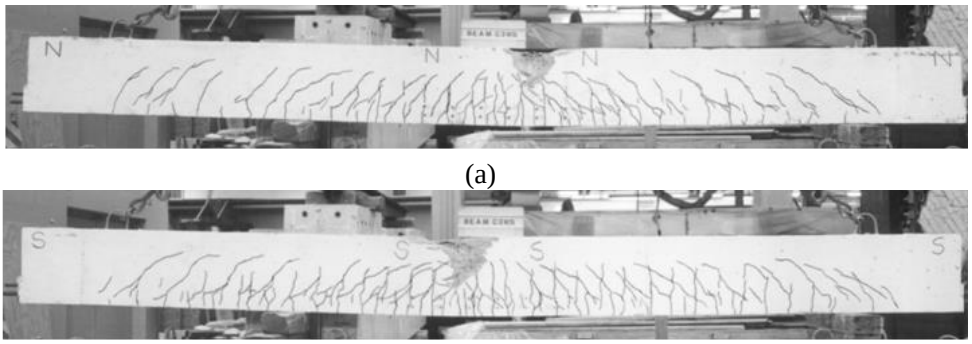

(a)

(b)

Figure 3-25: Case RB1. Experimental crack pattern at failure (load $P_{Exp} = 277kN$) (Vecchio & Shim 2004): a) north side, (b) south side

The yielding strain for the M10 reinforcing bars is equal to $\frac{315MPa}{200GPa} = 1.57 \times 10^{-3}$. The M10 reinforcing bars start to yield in compression at the load equal to 213kN (step 58). Figure 3-26 shows yielding of M10 reinforcing bars at step 70 (load $P = 254kN$).

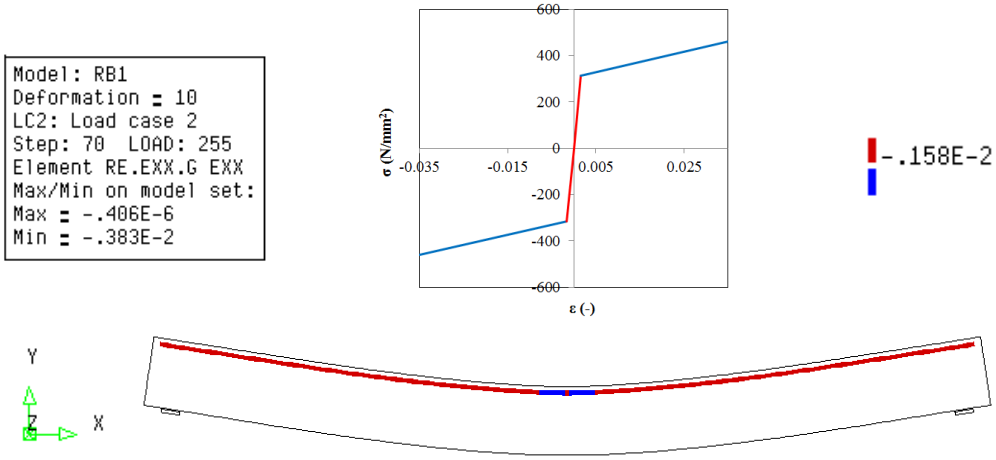

Figure 3-26: Case RB1. Yielding of reinforcing bars M10 at step 70 (load $P = 254kN$)

The yielding strain of stirrups is equal to $\frac{600MPa}{200GPa} = 3.0 \times 10^{-3}$. Stirrups start to yield at the load equal to 231kN (step 63). Figure 3-27 shows yielding of stirrups at step 80 (load $P = 267kN$).

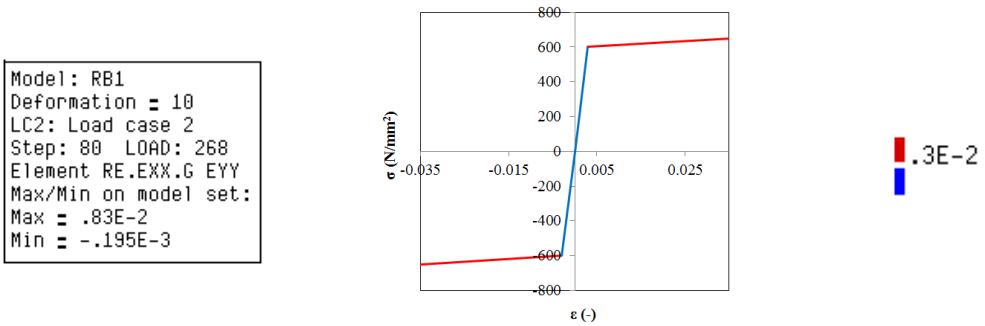

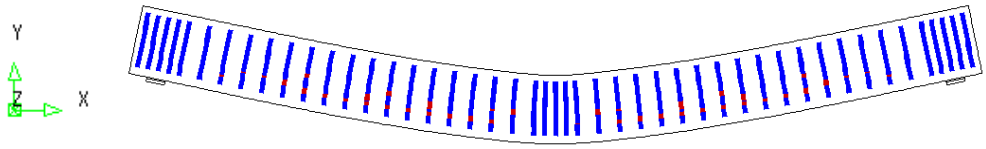

Figure 3-27: Case RB1. Yielding of stirrups at step 80 (load $P = 267kN$)

The yielding strain of the M30 reinforcing bars is equal to $\frac{436MPa}{200GPa} = 2.18\times10^{-3}$. The longitudinal M30 reinforcing bars start to yield in tension at the load equal to 251 kN (step 69). Figure 3-28 shows yielding of M30 reinforcing bars at step 75 (load $P = 263kN$).

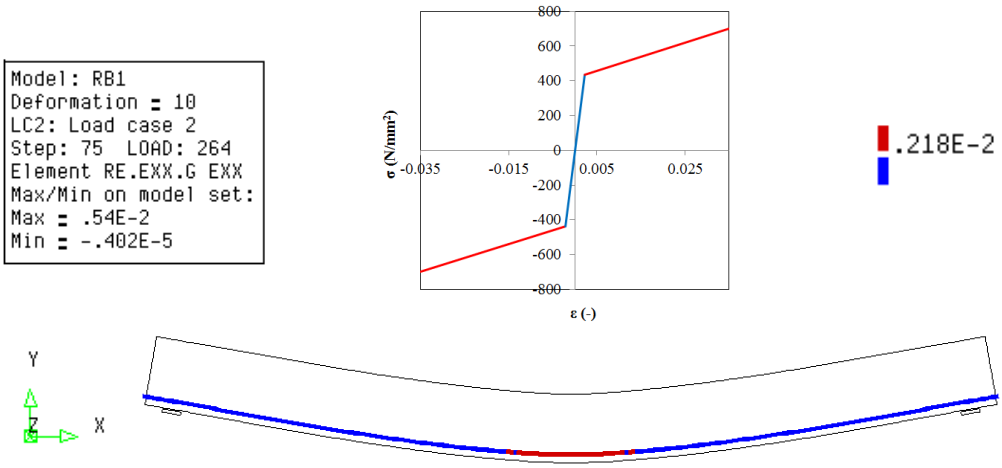

Figure 3-28: Case RB1. Yielding of reinforcing bars M30 at step 75 (load $P = 263kN$)

The yielding strain of the M25 reinforcing bars is equal to $\frac{445MPa}{220GPa} = 2.02\times10^{-3}$. The longitudinal M25 reinforcing bars start to yield at a load equal to 257 kN (step 71). Figure 3-29 shows yielding of M25 reinforcing bars at step 75 (load $P = 263kN$).

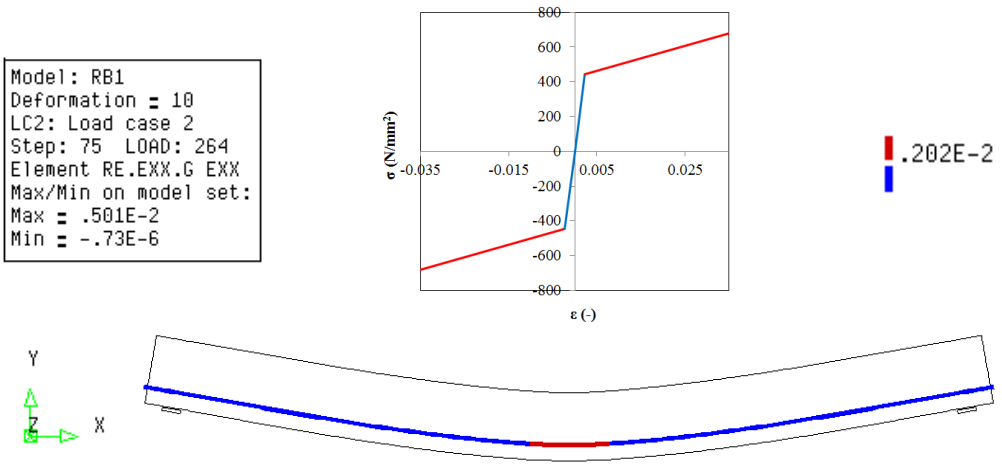

Figure 3-29: Case RB1. Yielding of M25 reinforcing bars at step 75 (load $P = 263kN$)

Figure 3-30shows principal strain state at the step 82 (peak load). The values of the minimum principal strain at the location of applied load are lower than -3.5×10^{-3} which

indicates crushing of concrete in this area. The peak value of applied load obtained from the NLFEA is equal to $P_u = 268kN$.

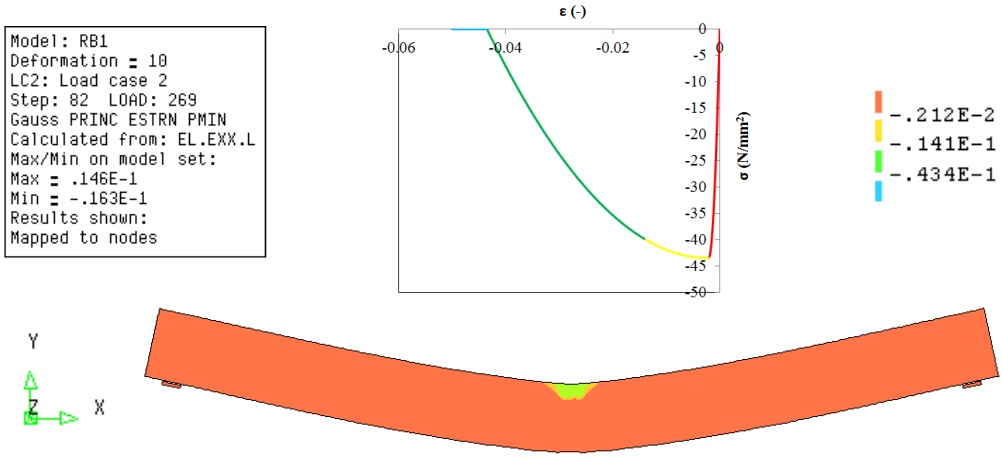

Figure 3-30: Case RB1. Minimum principal strain at step 82 (load $P_u = 268kN$)

Gauss point statistics

In Table 3-6 lists the number of cracking points, crushing points and yield points at step 58 (beginning of yielding of M10 reinforcing bars), at step 63 (beginning of yielding of stirrups), at step 67 (when the first element reaches minimum principal strains lower than -3.5×10^{-3}), at step 69 (beginning of yielding of M30 reinforcing bars), at step 71 (beginning of yielding of M25 reinforcing bars) and at step 82 (peak load). Crushing is defined as soon as the softening branch in compression is reached. In the current case, it is at the minimum principal strain of -2.1×10^{-3}.

Table 3-6: Case RB1; number of cracking points, crushing points, and yield points

YIELDING OF REINFORCING BARS M10						
STEP	**58**	**ITERATIONS**		17		
GROUP NAME	**PLAST**	**PRV. PL**	**CRITIC**	**PLAST NEW**	**PRV.PL NEW**	**CRITIC NEW**
BEAM	278	2	0	22	0	0
RETOPM10	18	0	0	18	0	0
CRUSHING	252	2	0	16	0	0
TOTAL MODEL	296	2	0	40	0	0
CRACKING LOGGING SUMMARY						
GROUP NAME	**CRACK**	**OPEN**	**CLOSED**	**ACTIVE**	**INACTI**	**ARISES**
BEAM	9725	9725	0	5725	4000	93
SHEAR	1799	1799	0	1031	768	34
TOTAL MODEL	9725	9725	0	5725	4000	93
CUMULATIVE REACTION:						
FORCE X			**FORCE Y**			
-0.24945D-09			-0.22759D+06			
YIELDING OF STIRRUPS						
STEP	**63**	**ITERATIONS**		12		
GROUP NAME	**PLAST**	**PRV. PL**	**CRITIC**	**PLAST NEW**	**PRV.PL NEW**	**CRITIC NEW**

BEAM	338	0	0	28	0	0
RETOPM10	27	0	0	12	0	0
STIRRUPS	2			2		
CRUSHING	280	0	0	18	0	0
SHEAR	3	0	0	3	0	0
TOTAL MODEL	367	0	0	42	0	0

CRACKING LOGGING SUMMARY

GROUP NAME	**CRACK**	**OPEN**	**CLOSED**	**ACTIVE**	**INACTI**	**ARISES**
BEAM	9774	9768	6	6184	3590	93
SHEAR	1731	1791	0	1059	732	39
TOTAL MODEL	9774	9768	6	6184	3590	93

CUMULATIVE REACTION:

FORCE X	**FORCE Y**
-0.63461D-09	-0.24465D+06

CRUSHING OF CONCRETE

STEP	**67**	**ITERATIONS**		7		
GROUP NAME	**PLAST**	**PRV. PL**	**CRITIC**	**PLAST NEW**	**PRV.PL NEW**	**CRITIC NEW**
BEAM	505	8	0	25	0	0
RETOPM10	54	0	0	6	0	0
STIRRUPS	20	0	0	4	0	0
CRUSHING	379	8	0	11	0	0
SHEAR	16	0	0	1	0	0
TOTAL MODEL	579	8	0	35	0	0

CRACKING LOGGING SUMMARY

GROUP NAME	**CRACK**	**OPEN**	**CLOSED**	**ACTIVE**	**INACTI**	**ARISES**
BEAM	10368	10368	0	7047	3321	86
SHEAR	2007	2007	0	1351	656	31
TOTAL MODEL	10368	10368	0	7047	3321	86

CUMULATIVE REACTION:

FORCE X	**FORCE Y**
-0.16393D-08	-0.26027D+06

YIELDING OF REINFORCING BARS M30

STEP	**69**	**ITERATIONS**		13		
GROUP NAME	**PLAST**	**PRV. PL**	**CRITIC**	**PLAST NEW**	**PRV.PL NEW**	**CRITIC NEW**
BEAM	555	10	0	21	0	0
RETOPM10	60	0	0	0	0	0
RETOPM30	14	0	0	14	0	0
STIRRUPS	26	0	0	4	0	0
CRUSHING	407	10	0	13	2	0
SHEAR	23	0	0	2	0	0
TOTAL MODEL	655	10	0	39	2	0

CRACKING LOGGING SUMMARY

GROUP NAME	**CRACK**	**OPEN**	**CLOSED**	**ACTIVE**	**INACTI**	**ARISES**
BEAM	10558	10558	0	6779	3779	111
SHEAR	2067	2067	0	1321	746	35

TOTAL MODEL	10558	10558	0	6779	3779	111
CUMULATIVE REACTION:						
FORCE X			**FORCE Y**			
-0.67223D-10			-0.26644D+06			
YIELDING OF REINFORCING BARS M25						
STEP	**71**	**ITERATIONS**		8		
GROUP NAME	**PLAST**	**PRV. PL**	**CRITIC**	**PLAST NEW**	**PRV.PL NEW**	**CRITIC NEW**
BEAM	607	8	0	25	0	0
RETOPM10	66	0	0	6	0	0
REBOTM30	50	0	0	24	0	0
REBOTM25	6	0	0	6	0	0
STIRRUPS	38	0	0	9	0	0
CRUSHING	435	8	0	15	0	0
SHEAR	31	0	0	4	0	0
TOTAL MODEL	767	8	0	70	0	0
CRACKING LOGGING SUMMARY						
GROUP NAME	**CRACK**	**OPEN**	**CLOSED**	**ACTIVE**	**INACTI**	**ARISES**
BEAM	10738	10738	0	6978	3760	93
SHEAR	2129	2129	0	1384	745	31
TOTAL MODEL	10738	10738	0	6978	3760	93
CUMULATIVE REACTION:						
FORCE X			**FORCE Y**			
-0.79772D-12			-0.27184D+06			
PEAK LOAD						
STEP	**82**	**ITERATIONS**		12		
GROUP NAME	**PLAST**	**PRV. PL**	**CRITIC**	**PLAST NEW**	**PRV.PL NEW**	**CRITIC NEW**
BEAM	302	446	0	5	210	0
RETOPM10	36	48	0	0	12	0
REBOTM30	104	0	0	4	0	0
REBOTM25	84	0	0	2	0	0
STIRRUPS	68	14	0	4	4	0
CRUSHING	220	298	0	3	62	0
SHEAR	18	30	0	0	6	0
TOTAL MODEL	594	509	0	9	226	0
CRACKING LOGGING SUMMARY						
GROUP NAME	**CRACK**	**OPEN**	**CLOSED**	**ACTIVE**	**INACTI**	**ARISES**
BEAM	11378	11378	0	6294	5084	62
SHEAR	2336	2336	0	1215	1121	22
TOTAL MODEL	11378	11378	0	6294	5084	62
CUMULATIVE REACTION:						
FORCE X			**FORCE Y**			
-0.72739D-10			-0.28331D+06			

3.5 Application of Safety Formats Model Code 2010

Table 3-7: Case RB1. Constitutive model parameters for concrete

	f_c (N/mm^2)	f_{ct} (N/mm^2)	E_c (N/mm^2)	ν	G_F (Nmm/mm^2)	G_C (Nmm/mm^2)
Mean measured	43.50	3.24	34925	Var.	0.144	35.99
Characteristic	35.50	2.27	32659	Var.	0.139	34.70
Mean GRF	30.17	2.91	30954	Var.	0.135	33.70
Design	23.67	1.51	28569	Var.	0.129	32.26

Table 3-8: Case RB1. Constitutive model parameters for reinforcing bars M10

	Φ (mm)	A_s (mm^2)	f_y (N/mm^2)	f_t (N/mm^2)	E_s (N/mm^2)	ε_{sy}
Mean measured	11.3	100	315.00	460.00	200000	0.00158
Characteristic	11.3	100	285.31	416.64	200000	0.00143
Mean GRF	11.3	100	313.84	458.31	200000	0.00157
Design	11.3	100	248.09	362.30	200000	0.00124

Table 3-9: Case RB1. Constitutive model parameters for reinforcing bars M25

	Φ (mm)	A_s (mm^2)	f_y (N/mm^2)	f_t (N/mm^2)	E_s (N/mm^2)	ε_{sy}
Mean measured	25.2	500	445.00	680.00	220000	0.00202
Characteristic	25.2	500	403.06	615.91	220000	0.00183
Mean GRF	25.2	500	443.36	677.50	220000	0.00202
Design	25.2	500	350.48	535.57	220000	0.00159

Table 3-10: Case RB1. Constitutive model parameters for reinforcing bars M30

	Φ (mm)	A_s (mm^2)	f_y (N/mm^2)	f_t (N/mm^2)	E_s (N/mm^2)	ε_{sy}
Mean measured	29.9	700	436.00	700.00	200000	0.00218
Characteristic	29.9	700	394.90	634.02	200000	0.00197
Mean GRF	29.9	700	434.39	697.42	200000	0.00217
Design	29.9	700	343.39	551.32	200000	0.00172

Table 3-11: Case RB1. Constitutive model parameters for reinforcing bars D4

	Φ (mm)	A_s (mm^2)	f_y (N/mm^2)	f_t (N/mm^2)	E_s (N/mm^2)	ε_{sy}
Mean measured	5.7	25.7	600.00	651.00	200000	0.00300
Characteristic	5.7	25.7	543.45	589.64	200000	0.00272
Mean GRF	5.7	25.7	597.79	648.60	200000	0.00299
Design	5.7	25.7	472.56	512.73	200000	0.00236

As proposed by the Model Code 2010 (fib, 2013) safety formats for non-linear finite element analyses include three numerical methods denoted as GRF (Global Resistance

Factor method), PF (Partial Factor method) and ECOV (Method of Estimation of a Coefficient of Variation of resistance). Application of the safety formats requires in total 4 non-linear analyses. In Table 3-7 - Table 3-11 the mechanical properties used in the non-linear analyses are summarized.

In Figure 3-31 the load-deflection curves obtained with mean measured, characteristic, mean GRF and design values of material strengths, calculated according to the Model Code 2010 (fib, 2013) are shown. In Figure 3-31 the peak loads of the analyses are presented. The aforementioned loads were defined as the highest load step which satisfied the imposed energy convergence tolerance of 1×10^{-3} or as the highest load value when the energy convergence norm was met in the subsequent steps. The peak loads are indicated with dots in Figure 3-31.

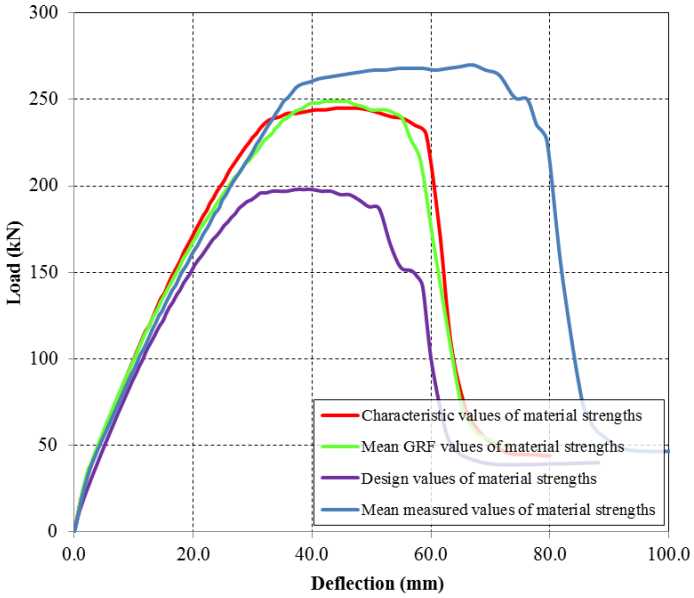

Figure 3-31: Case RB1. Load-deflection curves obtained with mean measured, characteristic, mean (GRF) and design values of material strengths calculated according to Model Code 2010 (fib, 2013)

The beam RB1 was analyzed with the analytical procedures proposed for sectional analysis an as well as numerically, with application of the safety formats for NLFEA as proposed by the Model Code 2010. Figure 3-32 shows the comparison of the analytical and numerical design values of the beam resistance expressed in terms of a percentage of the experimental ultimate value of applied load.

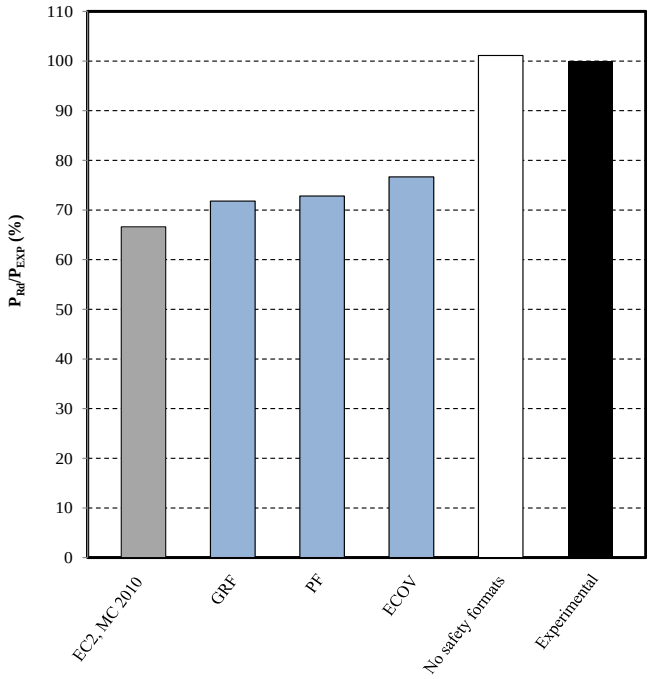

Figure 3-32: Case RB1. Analytical and numerical design values of beam resistance expressed in terms of a percentage of the experimental ultimate value of applied load, $P_{Exp} = 265kN$

In Table 3-12 the design values of beam resistances, expressed in terms of applied load P_{Rd}, obtained from numerical and analytical procedures are reported. The analytical beam resistance was obtained in section 3.2 with application of the sectional analysis according to Eurocode 2 (CEN, 2005) and Model Code 2010 (fib, 2013).

Table 3-12: Case RB1. Values of beam resistances, expressed in terms of applied load P_{Rd}

Experimental (kN)	EC2,MC2010 (kN)	GRF (kN)	PF (kN)	ECOV (kN)	No Safety Formats (kN)
265	181	190	193	203	268

3.6 Parametric study on crack models

A parametric study was carried out by varying sensitive input parameters of the concrete constitutive model, such as the crack model and the fracture energy of concrete in tension.
In Table 3-13 the material parameters applied in NLFE analyses performed in the parametric study are reported. Analysis 1 to Analysis 3 refer to the three analyses carried out by varying the aforementioned material parameters. All the analyses were performed considering mean measured values of material strengths. Parabolic law in compression and exponential law in tension were used for concrete, while an elasto-plastic law with hardening was adopted for steel. The analyses were carried out in load-control with arc-length control. A variable Poisson ratio was adopted for all analyses.
For all analyses a limit value of the reduction of the compressive strength of concrete due to lateral cracking was adopted:

$$\beta_{\sigma,\min} = \frac{f_{c,red}}{f_{cm}} = 0.6$$

The effect of the used values of the fracture energy of concrete in tension on the beam response was investigated by adopting the formulation proposed by Model Code 1990 (CEB-FIP, 1993) and the formulation proposed by Model Code 2010 (fib, 2013). The fracture energy of concrete in compression was considered for all analyses equal to $250G_F$ (Nakamura et al. 2001).
Within the fixed crack model a variable shear retention factor, which depends on the mean aggregate size d_{aggr}, the crack normal strain ε_n and the crack bandwidth value h is adopted:

$$\beta = 1 - \left(\frac{2}{d_{aggr}}\right)\varepsilon_n h$$

In Figure 3-33 the load-deflection curves obtained from the parametric study are plotted and the peak load of each analysis is indicated with a circular indicator. The peak load is defined as the highest load step where the energy norm ratio satisfies the fixed tolerance of 1×10^{-3}.
The peak load values are reported in Table 3-13.

Table 3-13: Case RB1. Data used for the parametric study

Analysis	Total strain crack model	Limit to β_σ	G_F	G_C	Peak load value (kN)
Analysis 1	rotating	0.6	MC2010	250 G_F	268
Analysis 2	rotating	0.6	MC1990	250 G_F	264
Analysis 3	fixed	0.6	MC2010	250 G_F	289

In Figure 3-33 the load-deflection curves resulting from the parametric study are plotted.

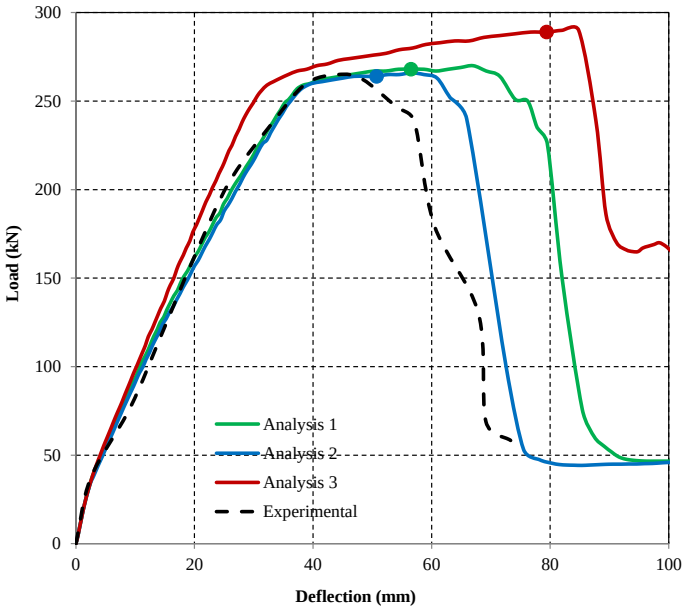

Figure 3-33: Case RB1. Load-deflection curves (Analysis 1 to 3)

The crack model and mechanical properties used in Analysis 1 were the same as those used to predict the design value of beam resistance from NLFE analyses.

From the comparison of analyses 1 and 2, the influence of the adapted values of the fracture energy of the concrete in tension ($G_{F,MC1990} = 0.106\,N/mm$ and $G_{F,MC2010} = 0.144\,N/mm$) and corresponding compressive fracture energy ($G_{C,MC1990} = 26.58\,N/mm$ and $G_{C,MC2010} = 35.99\,N/mm$) can be observed. Because of the fact that the beam failed in bending with crushing of concrete, the fracture energy of concrete in compression plays an important role on the ductility of the beam – especially on the peak and post-peak deformation.
Comparing analyses 1 till 3, it is clear that for beam RB1, the adopted crack model (total strain rotating or fixed crack model) has a moderate influence on the beam response, both in terms of peak load and in terms of peak deformation.

3.7 Parametric study on crack bandwidth

This section reports on (i) the sensitivity of analyses results on h, or actually G_F/h, and (ii) on post-analysis checks on the correctness of the a priori estimates for *h*.
Material models and parameters, element types and finite element mesh, boundary conditions and loading, load increments and convergence criteria are the same as those used for the analysis carried out with mean measured material strength (please refer to section 3.1.3).
Table 3-14 lists the *a priori* estimates for the crack bandwidth that are used in this study. Note that the compressive bandwidths h_C are unaltered. For practical reasons the variations of the crack bandwidths h were applied in the finite element models by variations of G_F. The exponential softening adopted for total strain crack models and exercised in the analysis can be formulated as given below:

$$\sigma = f_{ct} \exp\left(-\frac{\varepsilon}{\varepsilon_u}\right)$$

The fracture energy of concrete in tension G_F divided by the crack bandwidth *h* is:

$$G_F/h = -\varepsilon_u f_{ct} \cdot \exp\left(-\frac{\varepsilon}{\varepsilon_u}\right)\Big|_0^\infty = f_t \varepsilon_u$$

The ultimate crack strain results to be evaluated with:

$$\varepsilon_u = \frac{G_F}{h \cdot f_{ct}}$$

The maximum crack strain value $\varepsilon_{knn,\max}$ is defined as the crack strain corresponding to a residual stress equal to 1% of f_t:

$$\varepsilon_{knn,\max} = -\varepsilon_u \ln 0.001 = 4.6\varepsilon_u$$

The values of fracture energy of concrete in tension used as input data for the analyses and maximum crack strain values used in the contour plot are reported in Table 3-14.
Table 3-15 gives an overview of the obtained peak loads P_u.

Table 3-14: Case RB1. Estimates for the crack bandwidth *h* for quadratic plane stress quadrilaterals with 3×3 Gaussian integration

	Tension (mm)	**Compression (mm)**	G_F **(Nmm/mm²)**	G_C **(Nmm/mm²)**	$\varepsilon_{knn,max}$
Short-width	$h = ½\sqrt{A}\sqrt{2} = 20\sqrt{2}$	$h_c = \sqrt{A} = 40$	0.144	35.99	7.24×10^{-2}
Default	$h = \sqrt{A}\sqrt{2} = 40\sqrt{2}$	$h_c = \sqrt{A} = 40$	0.144	35.99	3.62×10^{-3}
Long-width	$h = 2\sqrt{A}\sqrt{2} = 80\sqrt{2}$	$h_c = \sqrt{A} = 40$	0.144	35.99	1.81×10^{-3}

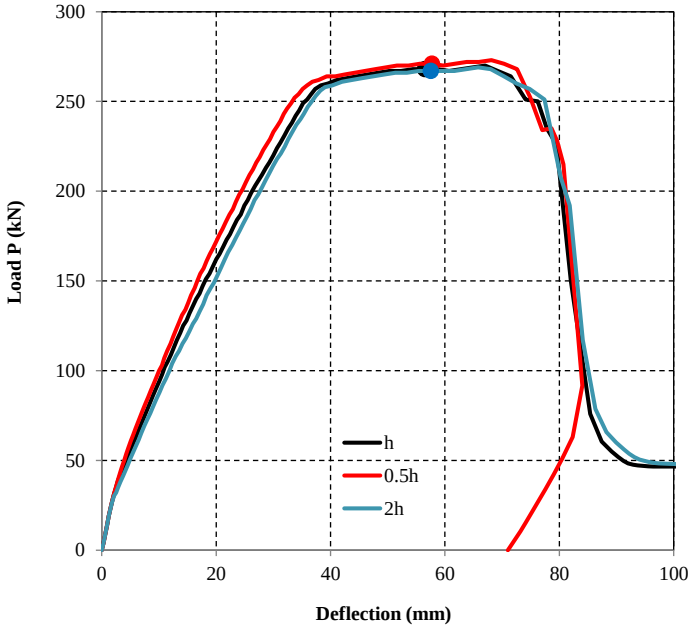

Figure 3-34: Case RB1. a) Load-deflection curves obtained with different crack bandwidth values

Table 3-15: Case RB1. Case studies and modifications

P_{Exp} (kN)	P_u (kN)		
	0.5*h*	***h***	**2*h***
265	271	268	255.98

Figure 3-34 shows the load-deflection curves for case RB1 obtained with different crack bandwidth values. The three ascending branches of the load-deflection graphs in show a comprehensible trend, with the "0.5*h*" branch above the "*h*" branch, and with the "*h*" branch above the "2*h*" branch. This does not hold true for the three descending branches in the Figure 3-32. A possible explanation is the sensitivity of the descending branches with respect to convergence criteria, especially for load controlled analysis with arc-length, see Section 3.8. A main observation is that the peak loads are hardly influenced by the choice of the crack bandwidth.

Figure 3-35 shows contour plots of the crack strain values for the corresponding peak values of the applied loads, obtained with different crack bandwidth values. In the contour plots the color ranges are adjusted to the (tensile) stress-strain relations: red denotes strains beyond the ultimate crack strain of the softening stress-strain diagram.

For a better assessment of the strain localization, mesh extractions from the marked regions in Figure 3-35 with indicated *a priori* estimates of *h* are illustrated in Figure 3-36.

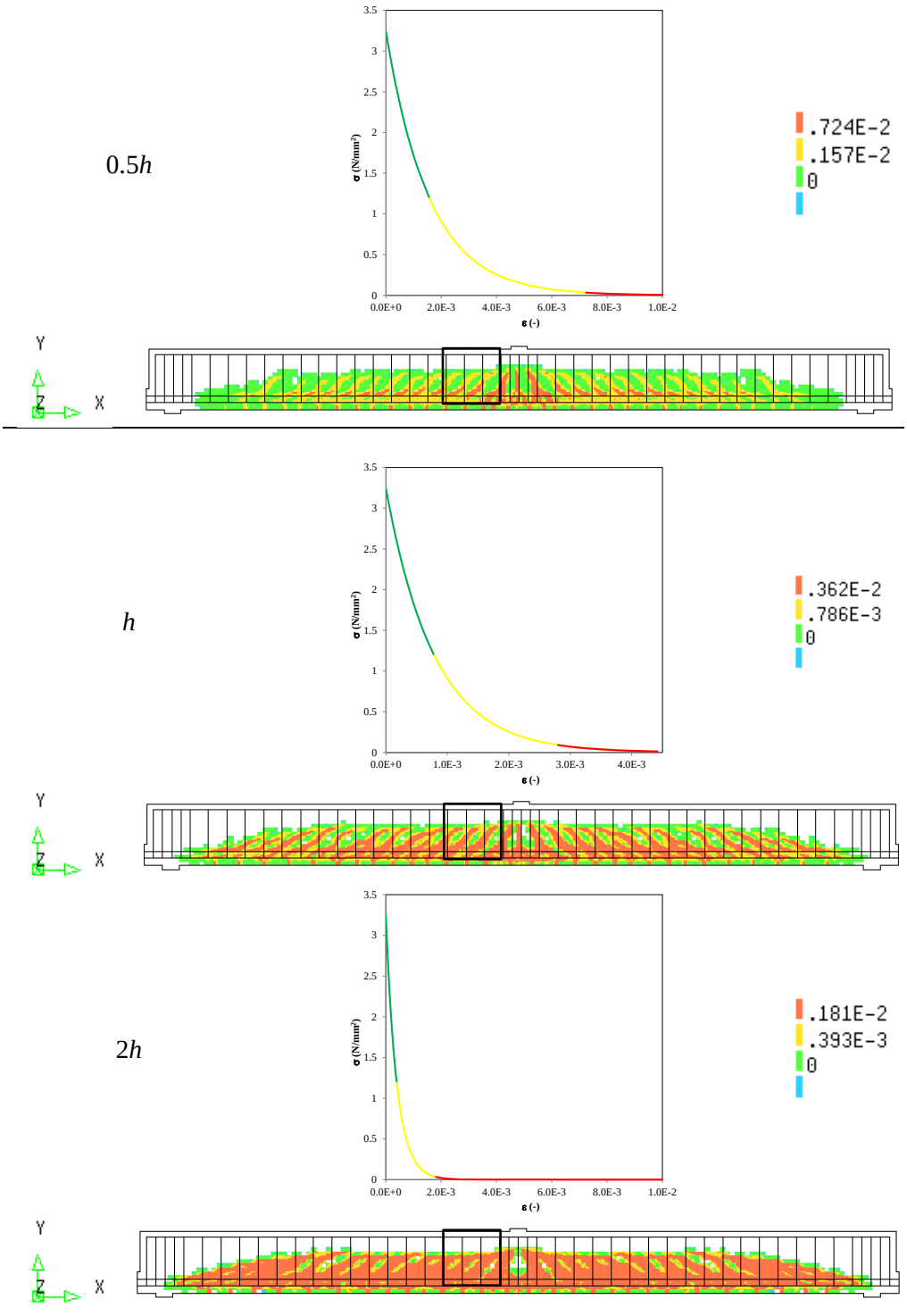

Figure 3-35: Case RB1. Maximum principal strain values obtained with different crack bandwidth values

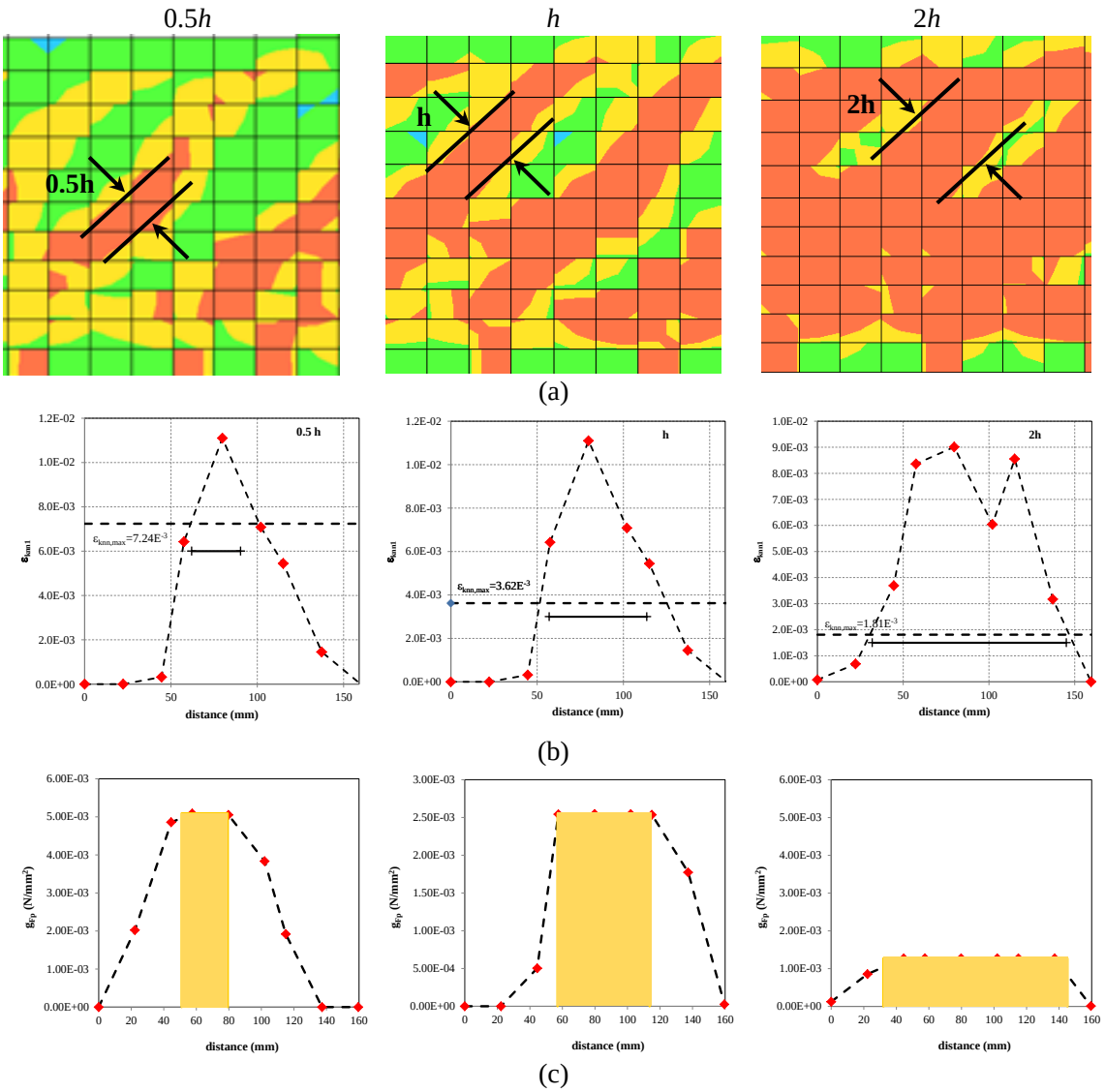

Figure 3-36: Case RB1. (a) Maximum principal strains for the area indicated in Figure 3-35. (b) Maximum principal strain-distance between integration points along the lines indicated above. The ultimate strain values are indicated by a red dashed line. (c) fracture energy over crack bandwidth-distance between integration points.

The dissipated fracture energy divided by the crack bandwidth (g_{Fp}) is plotted versus the distance between different integration points along a line considered perpendicular to the crack. In all graphs 9 integration points, as shown in Figure 3-37, are taken into account.

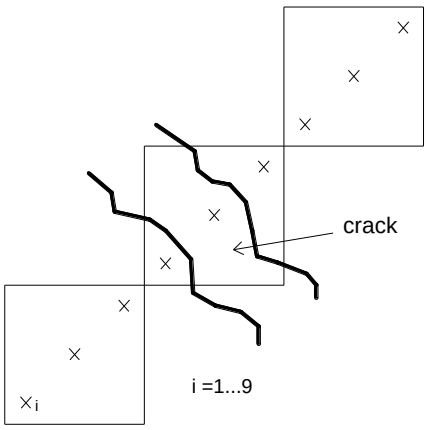

Figure 3-37: Case RB1. Example of integration points considered

The total dissipated fracture energy can be calculated with:

$$g_{Fp} = \varepsilon_u f_{ct} - \varepsilon_u f_{ct} \cdot \exp\left(-\frac{\varepsilon_i}{\varepsilon_u}\right) - \frac{1}{2}\sigma_i \varepsilon_i$$

The total dissipated fracture energy in the *i*-th integration point is illustrated in Figure 3-38, while the values of dissipated fracture energy in tension are calculated for different values of crack bandwidth in Figure 3-36 (c).

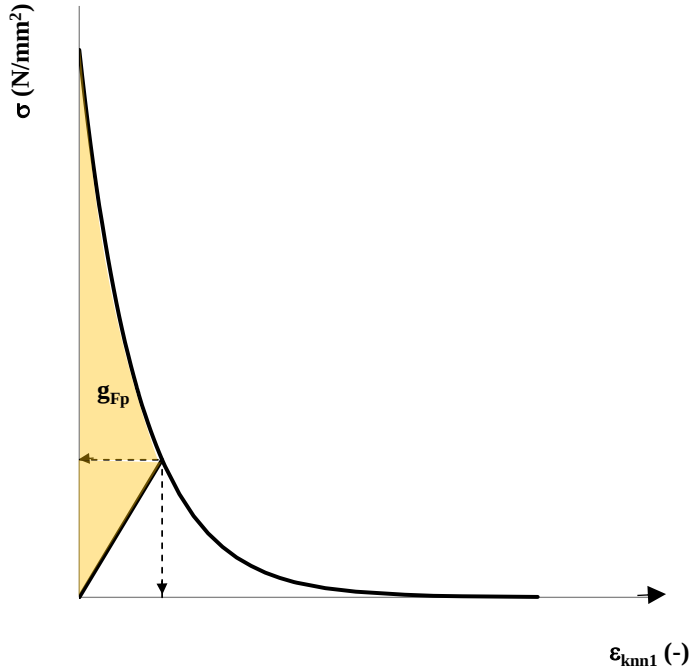

Figure 3-38: Fracture energy dissipated in the i- th integration point

From Figure 3-36 (c) the *a posteriori* crack bandwidths can be evaluated as the length characterized by maximum dissipated fracture energy of concrete in tension; this means the length characterized by principal strains higher than the ultimate crack strain in tension, $\varepsilon_{knn,max}$.

Remarkably, Figure 3-36 shows that by comparing the *a priori* crack bandwidths with the obtained *a posteriori* crack bandwidths, the results are quite close. None of the

three *a priori* crack bandwidths is clearly superior to the two remaining crack bandwidths.

3.8 Parametric study of convergence criteria

A sensitivity study were carried out with respect to (*i*) the fracture energy of concrete in compression, (*ii*) the convergence method, (*iii*) the convergence criteria and (*iv*) the maximum number of iterations, Table 3-16.
The current sensitivity study employs in the models the mean measured material parameters-material models and parameters as explained in section 3.3.

Table 3-16: Case RB1. Case studies and modifications

Case study	RB1
Compression model	Parabolic, low G_c — Parabolic, medium G_c — Parabolic, high G_c
Control	Load control with arc length
Max. number of iterat.	25 - 50

Table 3-17 presents the values for the fracture energy of concrete in compression. For "low", "medium" and "high" values of fracture energy of concrete in compression the ratio G_C/G_F equals 100, 250 and 500 respectively. The fracture energy of concrete in tension G_F was calculated with Model Code 2010 (fib, 2013).

Table 3-17: Case RB1. Values for the fracture energy of concrete in compression G_C

low G_C (Nmm/mm^2)	medium G_C (Nmm/mm^2)	high G_C (Nmm/mm^2)	G_F (Nmm/mm^2)
14.39	35.99	71.98	0.144

For analyses carried out in load control with arc-length method, Table 3-18 gives an overview of all analyses which were performed to determine the sensitivity of the analyses results to variations in the convergence criteria.

For low, medium and high values of fracture energy of concrete in compression G_C, 6 analyses were carried out:

- 3 different type of criteria: displacement (D), energy (E) and force (F)
- 2 levels of convergence tolerances ε: strict (1) and relatively loose (2)

As a main NLFEA result, the Table 3-18 presents the peak value of applied load P_u. Peak load values are identified in correspondence of the last step load values in which the convergence criterion is satisfied within the maximum number of iterations.

Table 3-18: Case RB1. Overview of NLFE analyses using load control and obtained peak values of the applied load P_u, ($P_{Exp} = 265kN$)

Comp. model	criterion	Analysis label	tolerance strict	P_u (kN)	Analysis label	tolerance loose	P_u (kN)
Low G_C	disp.	DA1L	1×10^{-2}	263	DA2L	5×10^{-2}	279
	energy	EA1L	1×10^{-3}	251	EA2L	5×10^{-3}	263
	force	FA1L	1×10^{-2}	27	FA2L	5×10^{-2}	42.3
Medium G_C	disp.	DA1M	1×10^{-2}	277	DA2M	5×10^{-2}	303

	energy	EA1M	1×10^{-3}	268	EA2M	5×10^{-3}	276
	energy (50 ite)	EA1M50	1×10^{-3}	267			
	force	FA1M	1×10^{-2}	27	FA2M	5×10^{-2}	39.4
	disp.	DA1H	1×10^{-2}	279	DA2H	5×10^{-2}	320
High G_C	energy	EA1H	1×10^{-3}	280	EA2H	5×10^{-3}	294
	force	FA1H	1×10^{-2}	268	FA2H	5×10^{-2}	259

Typical results for Case RB1 are given in Figure 3-39 where the convergence criteria was kept constant and the fracture energy of concrete in compression was varied. Because of the fact that beam RB1 fails due to bending after crushing of concrete, the ductility of the beam is increasing as the value of the fracture energy of concrete in compression is increased. In Figure 3-39 the peak load values are marked with the circular markers. The peak load values are identified in correspondence of the last step load values in which the energy convergence criterion is satisfied within the maximum number of iterations.

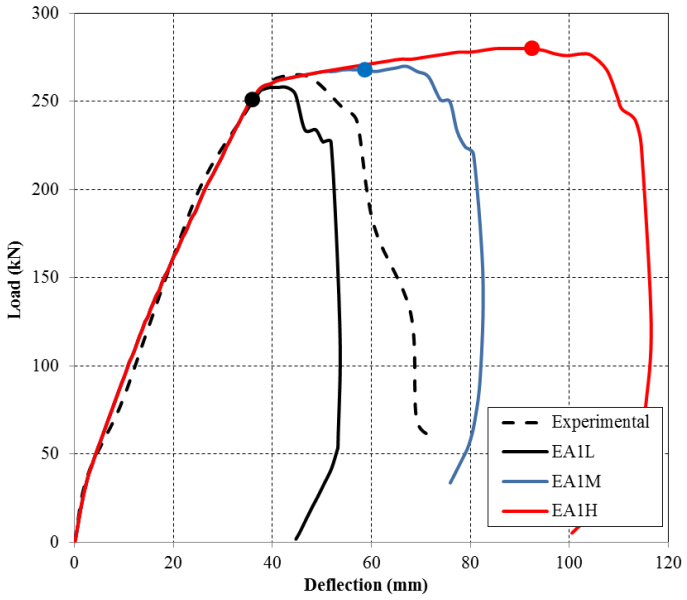

Figure 3-39: Case RB1. Load deflection curves for Case RB1 with varying the fracture energy of concrete in compression

Figure 3-40 presents the load-deflection curves obtained with the mean values of the fracture energy of concrete in compression and the varying convergence criteria. It can be observed that for the case of the analysis with the governing energy criterion and alternating number of iterations (25 and 50 iterations), no differences in the peak load value takes place. Moreover, from Figure 3-40 it is noted that for the analysis with the force convergence norm, the convergence criterion was satisfied within the maximum number of iterations for only few load steps.

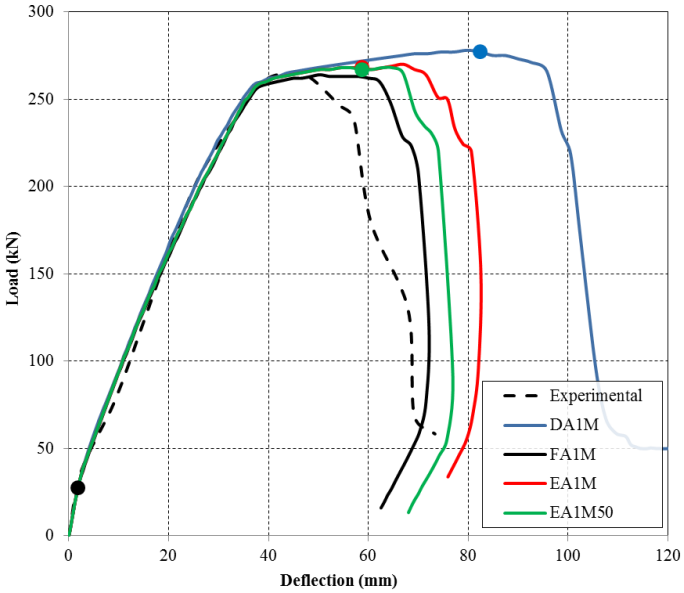

Figure 3-40: Case RB1. Load-deflection curves with varying the convergence criteria

Based on the recorded results in Table 3-18, a number of conclusions can be drawn.
The "loose" displacement norm is inappropriate for the estimation of load carrying capacity for the case under consideration. All analyses with the displacement criterion and the convergence tolerance of 5×10^{-2} resulted in the overestimated peak value when compared to the experimental failure load.
Good and consistent results were obtained by the "strict" energy norm. Based on the results of the analysis with an increased number of iterations per step as well as interpretations of the convergence graphs, a "strict" energy tolerance of 10^{-3} is recommended.

3.9 Estimating crack widths

In the current section, a way to estimate the crack width from the nonlinear finite element analyses results is proposed. The crack width was estimated from NLFE results in combination with the Model Code 2010 (fib, 2013).
The crack width is calculated at the Serviceability Limit State. The load at the Serviceability Limit State (P_{SLS}) was defined as:

$$P_{SLS} = \frac{P_u}{1.7}$$

where P_u is the peak value of applied load obtained from NLFEA. In this way the step corresponding to the Serviceability Limit State is identified.
In the following, the procedure for the determination of the crack width in case of development of bending and shear cracks is explained.

Bending cracks

In order to better evaluate the crack width of beam RB1, an equivalent tie with the same ratio of longitudinal reinforcement and the same effective area in tension as RB1 was modeled. Crack opening width values and crack spacing were evaluated both for the equivalent tie and for beam RB1 in correspondence of the same load level, equal to 268kN/1.7=157 kN.
In Figure 3-41(a) the cross section of the tie compared with the cross section of RB1 and the mechanical model of the equivalent tie (b) is shown.

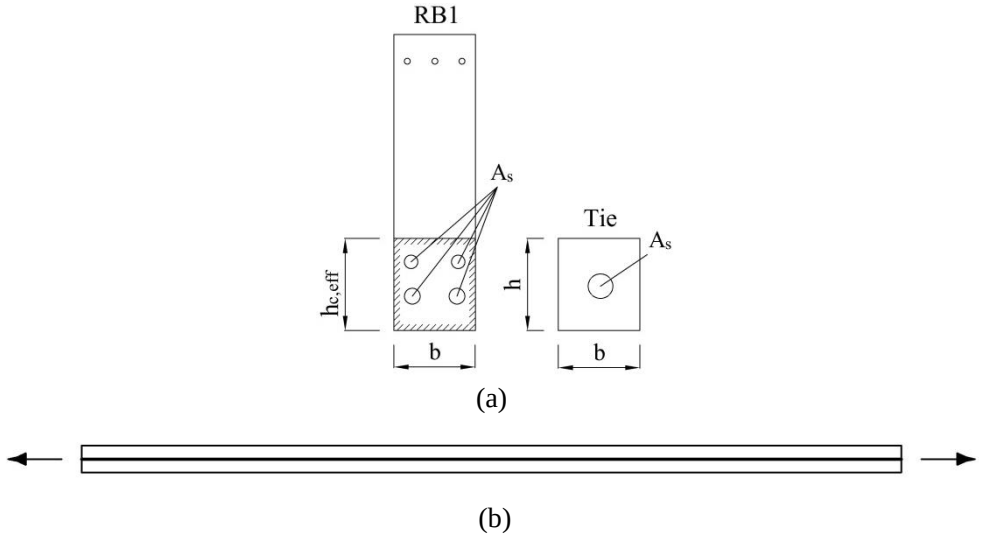

Figure 3-41: Case RB1. (a) Cross section and of the equivalent tie (b) Mechanical model of the tie

The characteristic crack width w_k was calculated according to the Model Code 2010 (*fib*, 2013) as follows:

$$w_k = 2l_{rs\max}(\varepsilon_{sm} - \varepsilon_{cm}) \tag{3-1}$$

where:

$l_{s,\max}$ length over which slip between concrete and steel occurs,

ε_{sm} average steel strain over the length $l_{s,max}$,

ε_{cm} average concrete strain over the length $l_{s,max}$,

The relative mean strain in equation (3-1) follows from:

$$\varepsilon_{sm} - \varepsilon_{cm} = \frac{\sigma_s - \beta\sigma_{sr}}{E_s} \tag{3-2}$$

Where:

σ_s the steel stress in a crack,

σ_{sr} maximum the steel stress in a crack in the crack formation stage, which for pure tension is $\sigma_{sr} = \frac{f_{ctm}}{\rho_{s,ef}}\left(1 + \alpha_e \rho_{s,ef}\right)$

Where:

$\alpha = \frac{E_s}{E_c}$, $h_{c,ef} = \min\left\{2.5(h-d); \frac{(h-x)}{3}\right\}$, $A_{c,fl} = bh_{c,ef}$, $\rho_{s,eff} = \frac{A_s}{A_{c,ef}}$ and σ_{sr} can be easily calculated from sectional analysis for bending.

For the length $l_{s,max}$ the following expression applies:

$$l_{s,\max} = k \times c + \frac{1}{4}\frac{f_{ctm}}{\tau_{bms}}\frac{\varphi_{eq}}{\rho_{s,ef}} \tag{3-3}$$

$k = 1$

$$\phi_{eq} = \frac{n_1\phi_1^2 + n_2\phi_2^2}{n_1\phi_1 + n_2\phi_2}$$

For a stabilized cracking stage and long term loading: $\tau_{bms} = 1.8 \times f_{ctm}$, $\beta = 0.4$

Because of beam RB1 fails due to bending, the crack opening width values obtained from NLFE analyses were calculated from the average value of strain of reinforcing steel M30, $\overline{\varepsilon_s}$, over the length $2l_{s,\max}$ at midspan. The average value of strain of reinforcing steel M30 obtained from the NLFEA was multiplied by the crack spacing $2l_{s,\max}$ obtained through Model Code 2010 (fib, 2013) formulation, equation.(3-3).

$$w_d = l_{s,\max}\overline{\varepsilon_s} \tag{3-4}$$

In Figure 3-42 the crack strain values of RB1 beam at the SLS (step 43, $P = 157kN$) are shown.

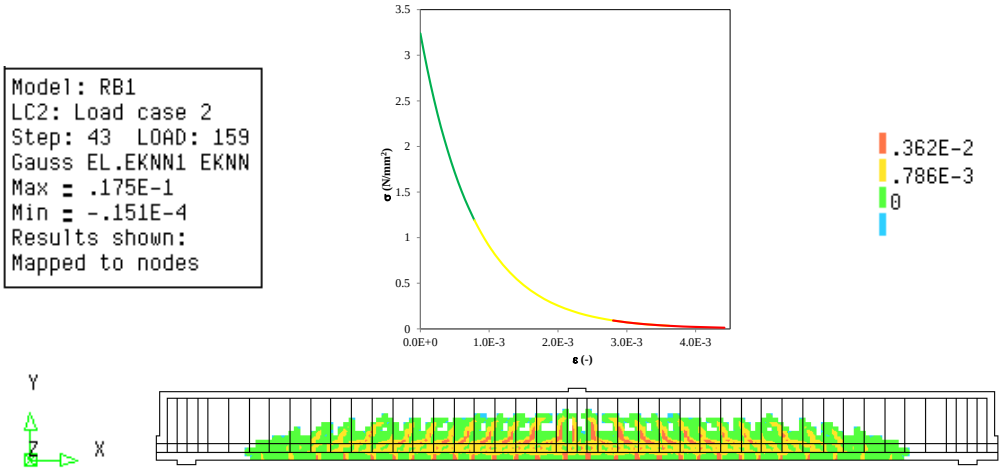

Figure 3-42: Case RB1. Crack strain values at step 43 ($P = 157kN$)

In Table 3-19 the crack spacing obtained from equation (3-3) and the crack width obtained from Model Code 2010 (fib, 2013) (equation (3-1)) and equation (3-4) are summarized.It can be noted that the crack opening width values mainly due to bending are well predicted with equation. (3-4) and on the safe side.

Table 3-19: Case RB1. Crack width according to Model Code 2010 (fib, 2013) formulation and equation (3-4))

$2l_{s,max}$ (mm)	w_d (mm)	w_d (mm)
236	0.297	0.318

3.10 Concluding remarks

The benchmark beam RB1 tested in the experimental program of Vecchio & Shim (2004) exhibited a flexural-compressive failure mode at a load equal to $P = 265kN$.
The analytical calculation based on sectional analysis demonstrated that beam RB1 fails due to bending. The shear force corresponding to the design value of moment resistance is lower than the design value of shear resistance. The design beam resistance evaluated with sectional analysis equals to $P_{Rd} = 176kN$.
The behavior of the beam is highly influenced by crushing of concrete beneath and adjacent to the loading plates. The disturbances around the loading plates introduce complex three-dimensional effects, making the modelling of interface elements placed between loading or supporting steel plates and the RC beam a fundamental aspect to be considered.
A flexural-compressive failure mode was achieved from NLFEA carried out with mean measured value of material strengths. The peak value of applied load obtained from

NLFEA is equal to 268 kN and the failure mode is characterized by crushing of concrete, yielding of M10 top bars, yielding of M30 and M25 bottom bars and yielding of stirrups.

Safety formats for non-linear finite element analyses as proposed by the Model Code 2010 (fib, 2013), were used to derive the design value of beam resistance.

The design value of beam resistance obtained from application of safety formats is higher than the design value of beam resistance obtained from analytical methods based on the sectional analysis. The maximum value was obtained with ECOV method and equals to $P_{Rd} = 203kN$.

Since the beam fails in bending, the failure mode is not heavily dependent on the crack model and tensile strengths adopted for concrete in tension, whereas the post-peak behavior appears to be sensitive to the stress-strain relation adopted for concrete in compression.

The first sensitivity study investigated the influence of the varying crack bandwidth (0.5*h*, *h*, 2*h*). *A priori* crack bandwidths (based on integration schemes) were compared with *a posteriori* crack bandwidths derived on the calculation of the dissipated fracture energy of concrete in tension. It was concluded that none of the three *a priori* crack bandwidths is clearly superior to the two remaining crack bandwidths

The second sensitivity study was carried out by varying the compression model for concrete, the convergence method, the convergence criteria and the maximum number of iterations. From the results, it was concluded that good and consistent results are obtained with the "strict" force and the "strict" energy convergence norms. Moreover, based on the above conclusions an energy norm with a tolerance of 10^{-3} is recommended.

Finally, the method to estimate the crack width from the results of nonlinear finite element analyses is proposed to satisfy performance requirements of serviceability limit states (SLS). It was shown that for beam RB1 the crack width values, mainly due to bending, can be evaluated with good accuracy by multiplying the average value of strain of reinforcing steel by the crack spacing $l_{s,max}$ calculated with expressions of the MC2010.

4 Case RB2: Collins and Kuchma (1999)

Case RB2 considers beam SE-50A-45 of the experimental program of Collins and Kuchma (Collins & Kuchma, 1999) and was reported in CEB bulletin 237 (CEB-FIB, 1997). In an international workshop on shear force held in Rotterdam, the Netherlands in 2007 this beam was used as a benchmark. It was then named "beam 8". The outline of the case is shown in Figure 4-1. The selection of the beam was made based on the failure mechanism which the beam had undergone. The failure was characterized as the diagonal-tension shear failure.

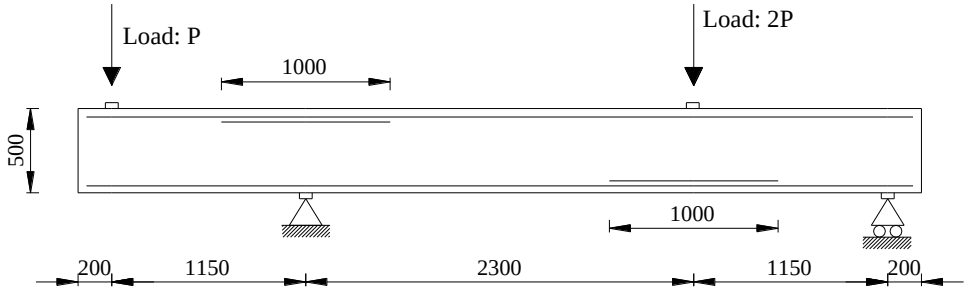

Figure 4-1: Case RB2. Dimensions (in mm), reinforcements and loading

4.1 Experimental setup and results

Geometry

The geometry of the beam and reinforcement is shown in Figure 4-2 and Figure 4-3. The beam has the total length of 5.0 m, depth of 0.5 m and width of 0.169 m.

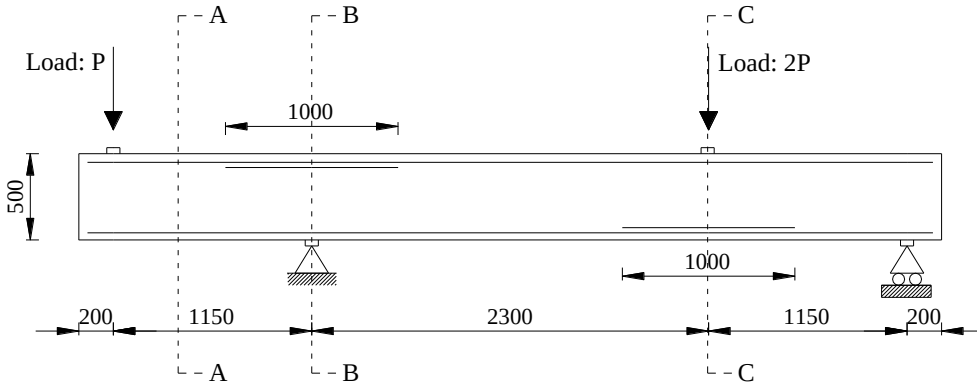

Figure 4-2: Case RB2. Dimensions (in mm), reinforcements layout and loading

The dimensions of the loading and support plates are not fully specified; it is assumed that the dimensions are 76×169×25 mm^3. Four #15 bars are placed as tensile and compressive reinforcement along the entire length of the beam. Additional four #15 bars are placed as tensile reinforcement over a length of 1 m in the region characterized by the maximum value of the applied bending moment. The sections corresponding to these regions are Section B-B and Section C-C in Figure 4-2.

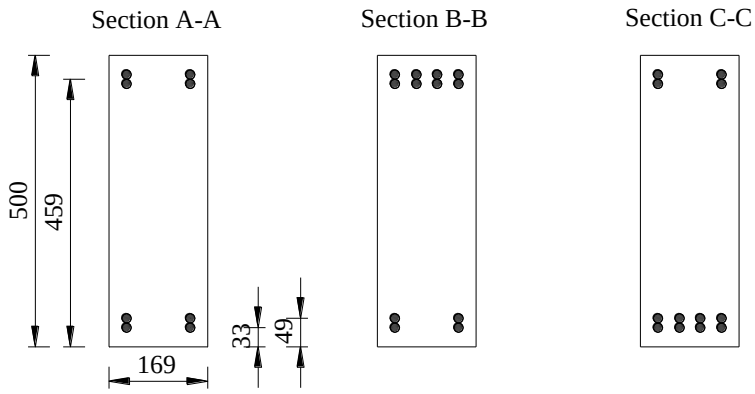

Figure 4-3: Case RB2. Cross section details (dimensions in mm)

Material Properties

The concrete and reinforcement properties, given in Collins & Kuchma (1999), are listed in Table 4-1.

Table 4-1: Case RB2. Concrete and reinforcement properties

Concrete properties				
f_{cm} **(N/mm^2)**			d_{max} **(mm)**	
53			10	
Reinforcement properties				
Φ **(mm)**	A_s **(mm^2)**	E_s **(N/mm^2)**	f_{ym} **(N/mm^2)**	f_{tm} **(N/mm^2)**
16.0	200	200000	400	600

Loading and Boundary Conditions

The loading and boundary conditions in the experimental setup are shown in Figure 4-4 and Figure 4-2. The beam is loaded by two concentrated loads: one load equal to *P* at the top left, and one load equal to *2P* at the middle right loading point, Figure 4-2.

Figure 4-4: Case RB2. Experimental setup

Experimental Results

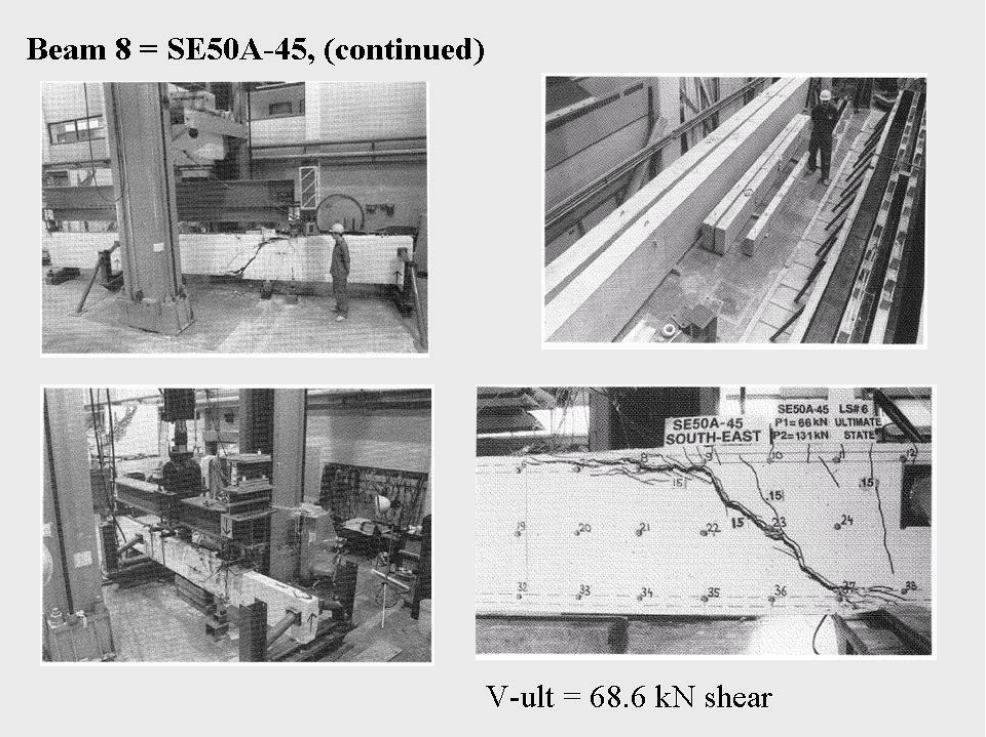

Figure 4-5: Case RB2. Failure mechanisms

The beam exhibited a typical brittle diagonal-tension failure mode, shown in Figure 4-5. The load-deflection curve is not given in the references; the experimental ultimate value of the applied load was equal to $P_{Exp} = 69kN$. In the second series of test on the same beam after strengthening failed at the applied load equal to $P_{Exp} = 81kN$.

4.2 Analytical analysis

In Figure 4-6 the load configuration at failure is shown. The distributed load representing the beam weight is equal to $q = 0.169m \times 0.5m \times 25\frac{kN}{m^3} = 2.113\,kN/m$.

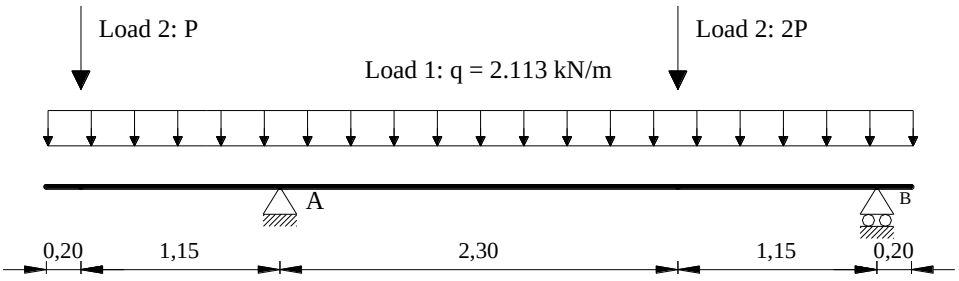

Figure 4-6: Case RB2. Load configuration (dimensions in m)

Load case 1
Figure 4-7 shows the value of applied moment and shear force due to load case 1.

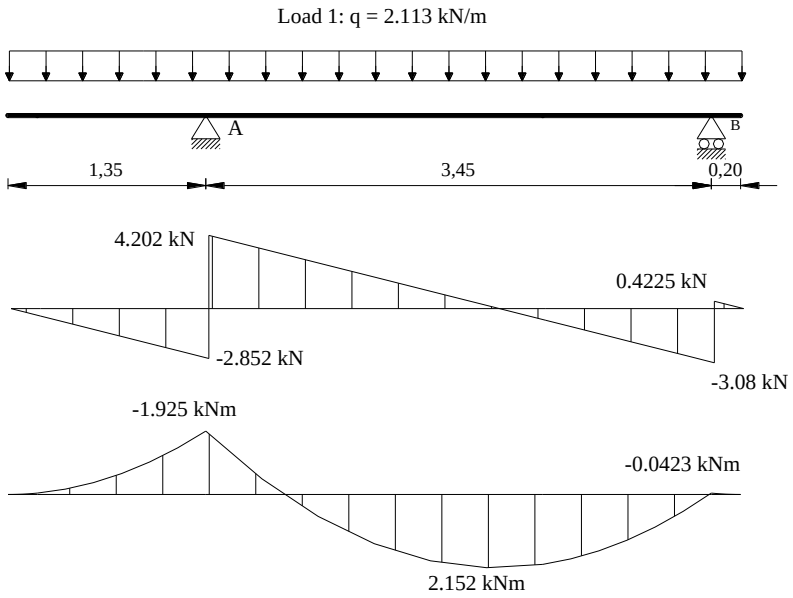

Figure 4-7: Case RB2. Load 1: Internal forces (dimensions in m)

Load case 2

The experimental ultimate value of the applied load is equal to $P_{Exp,1} = 69kN$. Figure 4-8 shows the maximum value of applied moment and shear force for load case 2.

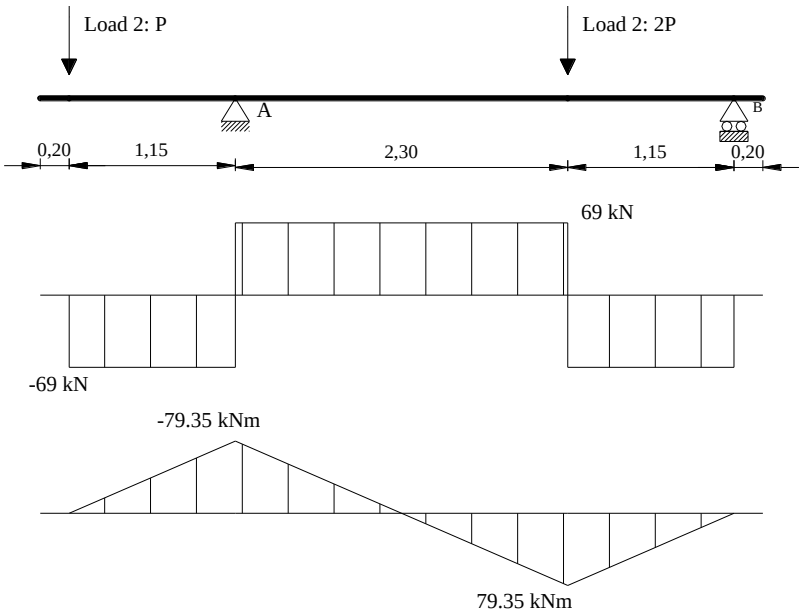

Figure 4-8: Case RB2. Load 2: Internal forces (dimensions in m)

Load 1 + Load 2

At failure the maximum value of the applied moment is

$M_{E,A,\min} = -1.925kNm - 79.35kNm = -81.28\,kNm$

and the maximum value of applied shear force is equal to:

$V_{Ed,\max} = 4.2kN + 69kN = 73.2kN$

The design value of moment resistance is evaluated with sectional analysis by assuming:

- the tensile strength of concrete is ignored,
- the compressive stresses in concrete are derived from parabola-rectangle relation,
- the stresses in reinforcing steel are derived from elastic-plastic stress-strain relation with hardening,
- the partial safety factor for the mechanical properties of reinforcing steel equals $\gamma_s=1.15$, the factor for concrete material properties equals $\gamma_c=1.5$.

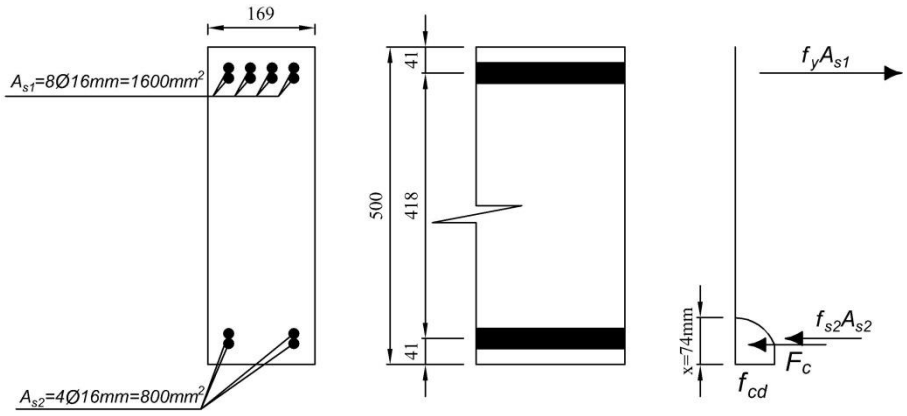

Figure 4-9: Case RB2. Stress block for determination of the design moment resistance

From the calculations with initially assumed yielding in both top and bottom reinforcement, it was concluded that the aforementioned assumption is not fulfilled for the compressive reinforcement. Consequently, the below presented computation of the moment resistance already includes the adjustment for the magnitude of the force below the yielding threshold.

The provided reinforcement yields when strains reach the value: $\varepsilon_s = \frac{f_{yd}}{E_s} = 1.74 \cdot 10^{-3}$

For the horizontal force equilibrium:

$$A_{s1} f_{yd} - A_{s2}\left(\frac{x-a_2}{x}\varepsilon_{cu2}\right)E_s - 0.8095 x b f_{cd} = 0 \rightarrow x = 74mm$$

Verification of the assumption for the calculated value of x:

$$\varepsilon_{s1} = \frac{\varepsilon_{cu2}(d_1 - x)}{x} = \frac{0.0035(459mm - 74mm)}{74mm} = 0.018 \rightarrow steel\ yields$$

$$\varepsilon_{s2} = \frac{\varepsilon_{cu2}(x - a_2)}{x} = \frac{0.0035(74mm - 41mm)}{74mm} = 1.561 \cdot 10^{-3} \rightarrow steel\ does\ not\ yield$$

thus the assumptions are fulfilled.

The design value of the moment resistance in calculated around the centre of the compression zone $0.416x$:

$$M_{Rd} = A_{s1} f_{yd}(d_1 - 0.416x) + A_{s2}\varepsilon_{s2} E_s(0.416x - a_2) = 235.76 kNm$$

A value of applied moment equal to

$$M_{E,A,\min} = -q\frac{(1.35m)^2}{2} - P \times 1.15m = -235.76\ kNm$$

Which results in the applied load:

$$P_{Rd} = \frac{1}{1.15m}\left(235.76 kNm - q\frac{(1.35m)^2}{2}\right) = 203.335\ kN\ .$$

The design value of shear resistance can be evaluated for an element without shear reinforcement with Eurocode 2 (CEN, 2005) as follows:

$$V_{Rdc} = db_W \left[C_{Rcd} k (100 \rho_\ell f_{ck})^{1/3} \right] = 459mm \times 169mm \times \left[\frac{0.18}{1.5} \times 1.66 \times (100 \times 0.0095 \times 45MPa)^{1/3} \right] =$$

$$= 54.03\,kN$$

The design value of shear resistance can be evaluated for an element without shear reinforcement with two levels of approximation as proposed in Model Code 2010 (fib, 2013).

Level I Approximation

The design shear resistance of members without shear reinforcement is given by:

$$V_{Rdc} = k_v \frac{\sqrt{f_{ck}}}{\gamma_c} z b_w = 0.119 \times \frac{\sqrt{45}}{1.5} \times 413.1mm \times 169mm = 37.06kN$$

Where:

$$k_v = \frac{180}{1000 + 1.25z} = \frac{180}{1000 + 1.25 \times 413.1mm} = 0.119$$

Level II Approximation

The state of strain required for the analysis is considered at the critical section located d from the edge of the support. In order to obtain a value of ε_x corresponding to the design shear resistance, an iterative procedure must be applied. After a number of iterations, the procedure results in:

$$V_{Ed}^{i-1} = 61019\,N$$

$$M_{Ed}^{i-1} = V_{Ed}^{i-1} d = 61019N \times (1150 - 459)mm = 42164483\,Nmm$$

$$\varepsilon_x^{i-1} = \frac{1}{2E_s A_s} \left(\frac{M_{Ed}^{i-1}}{z} + V_{Ed}^{i-1} \right) = \frac{1}{2 \times 200 \cdot 10^3 N/mm^2 \times 800mm^2} \left(\frac{42164483Nmm}{413.1mm} + 61019N \right) = 0.0005$$

$$k_{dg} = \frac{32}{16 + d_g} = \frac{32}{16 + 10} = 1.231 \geq 0.75$$

$$k_v^i = \frac{0.4}{1 + 1500 \cdot \varepsilon_x^{i-1}} \times \frac{1300}{1000 + k_{dg} z} = \frac{0.4}{1 + 1500 \times 0.0005} \times \frac{1300}{1000 + 1.231 \times 413.1mm} = 0.195$$

$$V_{Rd}^i = k_v^i \frac{\sqrt{f_{ck}}}{\gamma_c} z b_w = 0.195 \times \frac{\sqrt{45}}{1.5} \times 413.4mm \times 169mm = 60998\,N = 60.99\,kN$$

Concluding from the results of sectional analysis, it can be shown that the governing failure mode is caused by shear.

In Table 4-2 the design value of beam resistances expressed in terms of applied load P_{Rd} obtained with the Eurocode 2 (CEN, 2005) and the Model Code 2010 (fib, 2013) are summarized. These values are obtained by subtracting from the design shear resistance the shear force due to self-weight equal to 1.9 kN.

Table 4-2: Case RB2. Design value of beam resistance expressed in terms of applied load P_{Rd}

P_{Rd} (EC2) (kN)	P_{Rd} (MC2010 - Level I) (kN)	P_{Rd} (MC2010 - Level II) (kN)
52	35.2	59

4.3 Finite element model

Units

Units are N, m.

Material models and parameters

The concrete model is based on a total strain rotating crack model with

- exponential softening in tension and parabolic behavior in compression,
- variable Poisson's ratio of concrete dependent on crack strain values,
- reduction of compressive strength of concrete due to lateral cracking with a lower limit 0.6 according to (Vecchio, 1986),
- increase in compressive strength due to lateral confinement according to the model proposed by Selby and Vecchio (Selby and Vecchio, 1993).

The mechanical properties for concrete are summarized in Table 4-4. The uniaxial stress-strain curve is shown in Figure 4-10. In the input file of the analysis, the G_F value has been decreased with a factor $\sqrt{2}$ in order to compensate for an underestimation of the crack band width for cracks with an inclination angle of 45 degrees $G_{F,reduced} = 0.149/\sqrt{2} = 0.105$.

Table 4-3: Case RB2. Constitutive model parameters for concrete

	f_{cm} (N/mm^2)	f_{ctm} (N/mm^2)	E_c (N/mm^2)	ν	G_F (Nmm/mm^2)	G_C (Nmm/mm^2)
Mean measured values	53.0	3.80*	37485*	0.2	0.149*	37.29*

* Not specified in reference; estimated according to MC2010 (fib, 2013).

The model for the reinforcement bars is based on hardening plasticity. Geometrical and mechanical features of reinforcing bars are summarized in Table 4-4. The stress- strain curve for steel of the reinforcing bars is plotted in Figure 4-11.

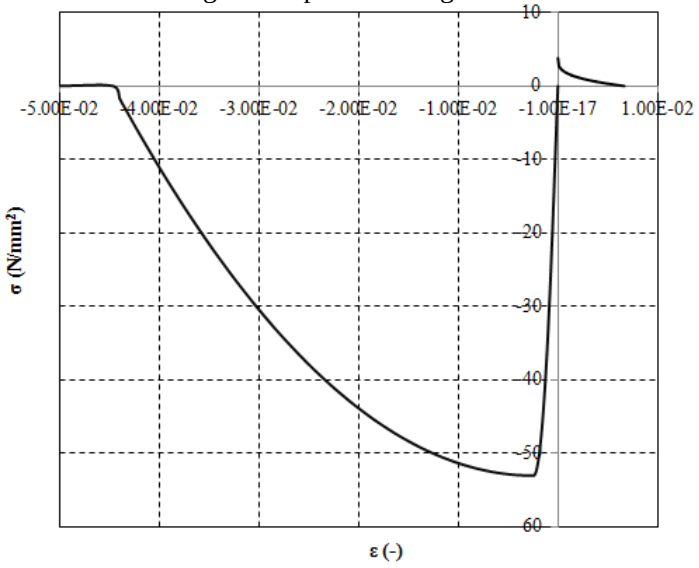

Figure 4-10: Case RB2. Stress-strain curve for concrete

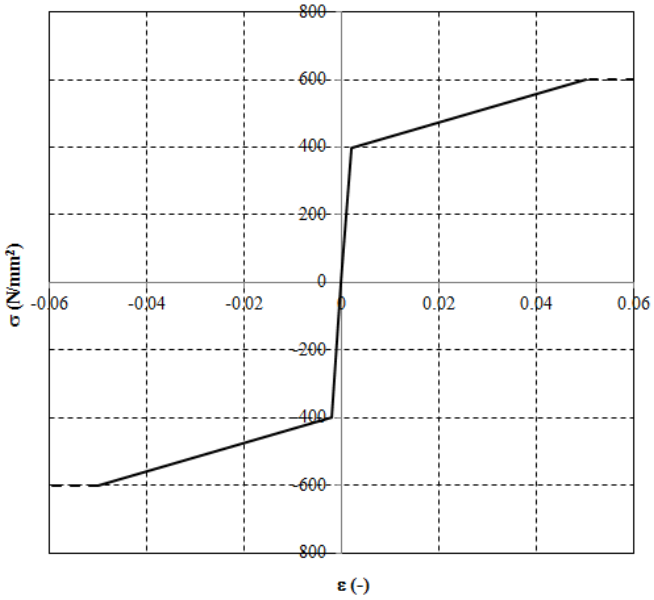

Figure 4-11: Case RB2. Stress-strain curve adopted for steel of reinforcing bars

For the steel plates a linear elastic behavior is assumed, see Table 4-4.

Table 4-4: Case RB2. Steel plates properties

E (N/mm^2)	ν
200000	0.3

Interface elements were used between the steel plates and the concrete beam at the supports and loading positions. The thickness of interface elements equals 10 mm. Stress-strain relation in compression was derived by assuming a stiffness equivalent to the stiffness of a layer of mortar 1 mm thick having a Young modulus derived from the mean measured compressive strength of concrete, Table 4-3. A bilinear behavior is assumed in the normal direction (see Figure 4-12) and a linear elastic relation is assumed in the shear direction. The normal stiffness in tension and the stiffness in shear direction were assumed almost equal to zero. For stableness of the analysis, horizontal displacements of one pair of nodes across the interface elements of support plates and loading plate were tied. The mechanical properties of the interface elements are summarized in Table 4-5.

Table 4-5: Case RB2. Interface properties

$K_{nn\ in\ tension}$ (N/mm^3)	$K_{nn\ in\ compression}$ (N/mm^3)	K_t (N/mm^3)
3.63×10^{-8}	$3.63\times10^{+4}$	3.63×10^{-8}

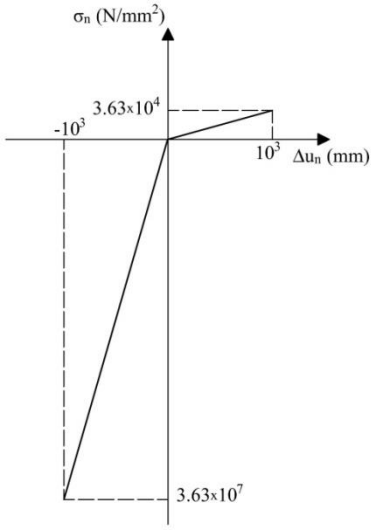

Figure 4-12: Case RB2. Traction-displacement diagram in normal direction for interfaces

Element types and finite element mesh

For the concrete 8-node membrane elements (CQ16M) are used for meshing the beam with a full Gauss integration scheme (3×3). The average element size is 25×30 mm^2.
The reinforcement bars are modelled with embedded truss elements with two Gauss integration points along the axis of the element. Perfect bond is assumed.
For the steel plates 8-node membrane elements (CQ16M) with a full Gauss integration scheme (3×3) are used.
The 6-node interfaces elements have three Lobatto integration points.
The adopted dimensions for the beam and for the transversal cross section of the beam are given in Figure 4-14 and Figure 4-3, respectively.

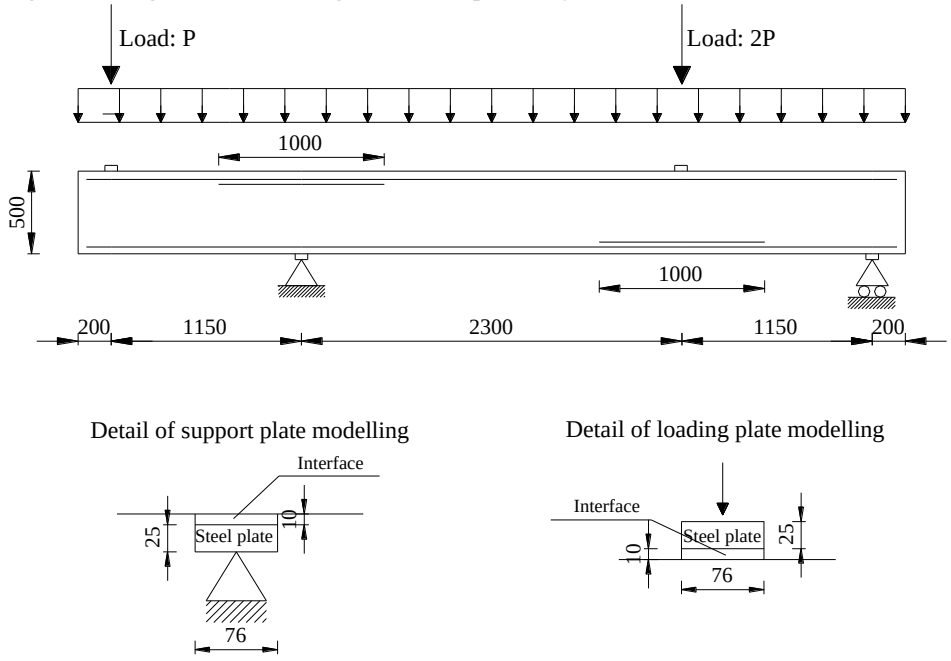

Figure 4-13: Case RB2. Dimensions adopted for the beam (in mm)

The mesh of the beam is presented in Figure 4-14(a). The different materials are indicated with different colors in Figure 4-14(b).

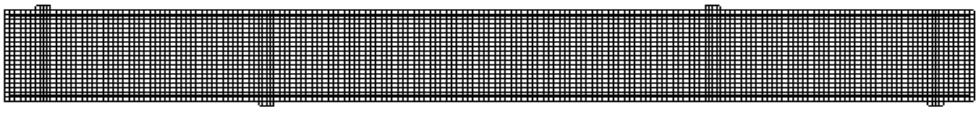

(a)

(b)

Figure 4-14: Case RB2. (a) Mesh and (b) material sets

Different groups of elements were defined to distinguish the concrete elements that can be subjected to cracking during the analysis and the steel elements that can yield during the analysis, Figure 4-15. These groups will be used in section 4.4 to monitor the failure mode during the analysis.

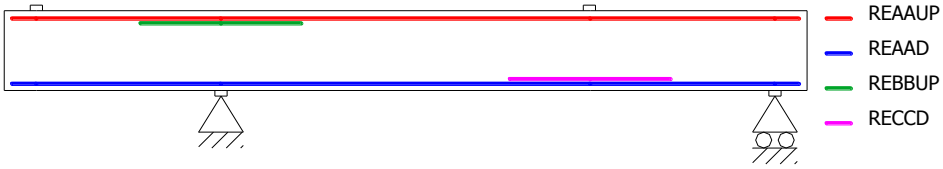

Figure 4-15: Case RB2. Groups of steel elements monitoring yielding

The internal stresses diagram, illustrated inFigure 4-8, shows that the entire beam is subjected to the maximum value of shear force, for this reason a group of concrete elements called SHEAR is used to monitor all the concrete elements of the beam which can be subjected to cracking, Figure 4-16.

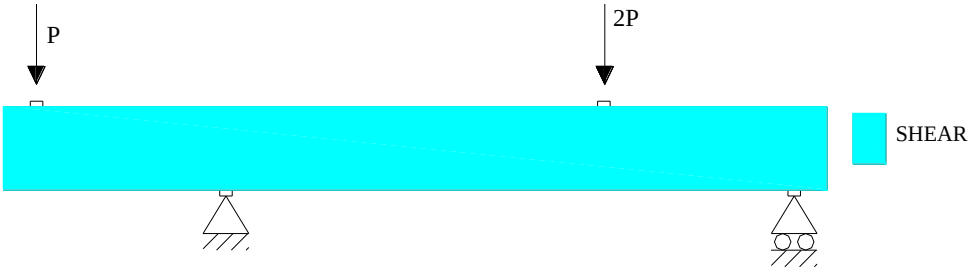

Figure 4-16: Case RB2. Groups of steel elements monitoring shear cracks

Boundary conditions and loading

The translations along x and y axes at a single node of the left steel plate (support 1) are constrained and the translation along y axis at a single node of the right steel plate (support 2) is constrained, Figure 4-17.

Dead load is applied in load case 1; load P and load $2P$ as a unit load of 1×10^3 N are added at load case 2 as concentrated loads applied at the middle node of the loading plates.

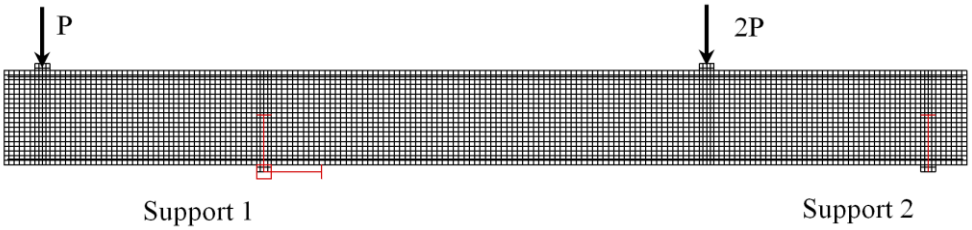

Figure 4-17: Case RB2. Boundary conditions and load case 2

Load increments and convergence criteria

Load case 1 is applied in a single step. The regular Newton-Raphson method with a maximum of 25 iterations is used. As convergence criteria, the norms of force and energy are selected. The analysis continues even if the convergence criteria are not satisfied. The convergence tolerance is equal to 5×10^{-2} for the case of force norm and 1×10^{-2} for the energy norm. A Line Search algorithm is used to improve the convergence performance.

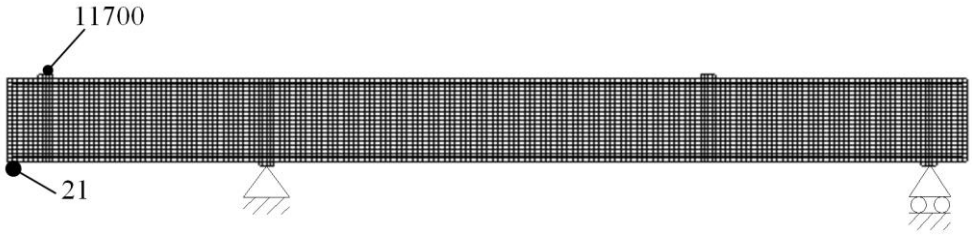

Figure 4-18: Case RB2. `Indirect Displacement control' technique applied referring to nodes 21 and 11700

Load case 2 is applied with automatic adaptive load increments based on energy. The initial load factor equals 5. The upper limit of the incremental load factor was set as 10 while the lower limit of the incremental load factor is equal to 0.5. The maximum number of steps is 150. The arc-length control was applied based on translation along y axis of nodes 21 and 11700 (“indirect displacement control”), Figure 4-18. The analysis continues even if the convergence criteria are not satisfied. The convergence tolerances are equal to 1×10^{-3} and 1×10^{-2} for energy and force, respectively. A maximum of 50 iterations is used. A Line Search algorithm is used to improve the convergence performance.

4.4 Nonlinear finite element analysis

Load deflection

The load-deflection curve is presented in Figure 4-19. The value of the peak load (step 74) is indicated with a marker. The deflection was measured for node 11700, Figure 4-18. From the outcome of the analysis, it is concluded that the beam failed in diagonal tension. This failure mechanism is typical for beams containing no shear reinforcement, is abrupt and follows shortly after formation of the major critical crack. After its formation, the crack propagates rapidly from the bottom to the top of the beams and continues as a large horizontal crack to the end of the beam. Due to a sudden and brittle nature of the shear failure, the beam displayed no ductility after the peak value

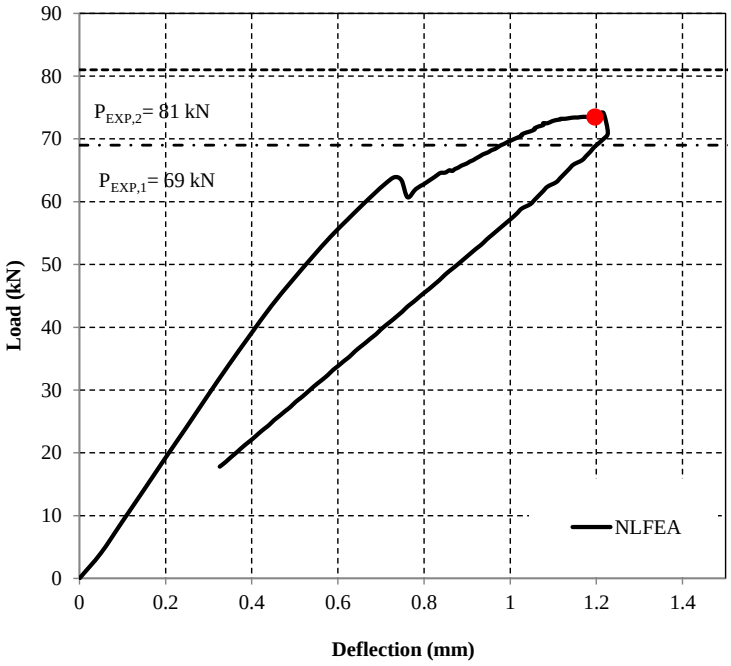

Figure 4-19: Case RB2. Load-deflection curves

Convergence behavior

For most steps convergence is achieved on the basis of the energy criterion, Figure 4-20 and Figure 4-21. For load case 2, the fixed convergence tolerances of energy norm is satisfied for the majority of the steps of the analysis preceding the peak load.The peak load is defined as the highest load step for which the energy norm ratio satisfies the fixed tolerance of 1×10^{-3} and it is marked Figure 4-20 and Figure 4-21 with a red dot. After step 74, for most of the steps, the analysis continues even if the energy and force convergence criteria are not satisfied within the maximum number of iterations equal to 50. The force norm ratio is higher than the fixed tolerance of 1×10^{-2} for most of the steps.

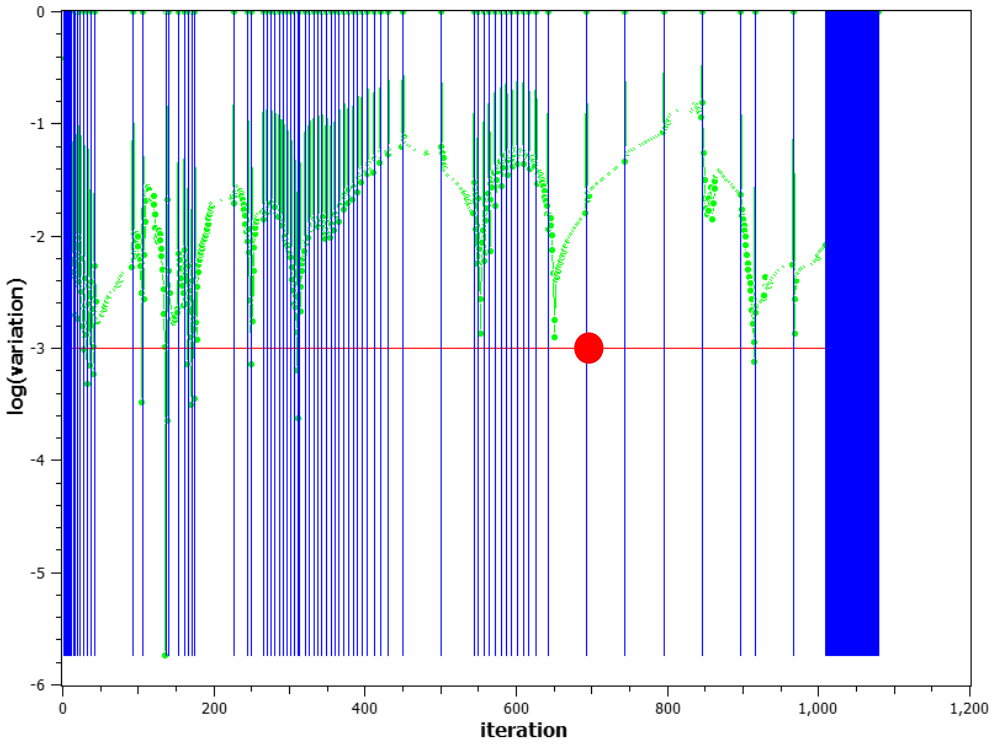

Figure 4-20: Case RB2. Evolution of the energy norm (blue lines indicate steps, red line indicates tolerance, green points indicate iterative results)

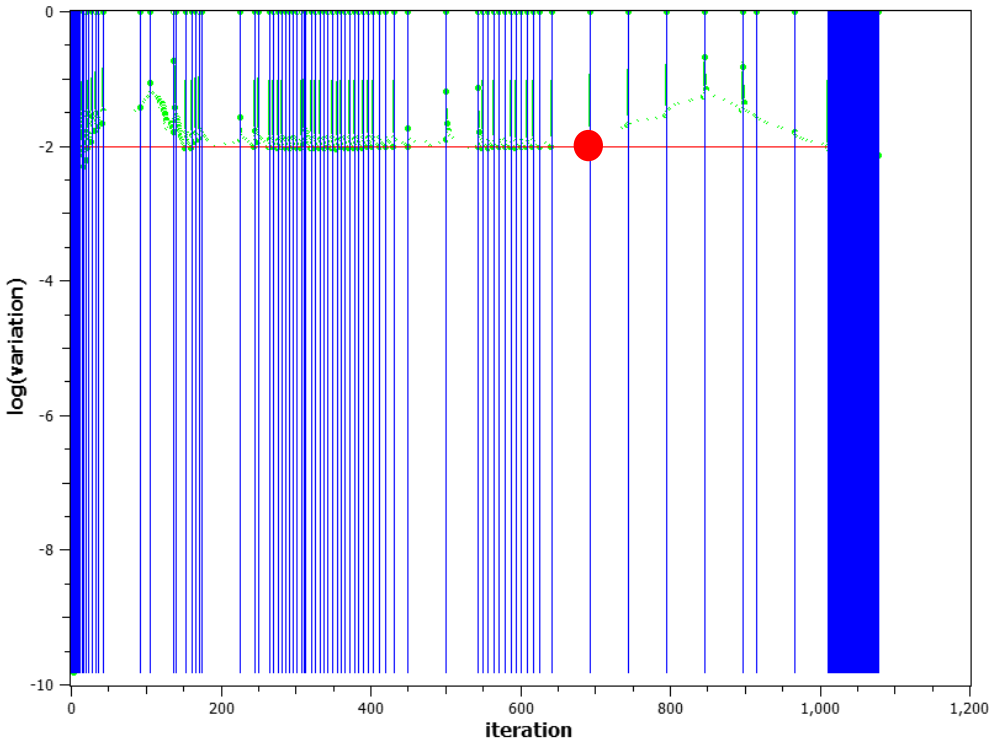

Figure 4-21: Case RB2. Evolution of the force norm (blue lines indicate steps, red line indicates tolerance, green points indicate iterative results)

Strains

Figure 4-22 shows the minimum principal strain values at the peak load (step 74, *P = 74.5 kN*). The minimum values of principal strain are higher than -3.5×10^{-3} because the shear failure was not accompanied by crushing of concrete in any element.

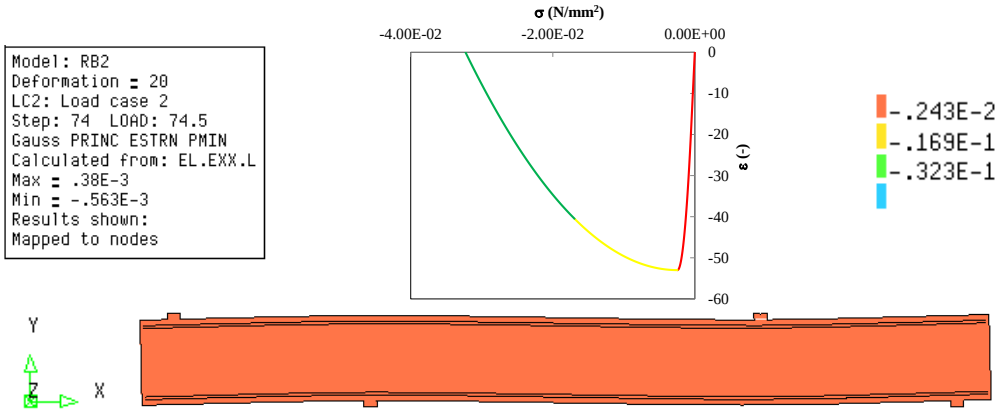

Figure 4-22: Case RB2. Minimum principal strain values at step 74 (*P=73.5 kN*)

Due to the fact that flexural failure is not the governing mechanism, strain values of reinforcing bars below 2.0×10^{-3} were noted, Figure 4-23.

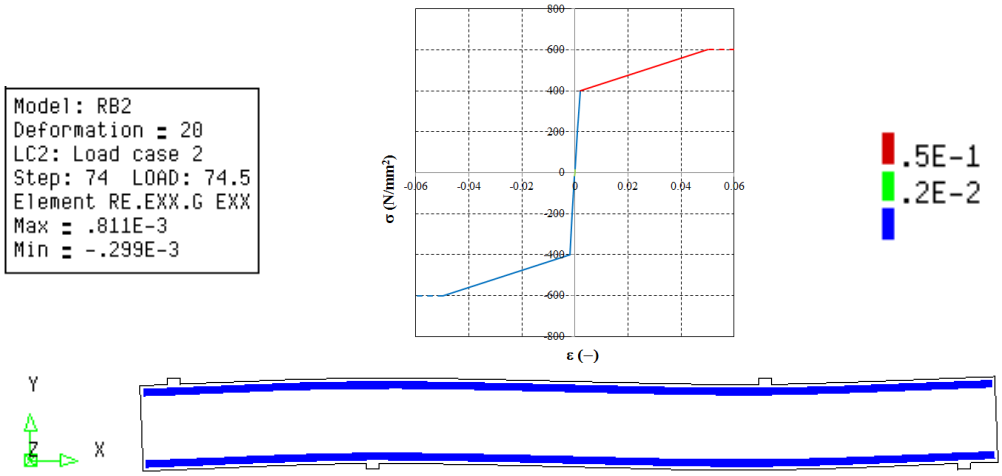

Figure 4-23: Case RB2. Strain values of reinforcing bars at step 74 (P=73.5 kN)

Figure 4-24 shows the crack strain values at the peak load. The crack strain values, reported in Figure 4-24, can be compared with the experimental crack pattern illustrated in Figure 4-5.
The first crack strain value plotted in Figure 4-24, equal to 9.9×10^{-4}, corresponds to the ultimate crack strain value calculated as $\varepsilon_{t,u} = \frac{G_F}{h \times f_{ctm}}$, while the third crack strain value, equal to 4.56×10^{-3}, is the crack strain value corresponding to a stress value equal to 1% of f_{ctm}. An intermediate crack strain value was added in the contour plot.
After the peak load the critical crack propagates rapidly and continues as a large horizontal crack towards the end of the beam, Figure 4-25.

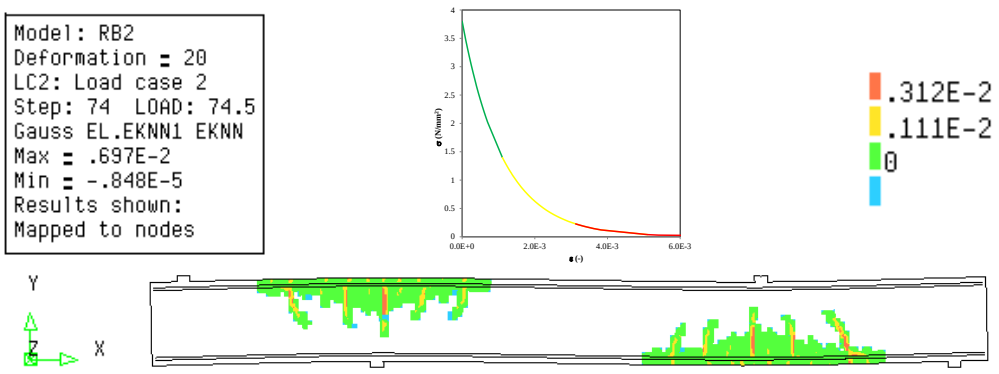

Figure 4-24: Case RB2. Crack strain values at step 74 (*P = 74.5 kN*)

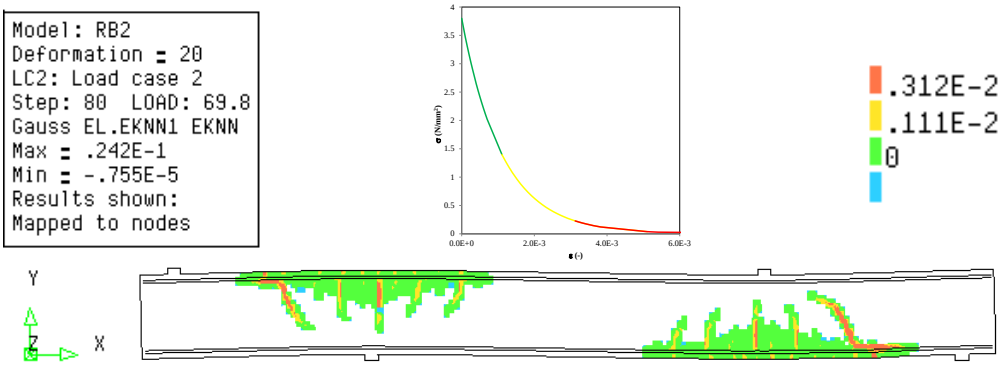

Figure 4-25: Case RB2. Crack strain values at step 80 (*P* = 68.8 *kN*)

Gauss point statistics

Table 4-6 lists the number of cracking points at step 74 (peak load) and at step 80 (post-peak behavior).

Table 4-6: Case RB2. Number of cracking points, crushing points, and yield points

PEAK LOAD						
STEP	**74**	**ITERATIONS**		15		
GROUP NAME	**PLAST**	**PRV. PL**	**CRITIC**	**PLAST NEW**	**PRV.PL NEW**	**CRITIC NEW**
TOTAL MODEL	0	0	0	0	0	0
CRACKING LOGGING SUMMARY						
GROUP NAME	**CRACK**	**OPEN**	**CLOSED**	**ACTIVE**	**INACTI**	**ARISES**
SHEAR	5232	5232	9	1291	3941	18
TOTAL MODEL	5232	5232	9	1291	3941	18
CUMULATIVE REACTION:						
FORCE X			**FORCE Y**			
-0.10431D-09			-0.23320D+06			
STEP	**80**	**ITERATIONS**		50		
GROUP NAME	**PLAST**	**PRV. PL**	**CRITIC**	**PLAST NEW**	**PRV.PL NEW**	**CRITIC NEW**
TOTAL MODEL	0	0	0	9	0	0

CRACKING LOGGING SUMMARY						
GROUP NAME	**CRACK**	**OPEN**	**CLOSED**	**ACTIVE**	**INACTI**	**ARISES**
SHEAR	5645	5632	13	676	4969	24
TOTAL MODEL	6832	6807	25	1520	5312	62
CUMULATIVE REACTION:						
FORCE X			**FORCE Y**			
-0.26268D-10			-0.21951D+06			

4.5 Application of Safety Formats Model Code 2010

The safety formats for non-linear finite element analyses as proposed by the Model Code 2010 (fib, 2013) comprise of the three numerical methods denoted as GRF (Global Resistance Factor method), PF (Partial Factor method) and ECOV (Method of Estimation of a Coefficient of Variation of resistance). In total this verification requires 4 non-linear analyses. In Table 4-7 and Table 4-8 the mechanical properties applied in the non-linear analyses are summarized.

Table 4-7: Case RB2. Constitutive model parameters for concrete

	f_c (N/mm^2)	f_{ct} (N/mm^2)	E_c (N/mm^2)	G_F (Nmm/mm^2)	G_C (Nmm/mm^2)
Mean measured	53.00	3.80	37485	0.149	37.293
Characteristic	45.00	2.66	35495	0.145	36.211
Mean GRF	38.25	3.41	33623	0.141	35.167
Design	30.00	1.77	31008	0.135	33.662
ν = variable for all the analyses starting with the value 0.2					

Table 4-8: Case RB2. Constitutive model parameters for reinforcing bars

	Φ (mm)	A_s (mm^2)	f_y (N/mm^2)	f_t (N/mm^2)	E_s (N/mm^2)	ε_{sy}
Mean measured	16	200	400.00	600.00	200000	0.00200
Characteristic	16	200	362.30	543.45	200000	0.00181
Mean GRF	16	200	398.53	597.79	200000	0.00199
Design	16	200	315.04	472.56	200000	0.00158

In Figure 4-26 the load-deflection curves obtained with mean measured, characteristic, mean GRF and design values of material strengths, calculated according to the Model Code 2010 (fib, 2013) are shown.
The peak loads are defined as the load of the highest load step for which the relative energy variation satisfies the convergence tolerance of 1×10^{-3} or as the highest load value when energy convergence tolerance of 1×10^{-3} is satisfied in the subsequent steps. The peak loads are indicated with dots in Figure 4-26.

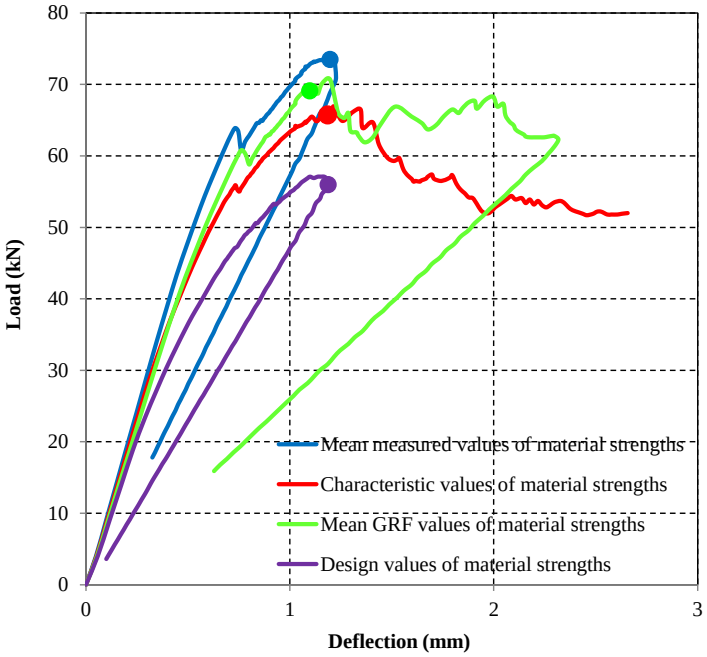

Figure 4-26: Case RB2. Load-deflection curves obtained with mean measured, characteristic, mean GRF and design values of material strengths

The specimen RB2 was analysed with sectional analysis and numerically with application of safety formats for NLFE analysis. In Figure 4-27, the comparison of the obtained design shear resistances is presented. The results are expressed in terms of a percentage of the average of the experimental ultimate applied loads.

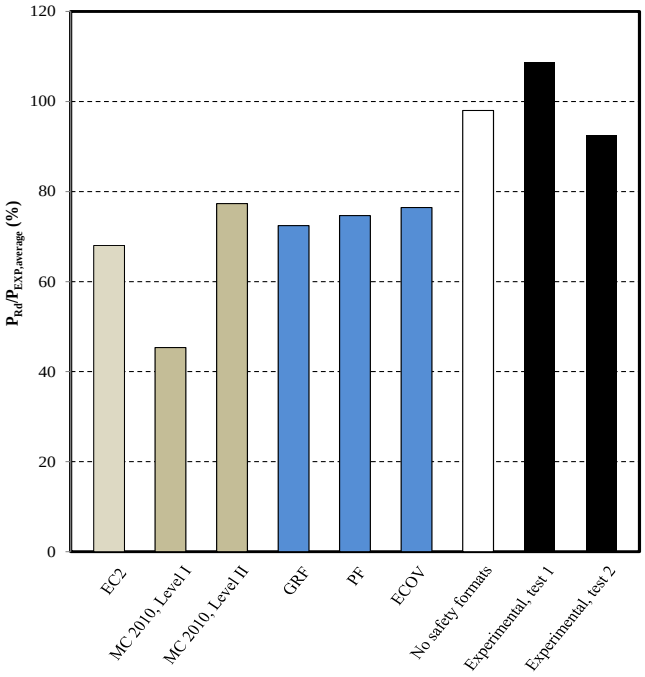

Figure 4-27: Case RB2. Analytical and numerical design values of beam resistance expressed in terms of a percentage of the average of the experimental ultimate values of applied load ($P_{Exp,average}$=75kN=100%)

In Table 4-9 the design values of beam resistances, expressed in terms of applied load P_{Rd}, obtained from numerical and analytical methods are reported. The analytical beam resistances were calculated with sectional analysis (see section 4.2) according to the Eurocode 2 (CEN, 2005) and the Model Code 2010 (fib, 2013).
From the comparison of the results it can be observed that the design values of beam resistance obtained with safety formats are higher than the values of shear resistance from sectional analysis. The exception constitutes the value of shear resistance calculated with the expressions of Level II Approximation. The reason for this discrepancy could be the particular layout of the rebars. Indeed, in the calculation of axial strain at mid-depth, as required by the procedure of Level II Approximation, the strain disturbance due to the additional four bars ϕ15, placed as the tensile reinforcement over the length of 1 m in the proximity of the section Sections B-B and C-C, cannot be considered. The crack patter shown in Figure 4-25 illustrates that NLFEA results are strongly dependent on the reinforcement layout. Consequently, it can be recognized as the reason why results of the NLFE analyses provide lower design values of the beam's shear resistance.

Table 4-9: Case RB2. Shear resistances expressed in terms of applied load P_{Rd}

$P_{Exp,1}$	$P_{Exp,2}$	Level I MC2010	Level II MC2010	EC2	GRF	PF	ECOV	No Safety Formats
(kN)	(kN)	(kN)	(kN)	(kN)	(kN)	(kN)	(kN)	(kN)
69	81	35.2	59	52	54	56	57	73

4.6 Parametric study on crack models

A parametric study was carried out by varying input parameters of the constitutive model, such as the crack model and the fracture energy of concrete in tension.
In Table 4-10 the material parameters used as the input in NLFE analyses carried out for the parametric study are tabularized. Analyses 1 to 3 refer to the three analyses carried out by varying the aforementioned material parameters. All the analyses were carried out considering mean measured values of material strengths. Parabolic law in compression and exponential law in tension were used for concrete, while an elasto-plastic law with hardening was adopted for steel. The analyses were carried out in load-control with the arc-length control. A variable Poisson ratio, reduced relative to the increasing crack strain, was adopted for all analyses.
For all analyses a limit value of the reduction of the compressive strength of concrete due to lateral cracking, equal to 0.6, was used.
The effects of the input value of the fracture energy of concrete in tension on the beam response was investigated by adopting the formulation of Model Code 1990 (CEB-FIP, 1993) and the formulation of Model Code 2010 (fib, 2013). The fracture energy of concrete in compression was considered for all analyses equal to $250G_F$ (Nakamura et al. 2001).
For the Total Strain fixed crack model, the aggregate size based shear retention was defined. According to this model, the shear stiffness of a crack diminishes together with opening of the crack until the value of the normal crack strain reaches the size of half the mean aggregate size. This implies loss of contact between crack planes. The linear decay of shear stiffness further depends on the crack bandwidth value *h*. The complete formulation is:

$$\beta = 1 - \left(\frac{2}{d_{aggr}} \right) \varepsilon_n h$$

In Table 6-2 the load-deflection curves obtained from the parametric study are plotted and the peak load of each analysis is indicated with a circular marker. The peak load is defined as the highest load step for which the relative energy variation satisfies the convergence tolerance of 1×10^{-3}. The peak load values are reported in Table 4-10.

Table 4-10: Case RB2. Data used for the parametric study

Analysis	Total strain crack model	Limit to β_σ	G_F	G_C	Peak load value (kN)
Analysis 1	rotating	0.6	MC2010	250 G_F	73
Analysis 2	rotating	0.6	MC1990	250 G_F	57
Analysis 3	fixed	0.6	MC2010	250 G_F	104

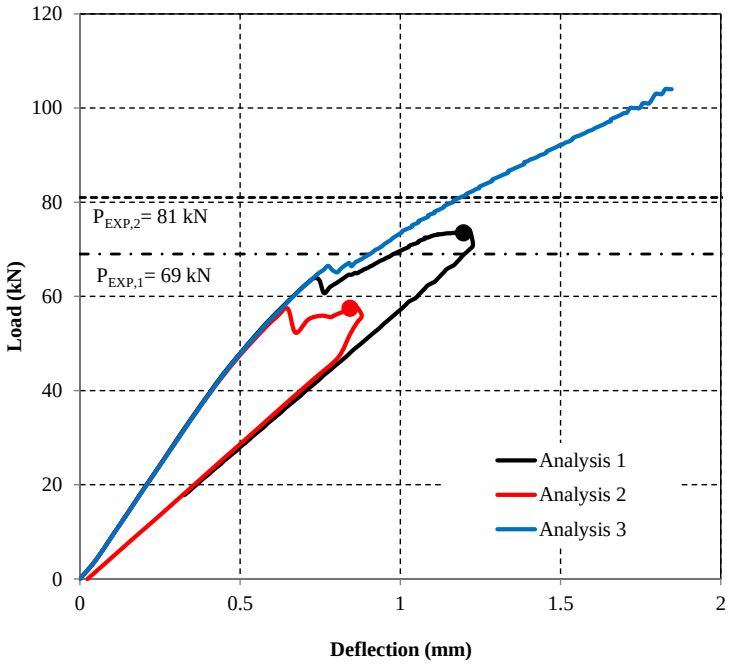

Figure 4-28: Case RB2 Load-deflection curves (Analysis 1 to 3)

The crack model and mechanical properties used in Analysis 1 were the same as those used to predict the design value of beam resistance from NLFE analyses. As expected, since the beam fails due to diagonal-tension, the results of NLFE analyses are considerably dependent on the crack model and the value of the fracture energy of concrete in tension.

4.7 Parametric study on crack bandwidth

This section reports on (*i*) the sensitivity of analyses results on h, or actually G_F/h and (*ii*) on post-analysis checks on the correctness of the a priori estimates for *h*.
Material models and parameters, element types and finite element mesh, boundary conditions and loading, load increments and convergence criteria are the same as those used for the analysis carried out with mean measured material strength (please refer to paragraphs 4.3).
Table 4-11 lists the *a priori* estimates for the crack bandwidth that are used in this study. Note that the compressive bandwidths h_C are unaltered. For practical reasons the variations of the crack bandwidths *h* were implemented in the finite element models as

variations of G_F. The exponential softening employed in the total strain crack models is formulated as explained in Chapter 3 – Case RB1. In Table 4-11, the values of fracture energy of concrete in tension used as the input data for the analyses and maximum crack strain values used in the contour plot are depicted. The following Table 4-12 gives an overview of the obtained peak loads P_u.

Table 4-11: Case RB2. Estimates for the crack bandwidth h for quadratic plane stress quadrilaterals with 3×3 Gaussian integration

	Tension (mm)	**Compression (mm)**	G_F **(Nmm/mm^2)**	G_C **(Nmm/mm^2)**	$\varepsilon_{knn,max}$
Short-width	$h = ½\sqrt{A}\sqrt{2} = 13\sqrt{2}$	$h_c = \sqrt{A} = 28$	0.149	37.29	9.12×10^{-3}
Default	$h = \sqrt{A}\sqrt{2} = 26\sqrt{2}$	$h_c = \sqrt{A} = 28$	0.149	37.29	4.56×10^{-3}
Long-width	$h = 2\sqrt{A}\sqrt{2} = 80\sqrt{2}$	$h_c = \sqrt{A} = 28$	0.149	37.29	2.28×10^{-3}

Table 4-12: Case RB2. Case studies and modifications

$P_{Exp,1}$ **(kN)**	$P_{Exp,2}$ **(kN)**	P_u **(kN)**		
		0.5*h*	***h***	**2*h***
69	81	93	73	55

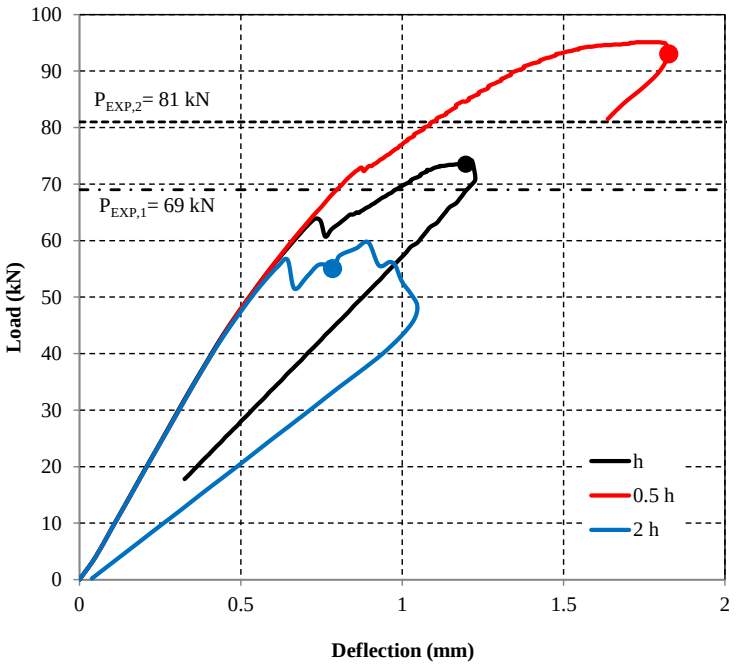

Figure 4-29: Case RB2. Load-deflection curves obtained with different crack bandwidth values

Figure 4-29 shows the load-deflection curves for case RB2 obtained with different crack bandwidth values. In contrast to Case RB1, the three peak values obtained from load-deflection curves in Figure 3-34 are clearly different. The three peak values show a comprehensible trend, with the "0.5*h*" peak load above the "*h*" peak load, and with the "*h*" peak load above the "2*h*" peak load. Again, the differences in the post peak ehavior are hard to explain, but might be related to the control procedure and the convergence behavior.

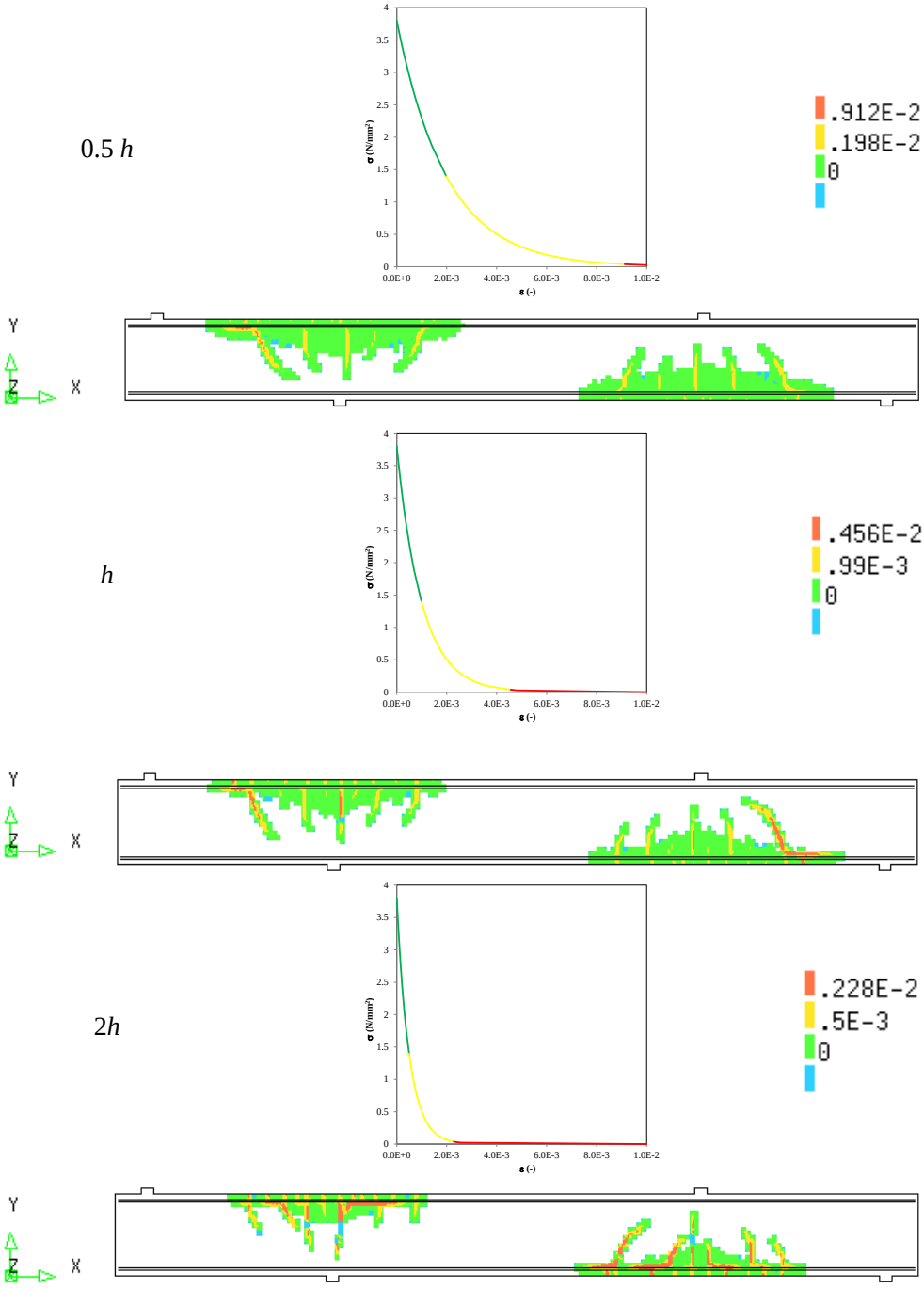

Figure 4-30: Case RB2. Maximum principal strain values obtained with varying crack bandwidth values

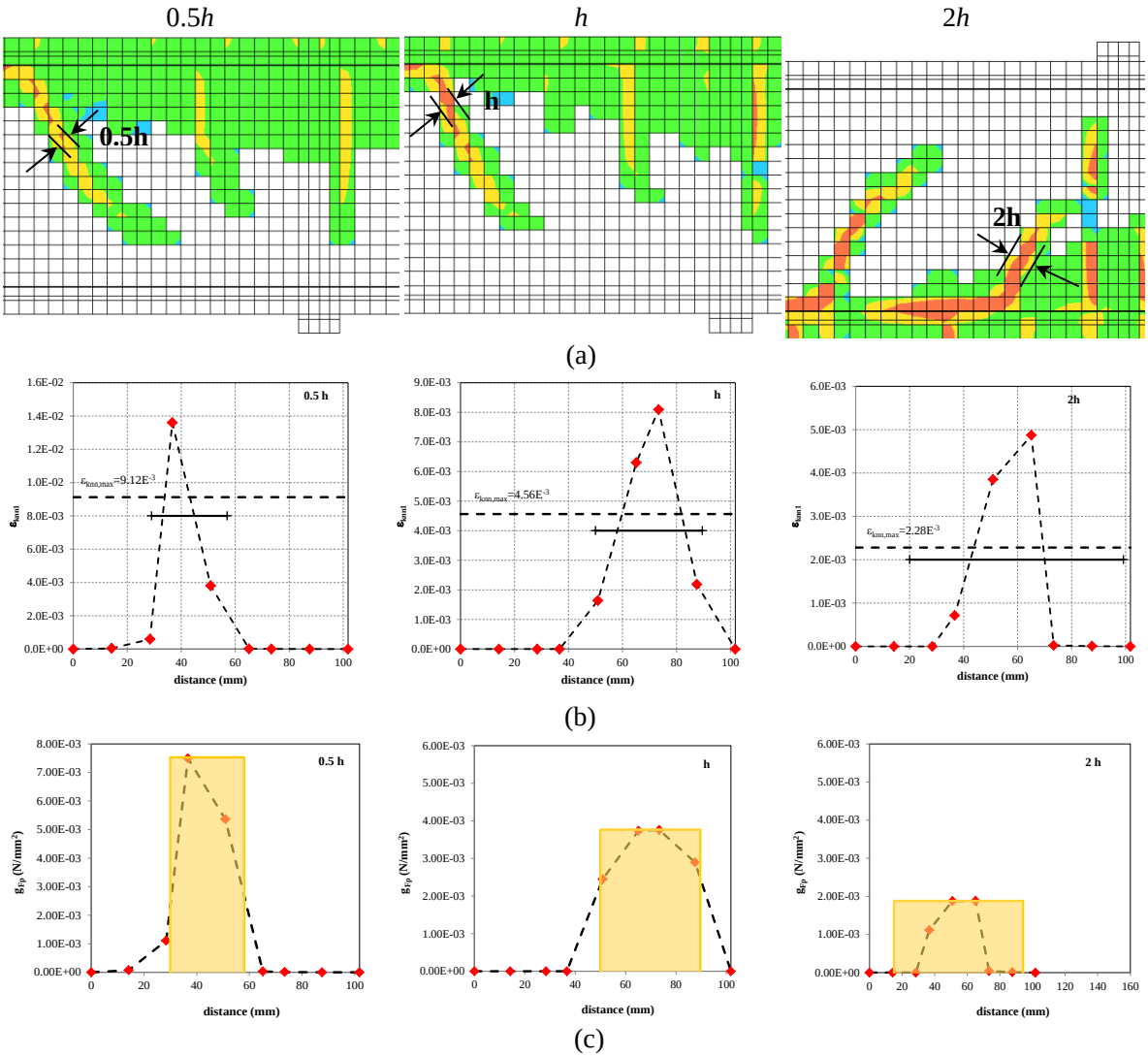

Figure 4-31: Case RB2. (a) Maximum principal strains (b) Maximum principal strain-distance between integration points along the lines indicated above. The ultimate strain value (red dashed line) (c) Fracture energy over crack bandwidth-distance between integration points

Figure 4-30 shows contour plots of the crack strain values some steps after the corresponding peak values of the applied loads, obtained with different crack bandwidth values. In the contour plots the color ranges are adjusted to the (tensile) stress-strain relations: red denotes strains beyond the ultimate crack strain of the softening stress-strain diagram. For a better assessment of the strain localization, Figure 4-31 magnifies the regions in the proximity of the location of the critical cracks depicted in Figure 4-30 to indicate the mesh and the *a priori* estimates for *h*.

The dissipated fracture energy divided by the crack bandwidth (g_F) is plotted against the distance between the subsequent integration points along the line perpendicular to the crack plane. In all graphs, 9 integration points are taken into account.

The values of dissipated fracture energy in tension are calculated for different values of crack bandwidth in Figure 4-31(c). From Figure 4-31(c) the *a posteriori* crack bandwidths can be evaluated as the length characterized by the maximum dissipated fracture energy of concrete in tension, that means the length characterized by principal strains higher than the ultimate crack strain in tension, $\varepsilon_{knn,max}$.

Remarkably, Figure 4-31(c) shows that by comparing the *a priori* crack bandwidths with the obtained *a posteriori* crack bandwidths, the results obtained with an *a priori* crack bandwidths of 2*h* provide an estimation which is too wide.

4.8 Parametric study of convergence criteria

A sensitivity study was carried out with respect to (*i*) the convergence criteria and (*ii*) the maximum number of iterations, Table 4-13. Mean measured values of the material parameters are used in this sensitivity study, material model and parameters are explained in section 4.3.

Table 4-13: Case RB2. Case studies and modifications

Case study	RB2
Compression model	Parabolic, medium G_C
Control	Load control with arc length
Max. number of iterat.	50-100

Table 4-14 presents the values for the fracture energy of concrete in compression and in tension. For a "medium" value of fracture energy of concrete in compression the ratio G_C/G_F equals 250. The fracture energy of concrete in tension G_F was calculated with Model Code 2010 (fib, 2013).

Table 4-14: Case RB2. Values for the fracture energy of concrete in compression G_C

medium G_C (Nmm/mm^2)	**G_F (Nmm/mm^2)**
37.29	0.149

Table 4-15 gives an overview of all analyses which were performed to determine the sensitivity of the results on variations in the convergence criteria. The total of six analyses was carried out:

- 3 different type of criteria: displacement (D), energy (E) and force (F)
- 2 levels of convergence tolerances ε: strict (1) and relatively loose (2)

The analyses were carried out in load control with arc-length method.

As a main NLFEA result, the Table 4-15 presents the peak value of applied load P_u. Peak load values are identified as the last load step values which satisfied the convergence criterion within the maximum number of iterations.

Table 4-15: Case RB2. Overview of NLFE analyses using load control and obtained peak values of the applied load P_u, ($P_{Exp,1}$ = 69kN and $P_{Exp,1}$ = 81kN)

Comp. model	Criterion	Analysis label	tolerance strict	P_u (kN)	Analysis label	tolerance loose	P_u (kN)
Medium G_C	displacement	DA1M	1×10^{-2}	69	DA2M	5×10^{-2}	74
	energy	EA1M	1×10^{-3}	65	EA2M	5×10^{-3}	71
	energy (100 ite)	EA1M100	1×10^{-3}	76			
	force	FA1M	1×10^{-2}	73	FA2M	5×10^{-2}	81

In the following the analyses results are presented by means of load-deflection graphs. For case RB2 a force criterion with a loose tolerance is not consistent with the other results. Consequently, this criterion should be excluded from considerations. It is

important to take into account that beam RB2 is a particular case because of its special reinforcement layout and the associated failure mode.

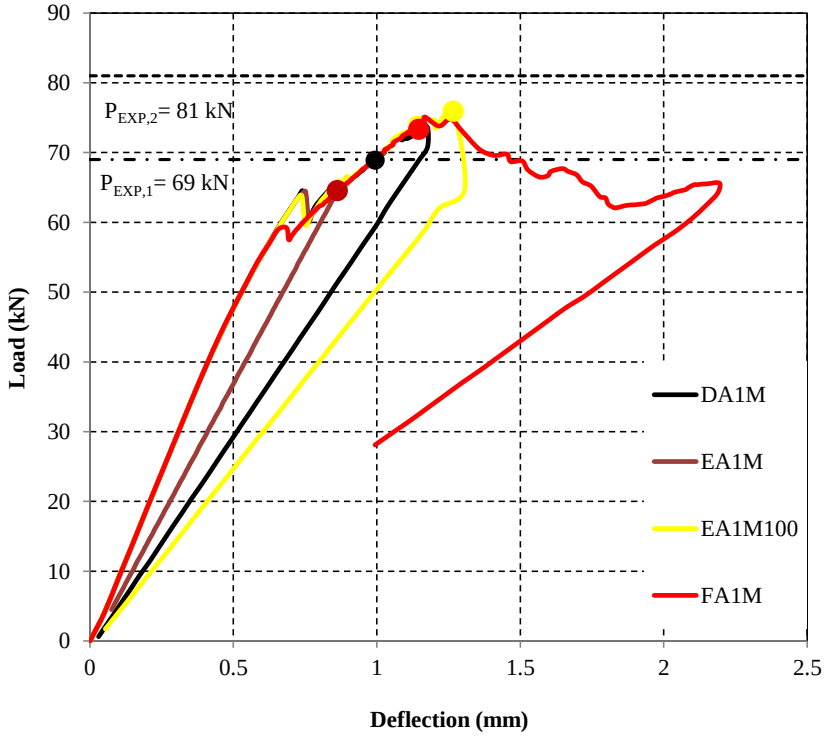

Figure 4-32: Case RB2. Load deflection curves with varying the convergence criteria

4.9 Concluding remarks

Beam RB2, tested by Collins and Kuchma (Collins & Kuchma, 1999), simulates the loading condition of continuous beams thus with regions influenced by high shear force in combination with substantial bending moment. The beam does not contain stirrups and fails due to shear in a brittle manner.

From the analytical calculations based on sectional analysis it was demonstrated that shear failure is the governing mechanism. The value of shear force corresponding to the design value of moment resistance is higher than the design value of resistance to shear force. The design shear resistance evaluated with the Eurocode 2 (CEN, 2005) is equal to P_{Rd} =51 kN, whereas the design shear resistances calculated with the Model Code 2010 (fib, 2013) are P_{Rd}=34 kN and P_{Rd}=58 kN for levels of approximation I and II respectively.

The beam was modeled with 8-node membrane elements for the concrete and embedded truss elements for the reinforcement. Perfect bond was assumed. The concrete model was based on a total strain rotating crack model with exponential softening in tension and parabolic behavior in compression. Moreover, a variable Poisson's ratio of concrete and reduction of compressive strength of concrete due to lateral cracking with a lower limit of 0.6 were adopted. The fracture energy of concrete in tension, calculated according to the Model Code 2010 (fib, 2013), was reduced by a factor equal to $\sqrt{2}$ to take into account the effect of crack orientation. The model for the reinforcement bars was based on hardening plasticity.

The governing failure mechanism resulting from NLFEA is diagonal-tension shear. This type of failure mode is typical for beams with no shear reinforcement, is abrupt, and occurs shortly after the formation of a "critical diagonal-tension crack".

Safety formats for non-linear finite element analyses as introduced by the Model Code 2010 (fib, 2013) were used in order to compute the design value of beam shear

resistance. The resulting resistances were expressed in terms of applied load and compared with experimental values and the analytical solution. The maximum design values of beam resistance obtained from safety formats equals to 57 kN. This value is higher than the design value of beam resistance obtained from Eurocode 2 and Level I of Approximation. The design shear resistance obtained with Level II Approximation is slightly higher than the values obtained with safety formats.

Since the beam failed due to diagonal tension, failure mode and ultimate shear resistance are heavily dependent on the crack model, concrete tensile strength and tensile fracture energy. At the same time, it can be concluded that the reduction of compressive strength of concrete due to lateral cracking and the Poisson's ratio are not very impactful on the results of NLFE analyses – both in terms of peak value of applied load as well as the obtained failure mode.

In the current study, two sensitivity studies were conducted. In the first study the varying parameter was the crack bandwidth. The values of the crack bandwidth ranged: 0.5h, h, 2h. From the resulting load-deflection curves it was deduced that the peak values decrease as the crack bandwidth values increase. By comparing the *a priori* crack bandwidths (based on integration schemes) with the obtained *a posteriori* crack bandwidths, is possible to conclude that a crack bandwidth value equal to 2h is excessive.

Another sensitivity study was carried out with respect to (*i*) the control procedure and (*ii*) the maximum number of iterations. The performance of the model of RB2 with a force convergence norm including a loose convergence tolerance is not consistent with the other results therefore this criterion should be disregarded. It is important to take into account that beam RB2 is a particular case due to its special reinforcement layout and the way it fails.

5 Case RB3: Grace (2001)

The experimental program of Grace (Grace, 2001) studied the effect of strengthening using fiber-reinforced polymer strips. The control beam of the so-called category II beams from this program is used as a case study.

5.1 Experimental setup and results

Geometry

The geometry of the beam and reinforcement is shown Figure 5-1and Figure 5-2. The beam has a total length of 8.230 m, a depth of 0.457 m, and a width of 0.250 m. The dimensions of the loading and support plates are not given; it is assumed that the dimensions are 0.22×0.10×0.25 m^3.

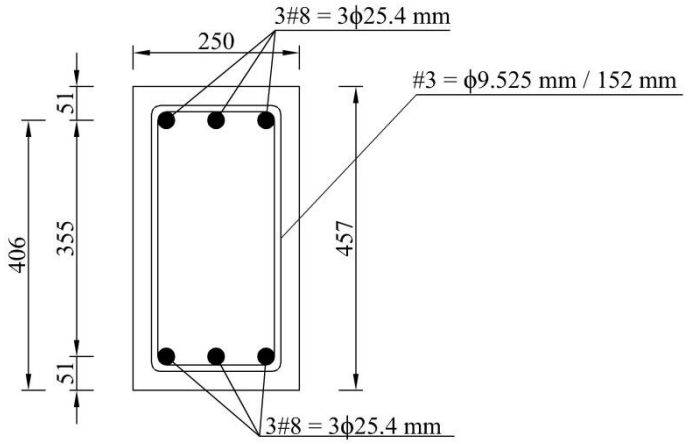

Figure 5-1: Case RB3. Cross section details (dimensions in mm)

The beam is reinforced with three #8 bars (Φ=25.4 mm) at the top and the bottom and #3 (Φ=9.525 mm) stirrups with a spacing of 152 mm. The concrete cover equals to 51 mm and the effective depth to main tension reinforcement equals to 406 mm.

Material Properties

The concrete and reinforcement properties, given in (Grace, 2001), are listed in Table 5-1.

Table 5-1: Case RB3. Concrete and reinforcement properties

Concrete properties					
	f_{cm} (N/mm^2)			d_{max} (mm)	
	31.2			19.0	
Reinforcement properties					
Bar	Φ (mm)	A_s (mm^2)	E_s (N/mm^2)	f_{ym} (N/mm^2)	f_{tm} (N/mm^2)
#3	9.525	71.25	200000	414	-
#8	25.4	506.70	200000	414	-

Loading and Boundary Conditions

The loading and boundary conditions in the experimental setup are show in Figure 5-2. It is not clear from the reference how the end support was constructed. It is assumed that the top and bottom of the beam is supported at the right-hand-side.

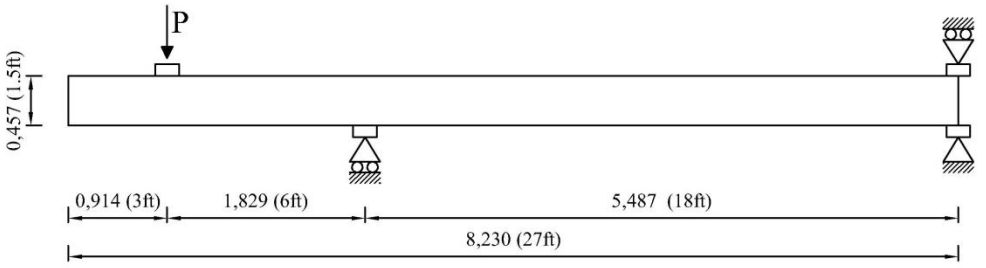

Figure 5-2: Case RB3. Loading and boundary conditions (dimensions in mm)

Experimental Results

The beam exhibited a flexural failure mode, Figure 5-3. The experimental ultimate value of applied load was equal to P_{Exp} = 141.9 kN.

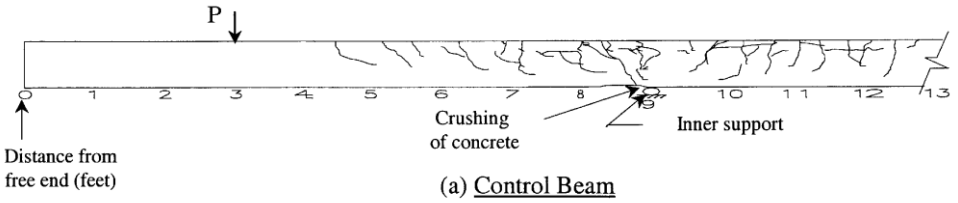

Figure 5-3: Case RB3. Failure mechanisms at experimental ultimate value of applied load (Grace 2001)

5.2 Analytical analysis

In Figure 5-4 the load configuration at failure is shown. The distributed load representing the beam weight is equal to $q = 0.25m \times 0.457m \times 25\,kN/m^3 = 2.856\,kN/m$.

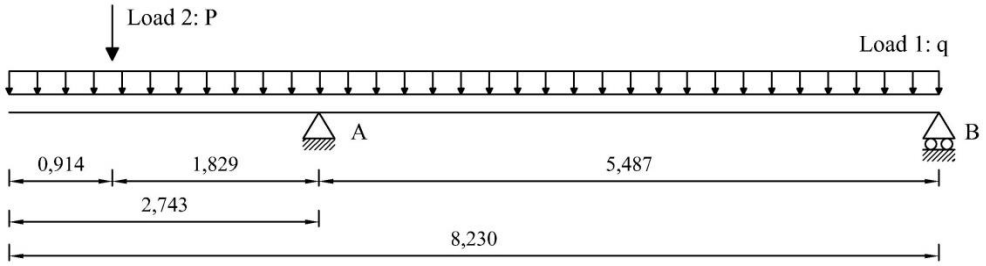

Figure 5-4: Case RB3. Load configuration (dimension in m)

Load case 1

Figure 5-5 shows that the maximum negative value of applied moment at the support A is equal to:

$$M^{-}_{E,A} = -2.856kN/m \times \frac{(2.743m)^2}{2} = 10.74\,kNm$$

and the value of applied shear force at support A is equal to:

$$V_{E,A,dx} = \frac{5.487m}{2} q + \frac{(2.743m)^2}{2} \times \frac{1}{5.487m} q = 9.794kN$$

$$V_{E,A,sx} = -2.856\,kN/m \times 2.743m = -7.83kN$$

The value of shear force at support B equals

$$V_{E,B} = -\frac{5.487m}{2}q + \frac{(2.743m)^2}{2} \times \frac{1}{5.487m}q = -5.877\ kN$$

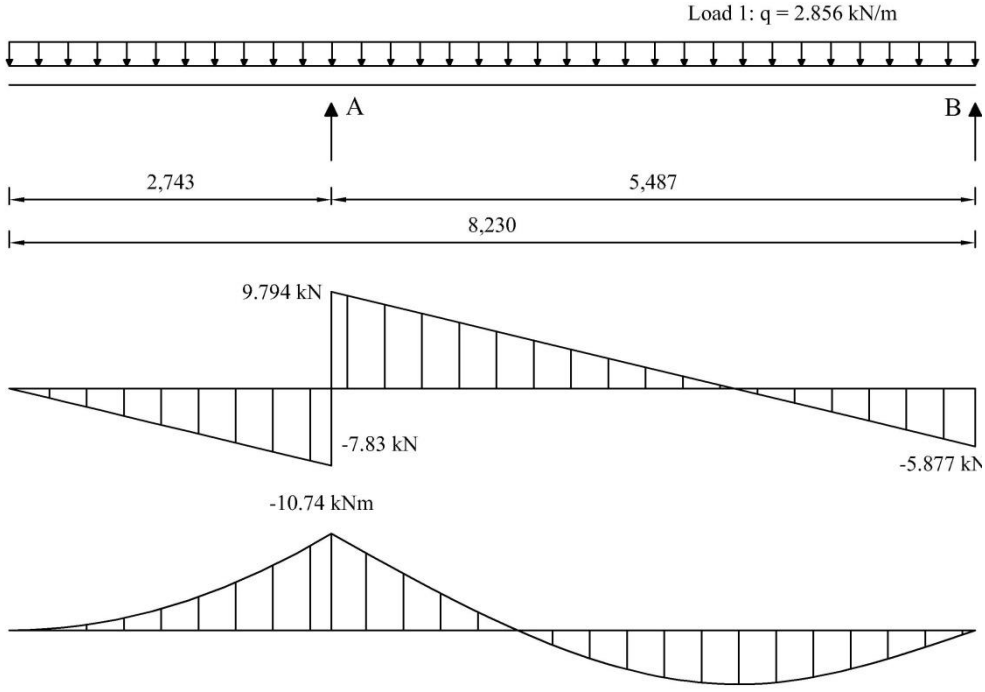

Figure 5-5: Case RB3. Load 1: Internal forces

Load case 2

The experimental ultimate value of applied load is equal to $P_{Exp} = 141.9kN$. Figure 5-6 shows that the minimum value of applied moment at the support A is equal to $M_{E,A}^{-} = -141.9kN \times 1.829m = -259.5\,kNm$ and the values of applied shear force at supports A and B are equal to $V_{E,A,sx} = -141.9\,kN$ and $V_{E,B} = 47.3\,kN$, respectively.

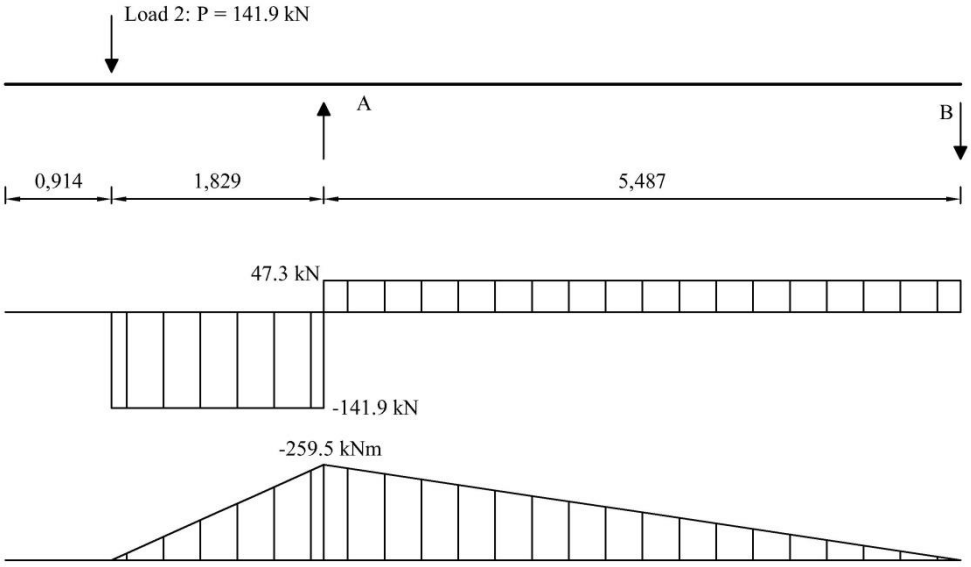

Figure 5-6: Case RB3. Load 2: Internal forces

Load 1 + Load 2

At failure the minimum value of applied moment is equal to $M^{-}_{E,A} = -259.5kNm - 10.74kNm = -270.24\ kNm$ and the minimum value of applied shear force equals to $V_{E,A,sx} = -141.9kN - 7.83kN = -149.73kN$

The design value of resistance moment is evaluated with sectional analysis by assuming that:

- tensile strength of concrete is ignored,
- the compressive stresses in concrete are derived from parabola-rectangle relation,
- the stresses in reinforcing steel are derived from elastic-plastic relation with hardening,
- partial safety factor for the mechanical properties of reinforcing steel equals $\gamma_s=1.15$ for concrete material properties equals $\gamma_c=1.5$.

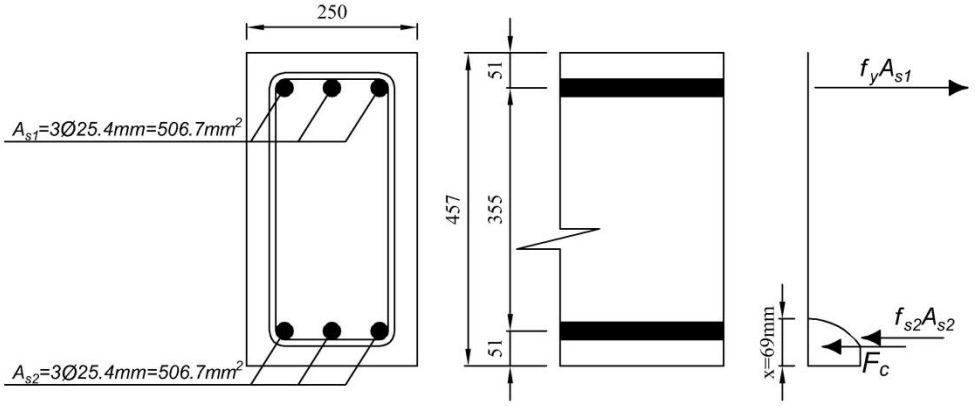

Figure 5-7: Case RB3. Stress block for determination of the design moment resistance

The design moment resistance is calculated assuming that the tensile reinforcement reaches the yield strain whereas the bottom reinforcement remains in the elastic strain range. For these assumptions, the height of the compression zone is calculated from the horizontal force equilibrium as follows:

$$A_{s1} f_{yd} - A_{s2}\left(\frac{x-a_2}{x}\right)\varepsilon_{cu2}E_s - 0.8095xbf_{cd} = 0 \rightarrow x = 69mm$$

Verification of the assumption for the calculated value of x:

$$\varepsilon_{s1} = \frac{\varepsilon_{cu2}(d_1 - x)}{x} = \frac{0.0035(459mm - 74mm)}{74mm} = 0.018 \rightarrow steel\ yields$$

$$\varepsilon_{s2} = \frac{\varepsilon_{cu2}(x - a_2)}{x} = \frac{0.0035(74mm - 41mm)}{74mm} = 1.561 \cdot 10^{-3} \rightarrow steel\ does\ not\ yield$$

therefore the assumptions hold.

The design value of the moment resistance in calculated around the centre of the compression zone $0.416x$:

$$M_{Rd} = A_{s1} f_{yd}(d_1 - 0.416x) + A_{s2}\varepsilon_{s2}E_s(0.416x - a_2) = 180.84kNm$$

The value of applied moment equal to

$$M^{-}_{E,A} = -q\frac{(2.743m)^2}{2} - 1.829m \times P = -180.84\ kNm$$

which after transformations leads to the maximum value of the applied load:

$$P_{Ed} = -q\frac{(2.743m)^2}{2 \cdot 1.829m} + \frac{180.84kNm}{1.829m} = 98.87\ kN\ .$$

The shear force resistance attributed to steel and crushing of concrete for the permitted range of the angle of inclination of compressive struts is presented in Figure 5-8.

The design value of shear resistance is equal to
$V_{Rd} = 270.57\ kN$.
The design shear resistance attributed to concrete is evaluated as follows:

$$V_{Rd,c} = 0.9 d b_w \alpha_c \nu_1 f_{cd} \frac{(\cot\alpha + \cot\theta)}{1+\cot^2\theta} =$$

$$= 0.9 \times 406mm \times 250mm \times 1 \times 0.6 \times \left(1 - \frac{23.2}{250}\right) \times 15.47MPa \frac{(0+2.43)}{1+2.43^2} = 270.57kN$$

while the design shear resistance provided by stirrups is:

$$V_{Rds} = 0.9 d \frac{A_{sw}}{s} f_{yd} (\cot\alpha + \cot\theta) \sin\alpha =$$

$$= 0.9 \times 406mm \times \frac{142mm^2}{152mm} \times 326.07MPa \times (0+2.43) \times 1 = 270.57kN$$

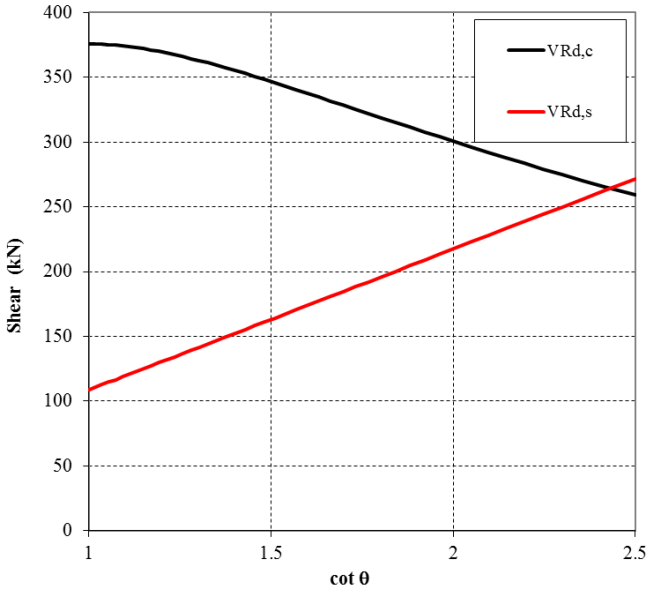

Figure 5-8: Case RB3. Shear resistance

The value of applied shear force corresponding to the bending capacity (equal to 98.87 kN) is lower than the design value of shear resistance (equal to 270.57 – 7.835 = 262.73 kN). As a result, according to the sectional analysis, the beam fails in bending. In Table 5-2 the design value of beam resistance expressed in terms of applied load P_{Rd} obtained with Eurocode 2 (CEN, 2005) is highlighted.

Table 5-2: Case RB3. Design value of beam resistance expressed in terms of applied load P_{Rd}

P_{Rd} (EC2) (kN)
98.87

5.3 Finite element model

Units

Units are N, m.

Material models and parameters

The concrete model is based on a total strain rotating crack model with

- exponential softening in tension and parabolic behavior in compression,
- variable Poisson's ratio of concrete dependent on crack strain values,
- reduction of compressive strength of concrete due to lateral cracking with a lower limit of 0.6 according to (Vecchio, 1986),
- increase in compressive strength due to lateral confinement according to the model proposed by Selby and Vecchio (Selby and Vecchio 1993).

The mechanical properties of concrete are summarized in Table 5-3. The uniaxial stress - strain curve is shown in Figure 5-9. In the input file of the analysis, the G_F value has been decreased with a factor $\sqrt{2}$ in order to compensate for an underestimation of the crack band width for cracks with an inclination angle of 45 degrees $G_{F,reduced} = 0.136/\sqrt{2} = 0.096$.

Table 5-3: Case RB3. Constitutive model parameters for concrete

	f_{cm} (N/mm^2)	f_{ctm} (N/mm^2)	E_c (N/mm^2)	ν	G_F (Nmm/mm^2)	G_C (Nmm/mm^2)
Mean measured values	31.20	2.44*	31297*	Var**	0.136*	33.90*

* Not specified in reference; estimated according to MC2010 (fib, 2013)
** Variable –reduced with the initial value of 0.15

The model for the reinforcement bars and stirrups is based on hardening plasticity. Geometrical and mechanical features of reinforcement are summarized in Table 5-1. The stress-strain curve of the #8 bars is plotted in Figure 5-10.

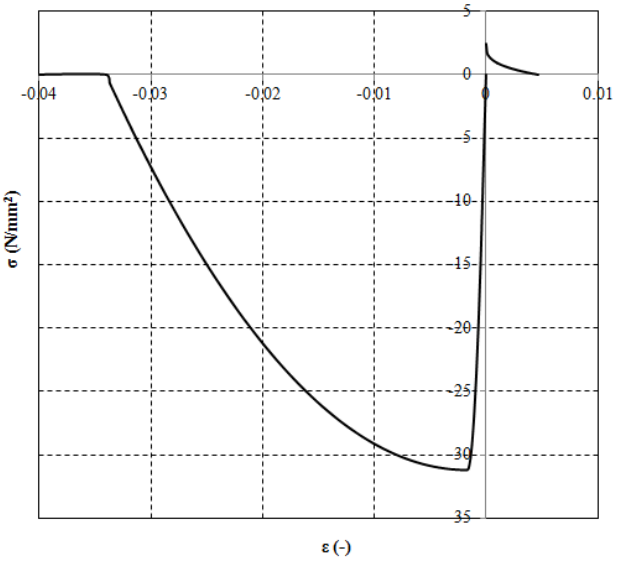

Figure 5-9: Case RB3. Stress-strain curve for concrete

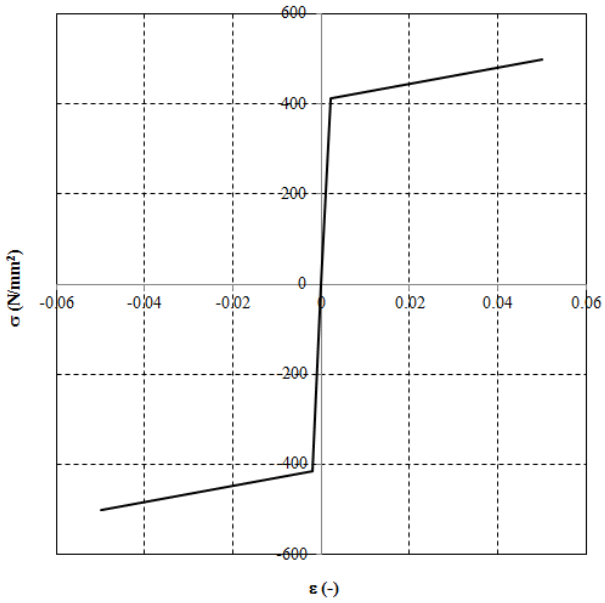

Figure 5-10: Case RB3. Stress-strain curve adopted for #8 bars

Table 5-4: Case RB3. Steel plates properties

E (N/mm^2)	ν
200000	0.3

For the steel plates a linear elastic behavior is assumed, see Table 5-4.
Interface elements were used between the steel plates and the concrete beam at the supports and the location of applied loading.
The thickness of interface elements equals 10 mm. Stress-strain relation in compression was determined by assuming stiffness equivalent to the stiffness of a layer of mortar 1 mm thick having a Young's modulus derived from the mean measured compressive strength of concrete as shown in Table 5-3. A bilinear behavior is assumed in the normal direction (see Figure 5-11) whereas for the shear direction the relation is linear elastic. The normal stiffness in tension and the stiffness in shear direction were assumed almost equal to zero. For stableness of the analysis, horizontal displacements of one pair of nodes across the interface elements of support plates and loading plate were tied. The mechanical characteristics of the interface elements are summarized in Table 5-5.

Table 5-5: Case RB3. Interface properties

$K_{nn\ in\ tension}$ (N/mm^3)	$K_{nn\ in\ compression}$ (N/mm^3)	K_t (N/mm^3)
3.13×10^{-8}	$3.13\times10^{+4}$	3.13×10^{-8}

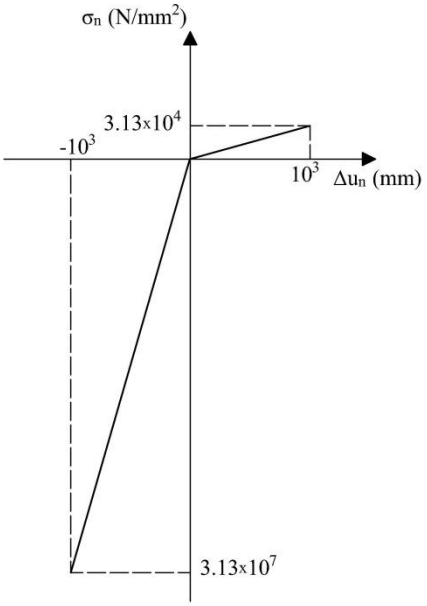

Figure 5-11: Case RB3. Traction-displacement diagram in normal direction for interfaces

Element types and finite element mesh

For meshing the concrete, 8-node membrane elements (CQ16M) with a full Gauss integration scheme (3×3) are used. The average element size is 50 mm. The reinforcement bars and stirrups are modelled with embedded truss elements with two Gauss integration points along the axis of the element. Perfect bond is assumed.
For the steel plates 8-node membrane elements (CQ16M) with a full Gauss integration scheme (3×3) are used. The 6-node interfaces element have three Lobatto integration points. The adopted dimensions for the beam and for the transversal cross section of the beam are given in Figure 5-12 and Figure 5-1, respectively.

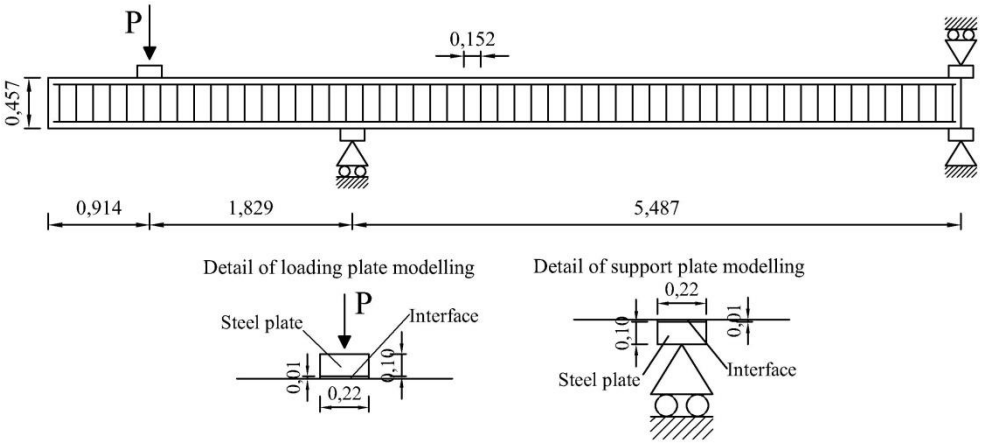

Figure 5-12: Case RB3. Dimensions adopted for the beam (in m)

The mesh of the beam is presented in Figure 5-13(a). Different materials are indicated with varying colors in Figure 5-13(b).

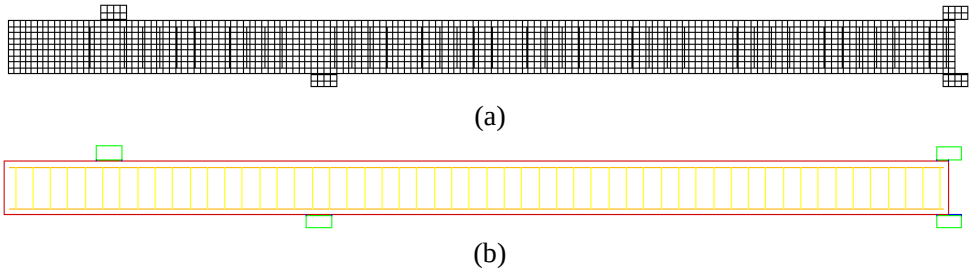

(a)

(b)

Figure 5-13: Case RB3. (a) Mesh and (b) material sets

Different groups of elements were defined to distinguish the concrete elements that can be subjected to crushing or cracking and reinforcement that can yield. These groups of elements will be used in section 5.4 to monitor the failure mode during the analysis. For monitoring steel yielding, the group REBAR (red) and STIRRUPS (black) refer to 3#8 reinforcing bars and #3 stirrups of the beam, see Figure 5-14.

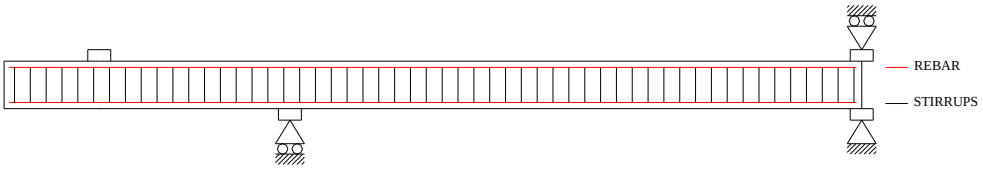

Figure 5-14: Case RB3. Groups of steel elements monitoring yielding

Figure 5-15 shows the groups of elements named CRUSHING, used for monitoring the inelastic behavior of concrete in compression due to bending near the support A. This group of elements has the length equal to 5 times the length of the supporting steel plate and the depth equal to the length of the supporting steel plate.

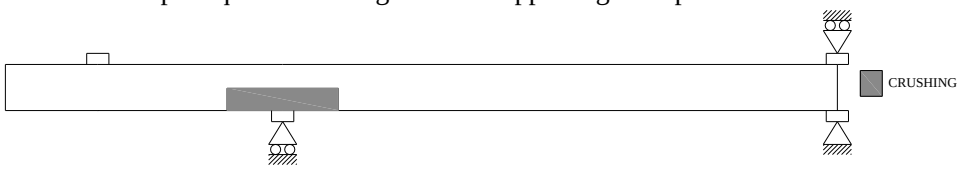

Figure 5-15: Case RB3. Group of concrete elements monitoring crushing due to bending

Figure 5-16 shows the group of elements named SHEAR where the inelastic behavior of concrete due to shear was monitored. Group SHEAR is lying between the REBAR group and the edges of the loading and the support steel plate.

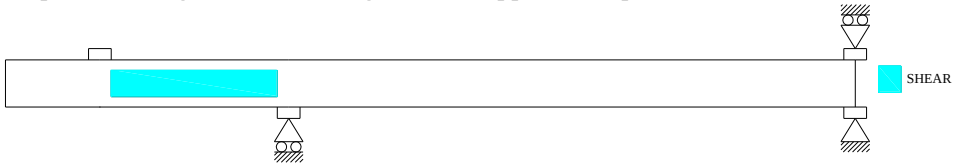

Figure 5-16: Case RB3. Group of concrete elements monitoring inelastic behavior due to shear

Boundary conditions and loading

The translations along *x* and *y* axes at a single node of the left steel plate (support A) is constrained as well as the translation along *y* axis at a single node of the bottom and the top right steel plates (support B), Figure 5-17.
Dead load is applied in load case 1. Load *P* as a unit load of 1×10^3 N is added in load case 2 as a concentrated load applied at the mid node of the loading plate, Figure 5-17.

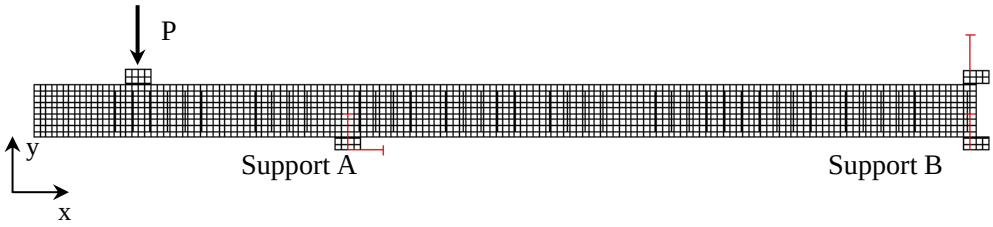

Figure 5-17: Case RB3. Boundary conditions and load case 2

Load increments and convergence criteria

Load case 1 is applied in a single step. The regular Newton-Raphson method with a maximum of 25 iterations is used. As convergence criteria, the norms of the force and energy are selected. The analysis continues even if the convergence criteria are not satisfied. The convergence tolerance is equal to 1×10^{-2} for the energy and force norms. A maximum number of iterations equal to 25 was chosen. A Line Search algorithm is used to improve the convergence performance.

Figure 5-18: Case RB3. `Indirect Displacement control' technique applied referring to node 1

Load case 2 is applied with automatic adaptive load increments based on energy. The initial load factor equals 5, the upper limit of the incremental load factor equals 10 and the lower limit of the incremental load factor equals 2. The maximum number of steps is 140. Arc-length control was applied based on translation along y axis of node 1 (line search- 'inddisp'), Figure 5-18. The analysis continues even if the convergence criteria are not satisfied. The convergence tolerances are equal to 1×10^{-3} and 1×10^{-2} for energy and force norms, respectively. A maximum number of iterations equal to 25 was selected. A Line Search algorithm is used to improve the convergence performance.

5.4 Nonlinear finite element analysis

Load deflection

The load-deflection curve is presented in Figure 5-19 together with the applied load values corresponding to the beginning of yielding of #8 longitudinal bars and yielding of the stirrups. The step at which the first integration point reaches a minimum principal strain value lower than -3.5×10^{-3} is defined crushing of concrete. The peak load is defined as the highest load step where the energy norm ratio satisfies the fixed tolerance of 1×10^{-3}. At the peak loads the ultimate strain of #8 rebars, assumed equal to of 5×10^{-2}, is achieved.

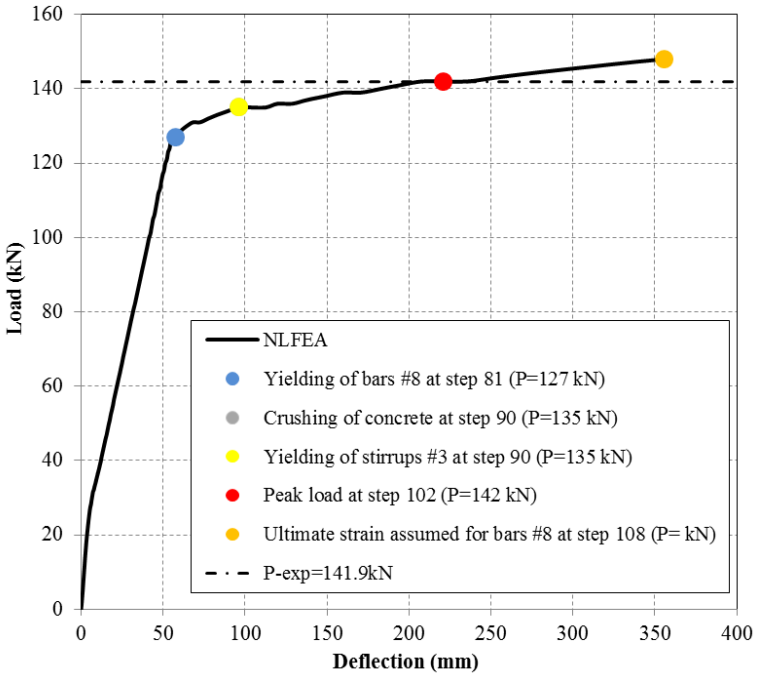

Figure 5-19: Case RB3. Load-deflection curves

Convergence behavior

For most steps convergence is achieved on the basis of the energy criterion, Figure 5-20 and Figure 5-21. For load case 2 the peak load is defined as the highest load step where the energy norm ratio satisfies the fixed tolerance of 1×10^{-3} and it is marked with a red marker.

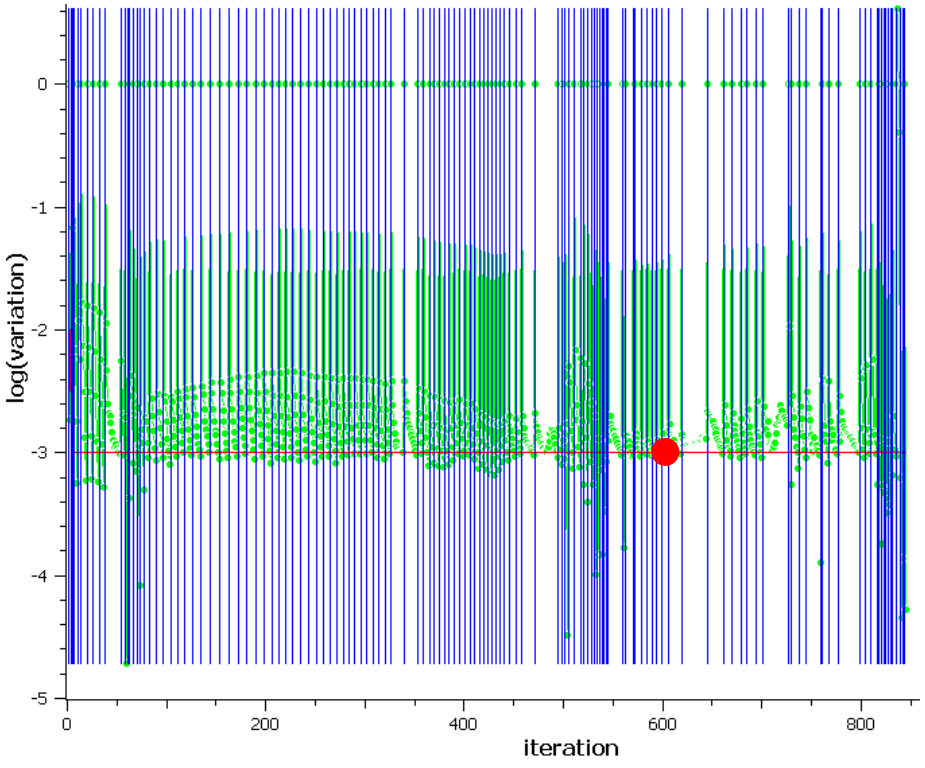

Figure 5-20: Case RB3. Evolution of the energy norm (blue lines indicate steps, red line indicates tolerance, green points indicate iterative results)

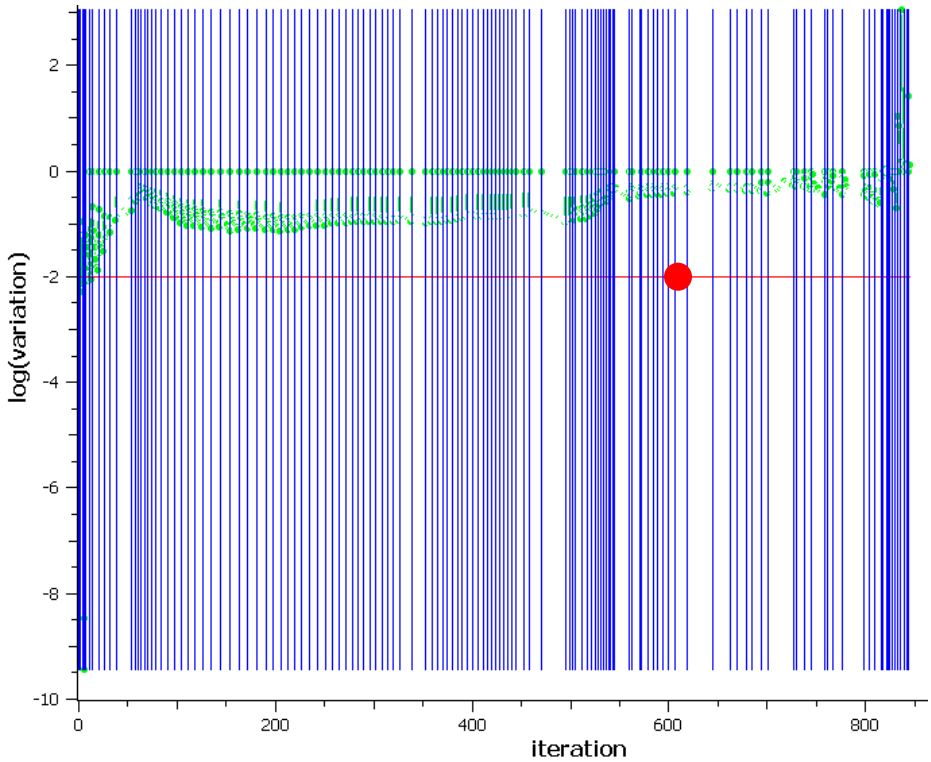

Figure 5-21: Case RB3. Evolution of the force norm (blue lines indicate steps, red line indicates tolerance, green points indicate iterative results)

Strains

Figure 5-22 shows the crack strain values at the peak value of applied load (step 102, P = 142 kN).

The first crack strain value plotted in Figure 5-22 equals to 7.86×10^{-4}, corresponds to the ultimate crack strain value calculated as $\varepsilon_{t,u} = \frac{G_F}{h \cdot f_{ctm}}$. The third crack strain value, equal to 3.62×10^{-3}, is the crack strain value corresponding to a stress value equal to 1% of f_{ctm}. An intermediate crack strain value was added in the contour plot.

The vertical crack pattern, which can be observed in the contour of the crack strain, shows that the failure is due to bending and can be compared with the experimental crack pattern illustrated in Figure 5-3.

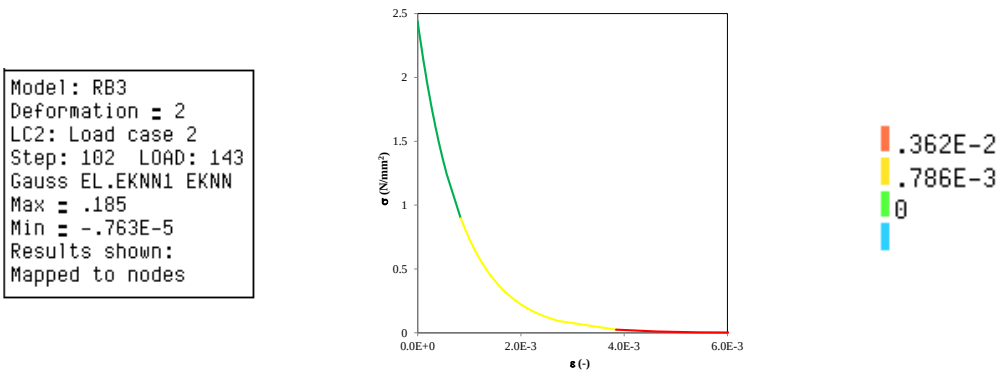

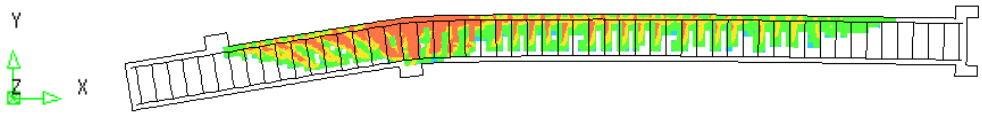

Figure 5-22: Case RB3. Crack strain values at step 102 (P=142 kN)

Figure 5-23 shows the minimum principal strain values, at the peak value of applied load obtained from NLFEA (step 114). The beam failed due to bending after yielding of the #8 reinforcing bars and consequently the beam displays a ductile behavior at failure. At the same time, crushing of concrete is not significant as it occurred in a small area near the supporting steel plate due to geometrical discontinuity.

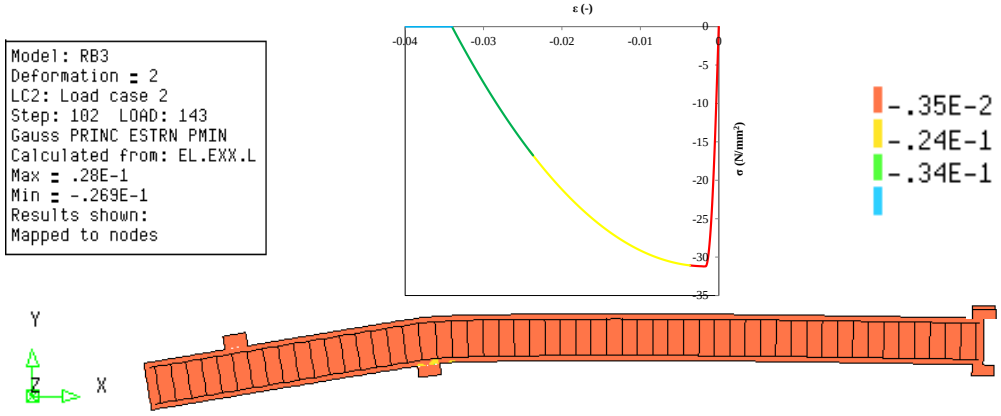

Figure 5-23: Case RB3. Minimum principal strain values at step 102 (peak load)

The yielding strain for the #8 reinforcing bars is equal to $414MPa/200GPa = 2.07 \times 10^{-3}$ The longitudinal #8 reinforcing bars start to yield in tension at a load equal to 127 kN (step 81). Figure 4-24 shows yielding of bars at step 102. The longitudinal #8 reinforcing bars reached the ultimate strain, assumed equal to 5×10^{-2} at the load equal to 148 kN (step 109) after the peak load.

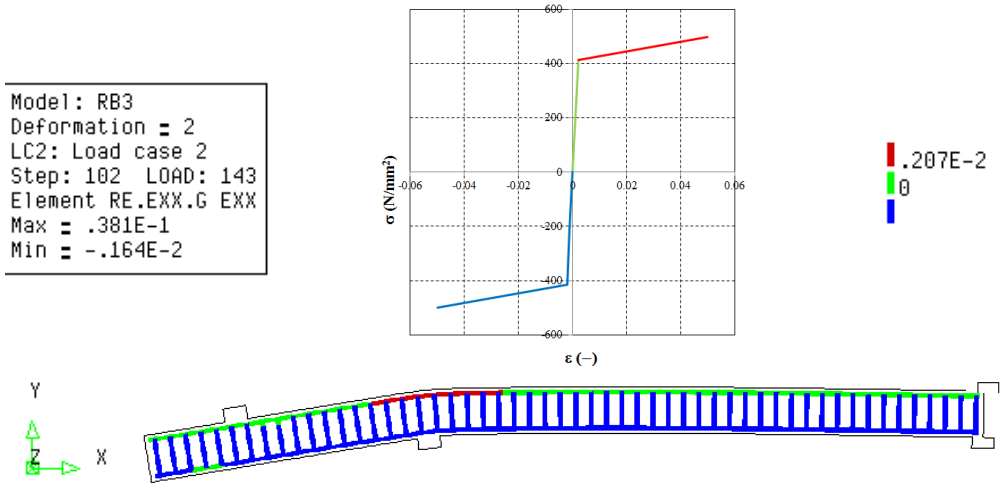

Figure 5-24: Case RB3. Yielding of #8 reinforcing bars at step 102 (P=142 kN)

The yielding strain for the stirrups is equal to $414MPa/200GPa = 2.07 \times 10^{-3}$. Because of the fact that the beam failed in bending, only localized yielding of stirrups at a low number of integration points can be recognized. Yielding or stirrups at the peak load is depicted in Figure 5-25.

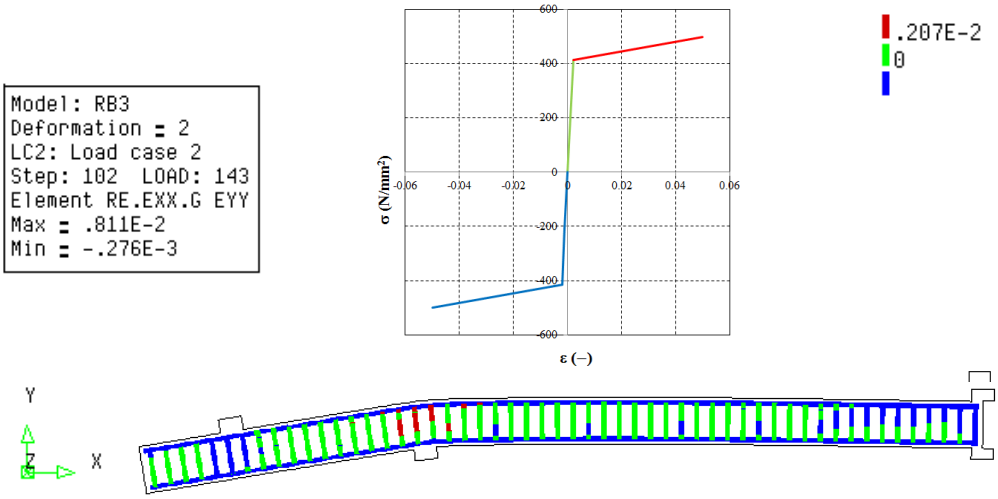

Figure 5-25: Case RB3. Yielding of the stirrups at the peak load (peak load P=142 kN)

Gauss point statistics

Table 5-6 lists the number of cracking points, crushing points, and yield points at step 81 (the beginning of yielding of #8 reinforcing bar), at step 90 (when the first element reaches minimum principal strains lower than -3.5×10^{-3} and yielding of stirrups) and at step 102 (the peak value of applied load obtained from NLFEA). Crushing is defined as soon as the softening branch in compression is reached. In the current, it is at the minimum principal strain of -1.7×10^{-3}.

Table 5-6: Case RB3. Number of cracking points, crushing points, and yield points

YIELDING OF #8 BARS						
STEP	**81**	**ITERATIONS**		5		
GROUP NAME	**PLAST**	**PRV. PL**	**CRITIC**	**PLAST NEW**	**PRV.PL NEW**	**CRITIC NEW**
BEAM	31	0	0	1	0	0
REBAR	7	0	0	0	0	0
CRUSHING	31	0	0	1	0	0
TOTAL MODEL	38	0	0	1	0	0
CRACKING LOGGING SUMMARY						
GROUP NAME	**CRACK**	**OPEN**	**CLOSED**	**ACTIVE**	**INACTI**	**ARISES**
BEAM	4559	4556	3	2742	1817	27
CRUSHING	198	198	0	133	65	6
SHEAR	681	681	0	432	249	5
TOTAL MODEL	4559	4556	3	2742	1817	27
CUMULATIVE REACTION:						
FORCE X			**FORCE Y**			
-0.56954D-09			-0.15049D+06			
CRUSHING OF CONCRETE AND YIELDING OF #3 STIRRUPS						
STEP	**90**	**ITERATIONS**		1		
GROUP NAME	**PLAST**	**PRV. PL**	**CRITIC**	**PLAST NEW**	**PRV.PL NEW**	**CRITIC NEW**
BEAM	79	0	0	11	0	0
REBAR	33	0	0	0	0	0
STIRRUPS	3	0	0	2	0	0
CRUSHING	78	0	0	10	0	0
TOTAL MODEL	115	0	0	13	0	0

CRACKING LOGGING SUMMARY						
GROUP NAME	**CRACK**	**OPEN**	**CLOSED**	**ACTIVE**	**INACTI**	**ARISES**
BEAM	4851	4848	3	3405	1446	37
CRUSHING	313	313	0	260	53	19
SHEAR	715	715	0	474	241	5
TOTAL MODEL	4851	4848	3	3405	1446	37
CUMULATIVE REACTION:						
FORCE X			**FORCE Y**			
-0.76775D-09			-0.15774D+06			
PEAK LOAD						
STEP	**102**	**ITERATIONS**		12		
GROUP NAME	**PLAST**	**PRV. PL**	**CRITIC**	**PLAST NEW**	**PRV.PL NEW**	**CRITIC NEW**
BEAM	91	34	0	3	18	0
REBAR	44	1	0	0	1	0
STIRRUPS	27	0	0	4	0	0
CRUSHING	79	33	0	3	18	0
TOTAL MODEL	162	35	0	7	19	0
CRACKING LOGGING SUMMARY						
GROUP NAME	**CRACK**	**OPEN**	**CLOSED**	**ACTIVE**	**INACTI**	**ARISES**
BEAM	5355	5352	3	3405	1950	54
CRUSHING	447	447	0	339	108	17
SHEAR	788	788	0	520	268	5
TOTAL MODEL	5355	5352	3	3405	1950	54
CUMULATIVE REACTION:						
FORCE X			**FORCE Y**			
-0.29341D-12			-0.16507D+06			

5.5 Application of safety formats Model Code 2010 (fib, 2013)

As proposed by the Model Code 2010 (fib, 2013),the safety formats for non-linear finite element analyses are three numerical methods denoted as GRF (Global Resistance Factor method), PF (Partial Factor method) and ECOV (Method of Estimation of a Coefficient of Variation of resistance). Application of the safety formats requires in total 4 non-linear analyses. In Table 5-7 - Table 5-9 the mechanical properties applied in the non-linear analyses are summarized.

Table 5-7: Case RB3. Constitutive model parameters for concrete

	f_c (N/mm^2)	f_{ct} (N/mm^2)	E_c (N/mm^2)	ν	G_F (Nmm/mm^2)	G_C (Nmm/mm^2)
Mean measured	31.20	2.44	31297	Var.	0.136	33.901
Characteristic	23.20	1.71	28382	Var.	0.129	32.140
Mean GRF	19.72	2.19	26900	Var.	0.125	31.214
Design	15.47	1.14	26602	Var.	0.120	29.878

Table 5-8: Case RB3. Constitutive model parameters for reinforcing bars #8

	Φ (mm)	A_s (mm^2)	f_y (N/mm^2)	f_t (N/mm^2)	E_s (N/mm^2)	ε_{sy}
Mean measured	25.4	471	414.00	500.00	200000	0.00207
Characteristic	25.4	471	374.98	452.87	200000	0.00187

Mean GRF	25.4	471	412.48	498.16	200000	0.00206
Design	25.4	471	326.07	393.80	200000	0.00163

Table 5-9: Case RB3. Constitutive model parameters for reinforcing bars #3

	Φ (mm)	A_s (mm^2)	f_y (N/mm^2)	f_t (N/mm^2)	E_s (N/mm^2)	ε_{sy}
Mean measured	9.5	71	414.00	500.00	200000	0.00207
Characteristic	9.5	71	374.98	452.87	200000	0.00187
Mean GRF	9.5	71	412.48	498.16	200000	0.00206
Design	9.5	71	326.07	393.80	200000	0.00163

In Figure 5-26 the load-deflection curves obtained with mean measured, characteristic, mean (GRF) and design values of material strengths, calculated according to Model Code 2010 (fib, 2013) are shown. The peak loads are defined as the load values for which the ultimate strain of #8 rebars, assumed to be 5×10^{-2} ,is reached

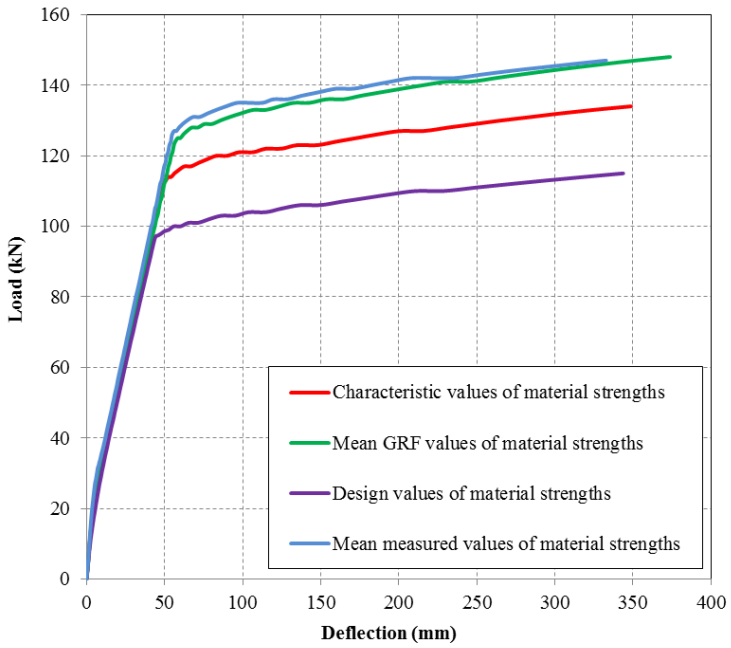

Figure 5-26: Case RB3. Load-deflection curves obtained with mean measured, characteristic, mean (GRF) and design values of material strengths

The RB3 beam was analyzed with analytical expressions for sectional analysis and numerical procedures proposed for NLFE analysis. Figure 5-27 shows the comparison of analytical and numerical design values of the beam resistance expressed in terms of a percentage of the experimental ultimate value of applied load.

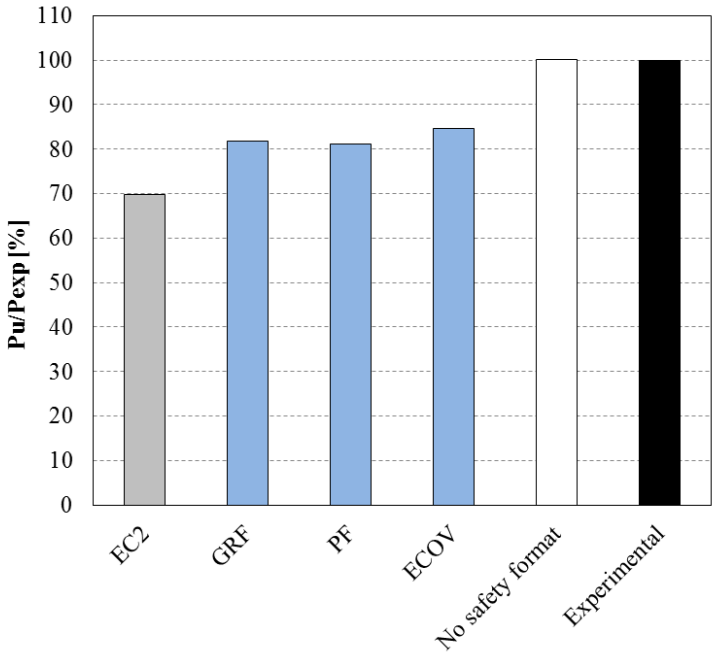

Figure 5-27: Case RB3. Analytical and numerical design values of beam resistance expressed in terms of a percentage of the experimental ultimate value of applied load, P_{Exp}=141.9 kN

Table 5-10 contains the design values of beam resistance, expressed in terms of applied load P_{Rd}, obtained from numerical analyses and analytical calculations. The analytical beam resistance was obtained with sectional analysis in section 5.2 according to Eurocode 2 (CEN, 2005) and Model Code 2010 (fib, 2013).

Table 5-10: Case RB3. Values of beam resistance, expressed in terms of applied load P_{Rd}

Experimental (kN)	EC2,MC2010 (kN)	GRF (kN)	PF (kN)	ECOV (kN)	No Safety Formats (kN)
141.9	98.97	116	115	120	142

5.6 Parametric study on crack models

A parametric study with different values of parameters of a concrete constitutive model, such as crack model and fracture energy of concrete in tension, was conducted. Table 5-11 lists material parameters applied in NLFEA of parametric study. Analyses 1 to 3 refer to three analyses performed by varying the aforementioned material parameters. All the analyses were carried out considering mean measured values of material strengths. The parabolic law in compression and the exponential law in tension were used for concrete, while the elasto-plastic law with hardening was applied for steel.

The load was applied incrementally with load-control procedure and active arc-length control. The analyses include a variable Poisson's ratio as well as the reduction of the compressive strength of concrete due to lateral cracking with the lower bound as follows from:

$$\beta_{\sigma,\min} = \frac{f_{c,red}}{f_{cm}} = 0.6$$

The effect of the applied value of the fracture energy of concrete in tension on the beam's response was investigated by adopting the formulation proposed by Model Code 1990 (CEB-FIP, 1993) and the formulation proposed by Model Code 2010 (fib, 2013). The fracture energy of concrete in compression was considered for all analyses equal to $250G_F$ (Nakamura et al. 2001).

For the Total Strain fixed crack model, the aggregate size based shear retention was defined. According to this model, the shear stiffness of a crack diminishes together with opening of the crack until the value of the normal crack strain reaches the size of half the mean aggregate size. This implies loss of contact between crack planes. The linear decay of shear stiffness further depends on the crack bandwidth value h. The complete formulation is:

$$\beta = 1 - \left(\frac{2}{d_{aggr}}\right)\varepsilon_n h$$

In Figure 5-28 the load-deflection curves resulting from the parametric study are plotted. The peak load values are given in Table 5-11.

Table 5-11: Case RB3. Data used for the parametric study

Analysis	Total strain crack model	Limit to β_σ	G_F	G_C	Peak load value (kN)
Analysis 1	rotating	0.6	MC2010	250 G_F	148
Analysis 2	rotating	0.6	MC1990	250 G_F	147
Analysis 3	fixed	0.6	MC2010	250 G_F	151

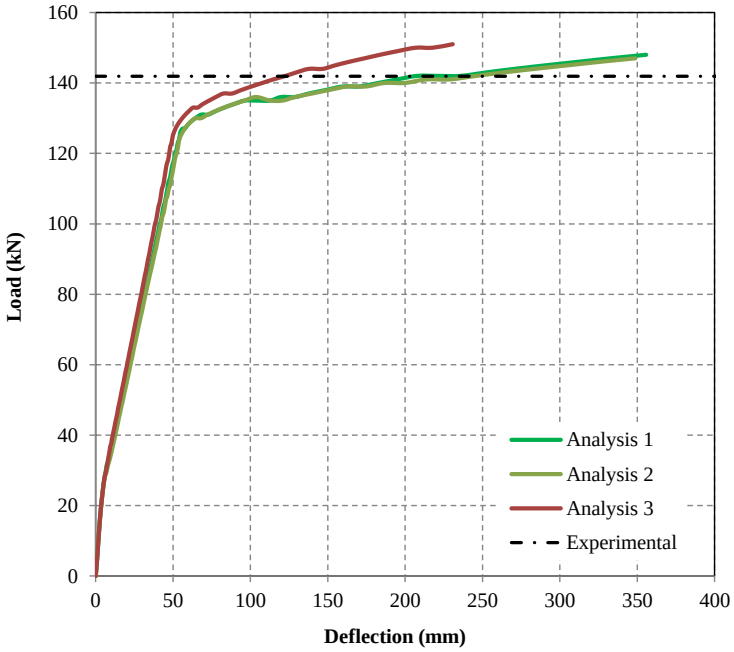

Figure 5-28: Case RB3. Load-deflection curves (Analyses 1 to 3)

The crack model and mechanical properties used in Analysis 1 were selected as for the safety formats for NLFEA to predict the design resistance. The peak loads are defined as the load values for which the ultimate strain of #8 rebars, assumed to be 5×10^{-2}, is reached.
As expected, since the beam fails in bending, the peak loads and the failure modes observed from NLFE analyses are not heavily dependent on the values of the fracture energy of concrete in tension. The fixed crack model provides a stiffer response after yielding of the #8 bars as well as after the crushing of concrete than the analyses with the applied rotating crack orientation.

5.7 Concluding remarks

The beam RB3 tested by Grace consists of an overhang at one end and a support constraining vertical translation at the other. The beam was loaded at the loose end and exhibited a ductile flexural failure. The ultimate value of the applied load in experiments was $P_{Exp} = 141.9kN$.

From the analytical calculation, based on sectional analysis, it was demonstrated that beam RB3 fails due to bending. This conclusion was drawn as the shear force corresponding to the design value of moment resistance is lower than the design value of shear resistance. The design beam resistance evaluated with the sectional analysis equals to $P_{Exp} = 95kN$.

The peak value of the applied load obtained from NLFEA, performed with the mean measured values of material strength, is equal to 142 kN. The displayed flexural failure mode is characterized by extensive yielding accompanied with high strain values in #8 top reinforcing bars and localized crushing of concrete and yielding of stirrups.
The peak loads are defined as the load magnitude for which the ultimate strain of #8 rebars – assumed to be 5×10^{-2} is reached.
In order to compute the design values of beam resistance, safety formats for non-linear finite element analyses, as introduced by the Model Code 2010 were used. The design values of beam resistance obtained from safety formats is higher than the design resistance estimated by means of an analytical approach. The maximum value resulting from the analyses with application of safety formats was obtained with ECOV approach which yields the resistance equal to $P_{Rd} = 120kN$.

Since the beam fails in bending, the failure mode is not heavily dependent on the crack model and tensile strengths of concrete in tension.

6 Case RB3A: Grace (2001)

The experimental program of Grace (Grace, 2001) studied the effect of strengthening using fiber-reinforced polymer strips. The control beam of the category I beams from this program is used as a case study.

6.1 Experimental setup and results

Geometry

The only difference between RB3 and RB3A is that the stirrups have a spacing of 0.457 m instead of 0.152 m. All the other dimensions and parameters remain the same.

Experimental Results

The beam exhibited a shear failure mode, Figure 6-1. The experimental ultimate value of applied load was equal to $P_{Exp} = 155.7kN$.

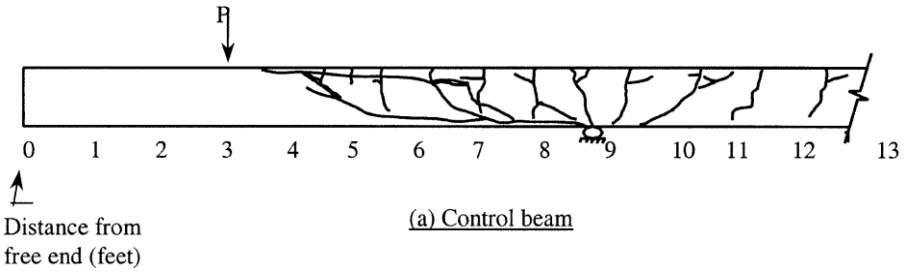

Figure 6-1: Case RB3A. Failure mechanisms at experimental ultimate value of applied load (Grace 2001)

6.2 Analytical analysis

In Figure 6-2, the load configuration at failure is depicted. The distributed load representing the beam weight is equal to $q = 0.25 \times 0.457 \times 25 = 2.856\ kNm$.

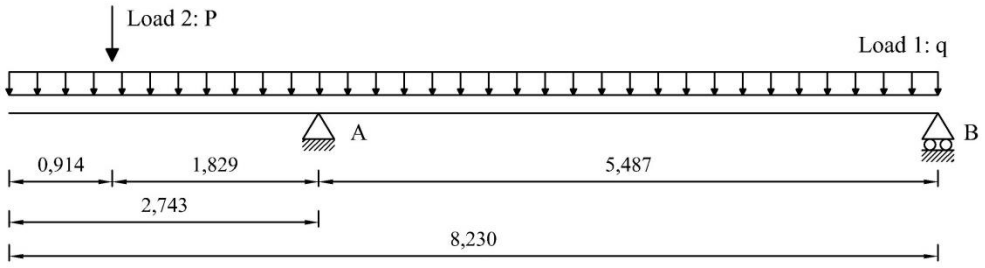

Figure 6-2: Case RB3A. Load configuration (dimension in m)

Load case 1

Figure 6-3 shows that the maximum negative value of applied moment at the support A is equal to:

$$M_{E,A}^{-} = -2.856kN/m \times \frac{(2.743m)^2}{2} = 10.74\,kNm$$

and the value of applied shear force at support A is equal to:

$$V_{E,A,sx} = -2.856\,kN/m \times 2.743m = -7.83kN$$

The value of shear force at support B equals:

$$V_{E,B} = -\frac{5.487m}{2}q + \frac{(2.743m)^2}{2} \times \frac{1}{5.487m}q = -5.877kN$$

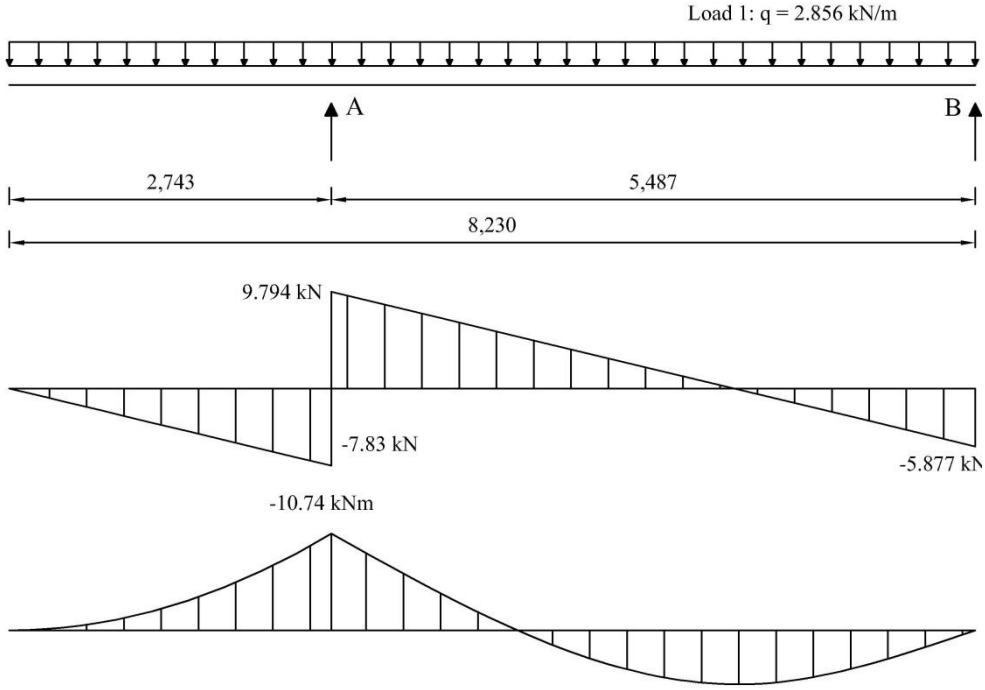

Figure 6-3: Case RB3. Load 1: Internal forces

Load case 2

The experimental ultimate value of applied load is equal to $P_{Exp} = 155.7kN$.

Figure 6-4 shows that the minimum value of applied moment at the support A is equal to:

$M^{-}_{E,A} = -155.7kN \times 1.829m = -284.78kNm$

and the values of applied shear force at supports A and B are equal to:

$V_{E,A,sx} = -155.7kN$ and $V_{E,B} = 51.9\,kN$.

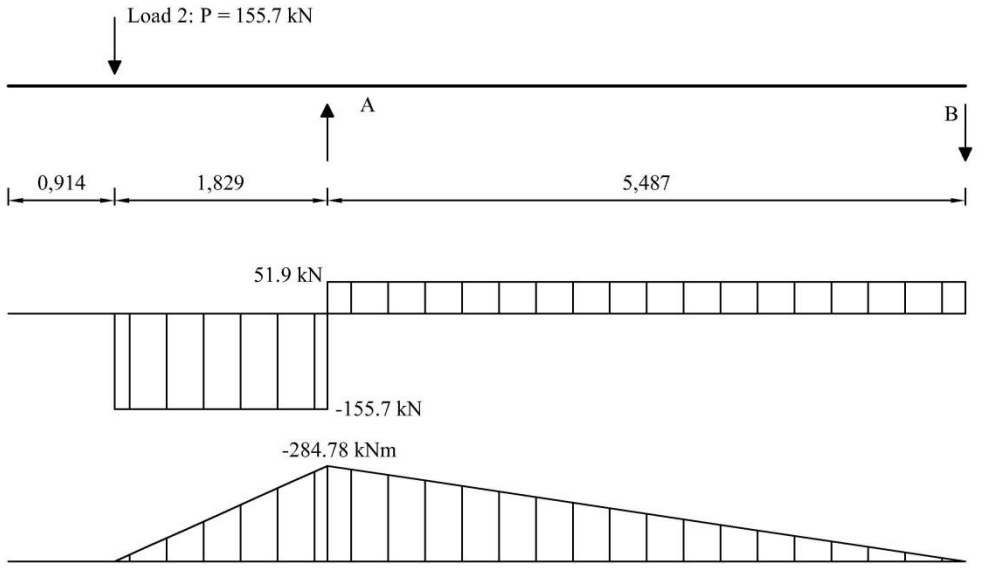

Figure 6-4: Case RB3. Load 2: Internal forces

Load 1 + Load 2

At failure the minimum value of applied moment is equal to:

$$M_{E,A}^{-} = -284.78kNm - 10.74kNm = -295.52kNm$$

and the minimum value of applied shear force:

$$V_{E,A,sx} = -155.7kN - 7.83kN = -163.3kN$$

The design value of resistance moment is evaluated with sectional analysis by assuming that:

- tensile strength of concrete is ignored,
- the compressive stresses in concrete are derived from parabola-rectangle relation,
- the stresses in the reinforcing steel are derived from elastic-plastic relation with hardening,
- the partial safety factor for the mechanical properties of reinforcing steel equals $\gamma_s = 1.15$, the factor for concrete material properties equals $\gamma_c = 1.5$.

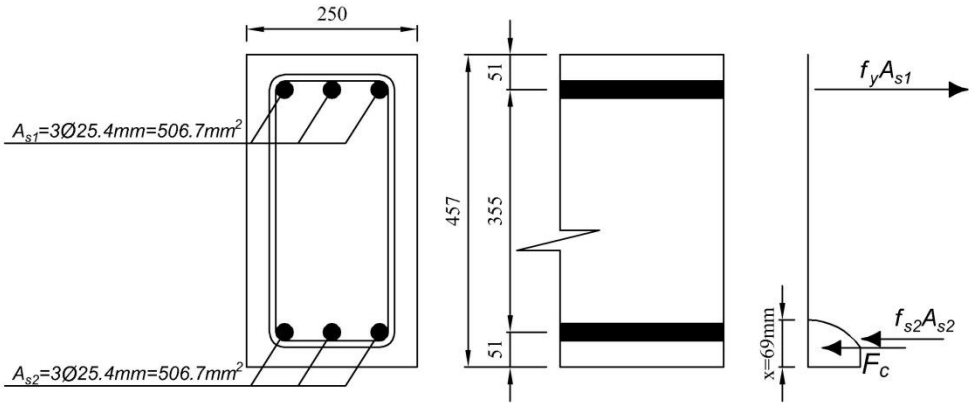

Figure 6-5: Case RB3A. Stress block for determination of the design moment resistance

The design moment resistance for the case study RB3A is not influenced by reduced spacing of stirrups. Under these circumstances, the procedure for computing bending capacity is the same as in the previous section. The cross-section of the beam is calculated assuming that the tensile reinforcement reaches the yield strain whereas the bottom reinforcement remains in the elastic strain range. For these assumptions, the height of the compression zone is calculated from the horizontal force equilibrium as follows:

$$A_{s1} f_{yd} - A_{s2}\left(\frac{x - a_2}{x}\right)\varepsilon_{cu2} E_s - 0.8095 x b f_{cd} = 0 \rightarrow x = 69mm$$

Verification of the assumption for the calculated value of x:

$$\varepsilon_{s1} = \frac{\varepsilon_{cu2}(d_1 - x)}{x} = \frac{0.0035(459mm - 74mm)}{74mm} = 0.018 \rightarrow steel\ yields$$

$$\varepsilon_{s2} = \frac{\varepsilon_{cu2}(x - a_2)}{x} = \frac{0.0035(74mm - 41mm)}{74mm} = 1.561 \cdot 10^{-3} \rightarrow steel\ does\ not\ yield$$

therefore the assumptions hold.

The design value of the moment resistance in calculated around the centre of the compression zone $0.416x$:

$$M_{Rd} = A_{s1} f_{yd}(d_1 - 0.416x) + A_{s2}\varepsilon_{s2} E_s(0.416x - a_2) = 180.84kNm$$

The value of applied moment equal to

$$M_{E,A}^{-} = -q\frac{(2.743m)^2}{2} - 1.829m \times P = -180.84\ kNm$$

which after transformations leads to the maximum value of the applied load:

$$P_{Ed} = -q\frac{(2.743m)^2}{2 \cdot 1.829m} + \frac{180.84kNm}{1.829m} = 98.87\ kN\ .$$

The design shear resistance provided by stirrups is evaluated with the expression 6.8 from the EC2 as follows:

$$V_{Rds} = 0.9d\frac{A_{sw}}{s} f_{yd} \cot\theta = 0.9 \times 406mm \times \frac{142mm^2}{457mm} \times 326.07N/mm^2 \times 2.5 = 92.55kN$$

The governing shear resistance is the minimum shear resistance restricted by yielding of stirrups and crushing of concrete. From Figure 6-6, it can be seen that the design shear resistance dictated by crushing of concrete is much higher than the design shear resistance attributed to stirrups. Consequently, the governing shear resistance is:

$V_{Rd} = \min(V_{Rdc}, V_{Rds}) = 92.55\ kN$

and follows from yielding of shear reinforcement.

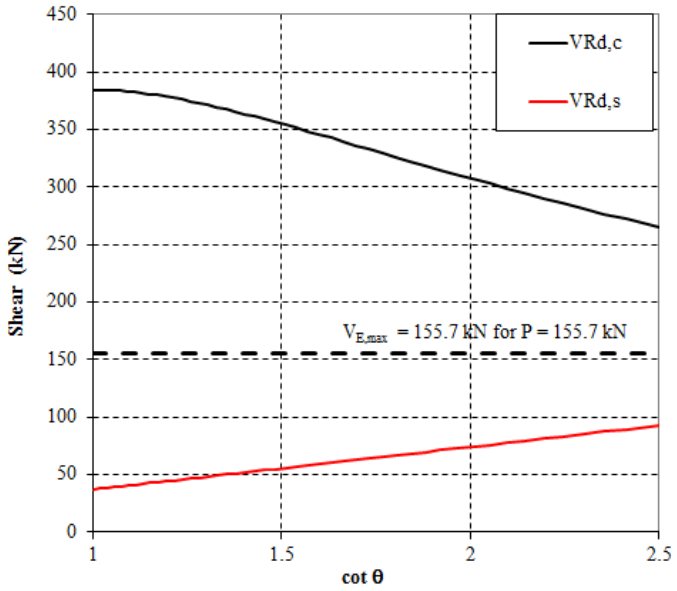

Figure 6-6: Case RB3A. Shear resistance

From the comparison of the values of applied load corresponding to shear resistance, $P_{E,\max} = 92.55kN - 6.675kN = 85.875kN$ and bending moment resistance $P_{BM} = 98.97kN$, it can be concluded that because $P_{E,\max} < P_{BM}$, the beam fails due to shear. It is thus in agreement with the observation from the experiments.

Besides the calculations according to the EC2, the design value of shear resistance for an element containing shear reinforcement was evaluated with three levels of approximation as given in the Model Code 2010 (fib, 2013).

Level I Approximation

The design shear resistance of members with shear reinforcement is given by:

$V_{Rd} = V_{Rd,s} \le V_{Rd,\max}$

For reinforced concrete members $\theta_{\min} = 30^{\circ}$, $\cot(\theta) = 1.732$.

$$V_{Rd,s} = \frac{A_{sw}}{s_w} z f_{ywd} \cot\theta = \frac{2 \times 71.26mm^2}{457mm} 365.4mm \times 326N/mm^2 \times 1.732 = 64.34\ kN$$

$$V_{Rd,\max} = k_c \frac{f_{ck}}{\gamma_c} b_w z \sin\theta \cos\theta = 0.55 \cdot \frac{23.2 N/mm^2}{1.5} 250mm \times 365.4mm \times \sin 30^\circ \cos 30^\circ = 336.5\ kN$$

where:

$z = 0.9d = 0.9 \times 406mm = 365.4mm$

$k_c = k_\varepsilon \eta_{fc} = 0.55 \times 1 = 0.55$

$k_\varepsilon = 0.55$

$$\eta_{fc} = \left(\frac{30}{f_{ck}}\right)^{1/3} \le 1 \Rightarrow \eta_{fc} = 1$$

Level II Approximation

To calculate the design value of shear resistance, it is required to determine the state of stress ε_x. The strain parameter ε_x is calculated iteratively at the critical section located d from the edge of the support. After a number of iterations, calculations result in:

$V_{Ed}^{i-1} = 75.82kN$

$M_{Ed}^{i-1} = V_{Ed}^{i-1}(1829mm\text{-}d) = 75.82kN \times (1.829m - 0.406m) = 107.890\,kNm$

$$\varepsilon_x^{i-1} = \frac{1}{2E_s A_s}\left(\frac{M_{Ed}^{i-1}}{z} + V_{Ed}^{i-1}\right) == \frac{1}{2 \times 200GPa \times 1520mm^2}\left(\frac{107.890kNm}{365.4mm} + 75.82kN\right) = 6.103 \times 10^{-4}$$

$\theta^{i-1} = 20^\circ + 10000\varepsilon_x = 26.103^\circ$

$\varepsilon_1^{i-1} = \varepsilon_x^{i-1} + (\varepsilon_x^{i-1} + 0.002)\cot^2\theta^{i-1} = 0.01148$

$$k_\varepsilon^{i-1} = \frac{1}{1.2 + 55\varepsilon_1} = 0.546$$

$$\eta_{fc} = \left(\frac{30}{f_{ck}}\right)^{1/3} \le 1 \Rightarrow \eta_{fc} = 1$$

$k_c^{i-1} = k_\varepsilon^{i-1} \eta_{fc} = 0.546$

$$V_{Rd,s}^i = \frac{A_{sw}}{s_w} z f_{ywd} \cot\theta^{i-1} = \frac{2 \times 71.26mm^2}{457mm} 365.4mm \times 326N/mm^2 \times 2.033 = 75.82\ kN$$

$$V_{Rd,\max}^i = k_c^{i-1} \frac{f_{ck}}{\gamma_c} b_w z \sin\theta^{i-1} \cos\theta^{i-1} = 0.546 \times \frac{23.2N/mm^2}{1.5} 250mm \times 365.4N/mm^2 \times 0.44 \times 0.90 =$$

$= 304.8\ kN$

Level III Approximation

A similar procedure to that of LoA II was adopted. In LoA III, the contribution of concrete can be accounted for when $V_{Ed} < V_{Rd,\max}$. After a number of iterations it results in:

$V_{Ed}^{i-1} = 104.32\,kN$

$M_{Ed}^{i-1} = V_{Ed}^{i-1}(1829mm - d) = 104.32 \times (1.829m - 0.406m) = 148.45kNm$

$$\varepsilon_x^{i-1} = \frac{1}{2E_s A_s}\left(\frac{M_{Ed}^{i-1}}{z} + V_{Ed}^{i-1}\right) =$$

$$= \frac{1}{2 \times 200GPa \times 1520mm^2}\left(\frac{148.45kNm}{365.4mm} + 104321N\right) = 0.00084$$

$\theta_{\min}^{i-1} = 20^\circ + 10000\varepsilon_x^{i-1} = 28.40^\circ$

$\varepsilon_1^{i-1} = \varepsilon_x^{i-1} + (\varepsilon_x^{i-1} + 0.002)\cot^2\theta^{i-1} = 0.0106$

$$k_\varepsilon^{i-1} = \frac{1}{1.2 + 55\varepsilon_1} = 0.562$$

$$\eta_{fc} = \left(\frac{30}{f_{ck}}\right)^{1/3} \leq 1 \Rightarrow \eta_{fc} = 1$$

$$k_c^{i-1} = k_\varepsilon^{i-1}\,\eta_{fc} = 0.562$$

$$V_{Rd,s}^{i} = \frac{A_{sw}}{s_w} z f_{ywd} \cot\theta_{\min}^{i-1} = \frac{2\times 71.26 mm^2}{457 mm} 365.4 mm \times 326 N/mm^2 \times 1.83 = 68.71 kN$$

$$V_{Rd,\max}^{i} = k_c^{i-1}\frac{f_{ck}}{\gamma_c} b_w z \sin\theta_{\min}^{i-1}\cos\theta_{\min}^{i-1} = 0.562\times\frac{23.2 N/mm^2}{1.5} 250 mm\times 365.4 mm\times 0.476\times 0.88 =$$

$$= 331.97\ kN$$

$$k_v^{i-1} = \frac{0.4}{1+1500\varepsilon_x^{i-1}}\left(1-\frac{V_{Ed}}{V_{Rd,\max}\left(\theta_{\min}^{i-1}\right)}\right) = \frac{0.4}{1+1500\times 0.00084}\left(1-\frac{104.321}{331.87}\right) = 0.121$$

$$V_{Rd,c}^{i} = k_v^{i-1}\frac{\sqrt{f_{ck}}}{\gamma_c} b_w z = 0.121\frac{\sqrt{23.2}}{1.5} 250 mm\times 365.4 mm = 35.61 kN$$

$$V_{Rd}^{i} = V_{Rd,s}^{i} + V_{Rd,c}^{i} = 68.71 kN + 35.61 kN = 104.32\ kN$$

Shear resistance obtained with LoA III after extraction of the self-weight (equal to 6.675kN at location d from the support) is 97.65kN. This value is marginally lower than the maximum load $P_{Rd} = 98.78 kN$ which, according to the above calculations, would lead to failure in flexure.
Consequently, it can be stated that from the consideration of both methods i.e. Eurocode 2 (CEN, 2005) and Model Code 2010 (fib, 2013) shear failure is predicted to be the governing mechanism. The results of the analytical solution are summarized in Table 6-1.

Table 6-1: Case RB3A. Design value of beam resistance expressed in terms of applied load P_{Rd}

P_{Rd} (EC2) (kN)	P_{Rd} (MC2010 - Level I) (kN)	P_{Rd} (MC2010 - Level II) (kN)	P_{Rd} (MC2010 - Level II) (kN)
85.88	57.67	69.15	97.65

6.3 Finite element model

A similar model to the finite element model of RB3 was used for RB3A. The only modification comprised of a different spacing of the stirrups.

Material models and parameters

The concrete model is based on a total strain rotating crack model with

- exponential softening in tension and parabolic behavior in compression,
- variable Poisson's ratio of concrete dependent on crack strain values,
- reduction of compressive strength of concrete due to lateral cracking with a lower limit of 0.6 according to (Vecchio, 1986),
- increase in compressive strength due to lateral confinement according to the model proposed by Selby and Vecchio (Selby and Vecchio, 1993).

The mechanical properties for concrete are summarized in Table 6-2. In the input file of the analysis, the G_F value has been decreased with a factor $\sqrt{2}$ in order to

compensate for an underestimation of the crack band width for cracks with an inclination angle of 45 degrees $G_{F,reduced} = 0.136/\sqrt{2} = 0.096$.

Table 6-2: Case RB3A. Constitutive model parameters for concrete

	f_{cm} (N/mm^2)	f_{ctm} (N/mm^2)	E_c (N/mm^2)	ν	G_F (Nmm/mm^2)	G_C (Nmm/mm^2)
Mean measured values	31.20	2.44*	31297*	Var.**	0.136*	33.90*

* Not specified in reference; estimated according to MC2010 (fib, 2013)
** Variable –reduced with the initial value of 0.15

Element types and finite element mesh

The specified dimensions of the beam and for the transversal cross section of the beam are given in Figure 6-7 and Figure 6-8, respectively.

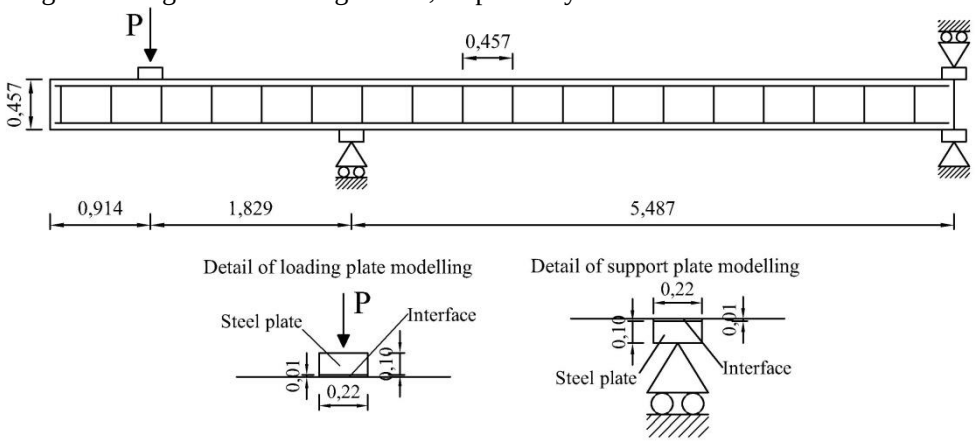

Figure 6-7: Case RB3A. Dimensions adopted for the beam (in m)

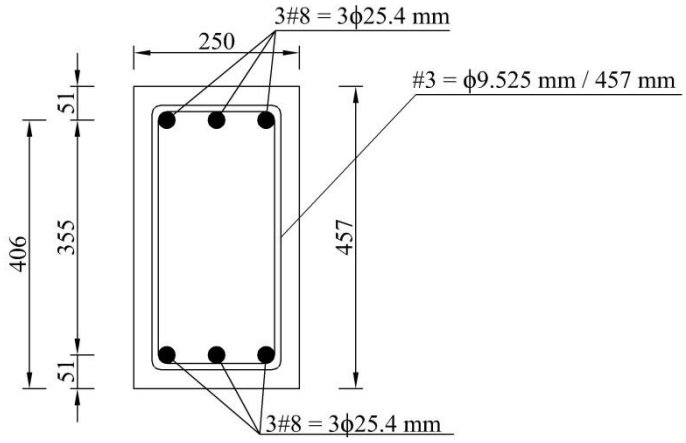

Figure 6-8: Case RB3A. Dimensions adopted for the transversal cross section of the beam (in mm)

The mesh of the beam is presented in Figure 6-9 (a). Different materials are indicated in colors in Figure 6-9(b).

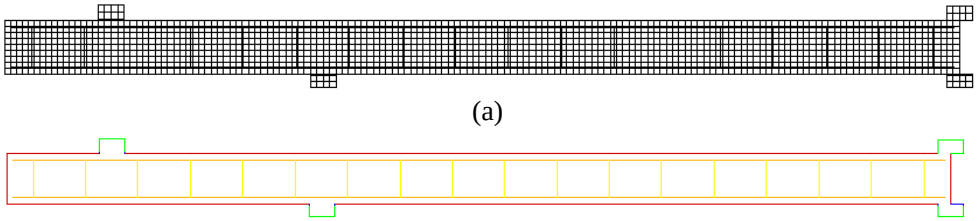

(a)

(b)

Figure 6-9: Case RB3A. (a) Mesh and (b) material sets

Different groups of elements were defined to distinguish the concrete elements that can be subjected to crushing, cracking or yielding in case of reinforcement. These groups of elements will be used in section 6.4 to monitor the failure mode during the analyses. For monitoring yielding of reinforcement, the groups REBAR and STIRRUPS referring to #8 reinforcing bars and #3 stirrups are used, see Figure 6-10.

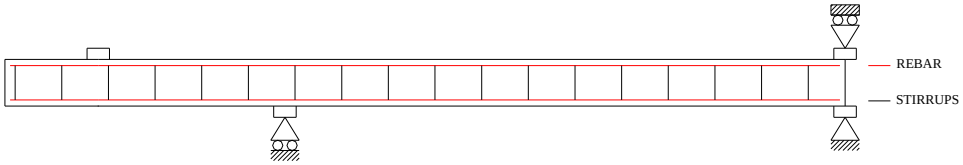

Figure 6-10: Case RB3A. Groups of steel elements monitoring yielding

Figure 6-11 shows the groups of elements called CRUSHING used for monitoring the inelastic behavior of concrete in compression due to bending near the support A. This group of elements has a length equal to 5 times the length of the supporting steel plate and the depth equal to the length of the supporting steel plate.

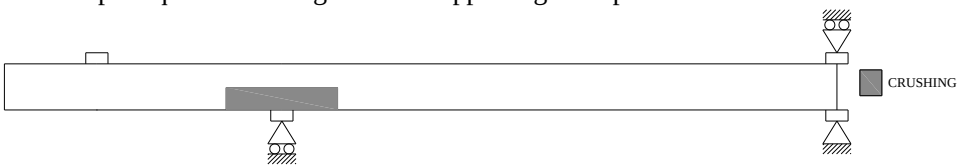

Figure 6-11: Case RB3A. Group of concrete elements monitoring crushing due to bending

Figure 6-11 shows the group of elements named SHEAR where the inelastic behavior of concrete due to shear was monitored. The group SHEAR is lying between the REBAR group and between the edges of the load and support steel plate.

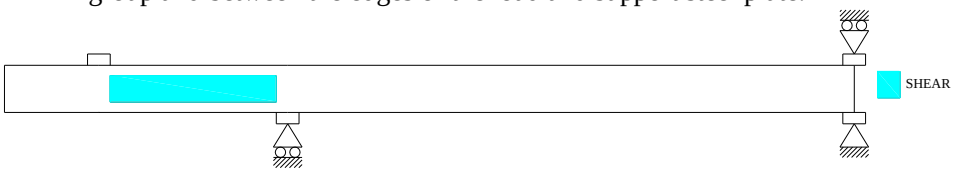

Figure 6-12: Case RB3A. Group of concrete elements monitoring inelastic behavior due to shear

Boundary conditions and loading

Constraint translations, Figure 6-13:

- along *x* and *y* axes at a single node of the left steel plate (support A)
- along *y* axis at a single node of the bottom and top right steel plates (support B).

Dead load is applied in load case 1. Load P as a unit load of 1×10^3 N is added in load case 2 as a concentrated load applied at the mid node of the loading plate,

Figure 6-13.

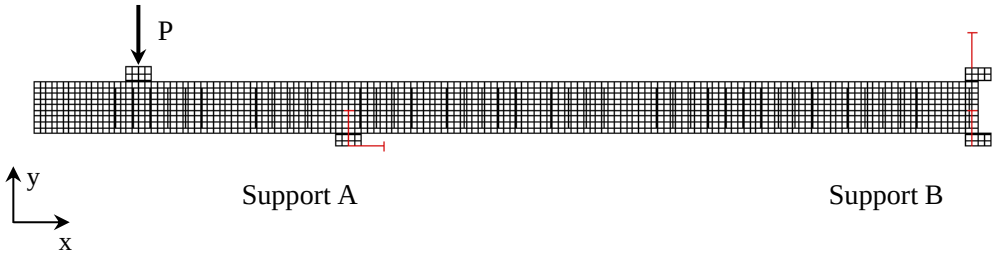

Figure 6-13: Case RB3. Boundary conditions and load case 2

Load increments and convergence criteria

Load case 1 is applied in a single step. The regular Newton-Raphson method with a maximum of 25 iterations is used. As convergence criteria, the norms of the force and energy are selected. The analysis continues even if the convergence criteria are not satisfied. The convergence tolerance is equal to 1×10^{-2} for the energy and force norms. A maximum number of iterations equal to 25 was selected. A Line Search algorithm is used to improve the convergence performance.

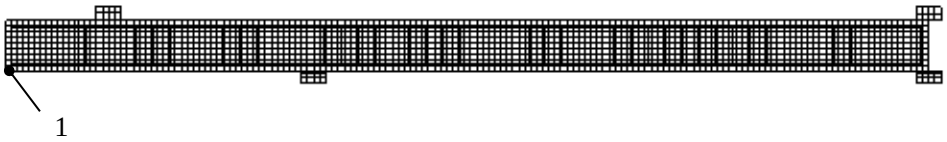

Figure 6-14: Case RB3. `Indirect Displacement control' technique applied referring to node 1

Load case 2 is applied with automatic adaptive load increments based on energy. The initial load factor equals 5, the upper limit of the incremental load factor is 10 and the lower limit of the incremental load factor equals 2. The maximum number of steps is 140. Arc-length control was applied based on translation along y axis of node 1 (line search- 'inddisp'), Figure 6-14. The analysis continues even if the convergence criteria are not satisfied. The convergence tolerances are equal to 1×10^{-3} and 1×10^{-2} for energy and force norms respectively. A maximum number of iterations equal to 50 was selected. A Line Search algorithm is used to improve the convergence performance.

6.4 Nonlinear finite element analysis

Load deflection

The load-deflection curve is presented in Figure 6-15. The applied load values corresponding to the beginning of yielding of the #8 longitudinal bars, yielding of the stirrups and crushing of concrete are indicated. The peak load was defined in as the highest load step (step 98) for which the energy norm ratio satisfies the fixed tolerance of 1×10^{-3}. After step 98 the ultimate strain of #8 bars, assumed to be equal to of 5×10^{-2}, was reached. The beam failed in a mix mode due to shear and bending after the yielding of the #8 reinforcing bars and stirrups.

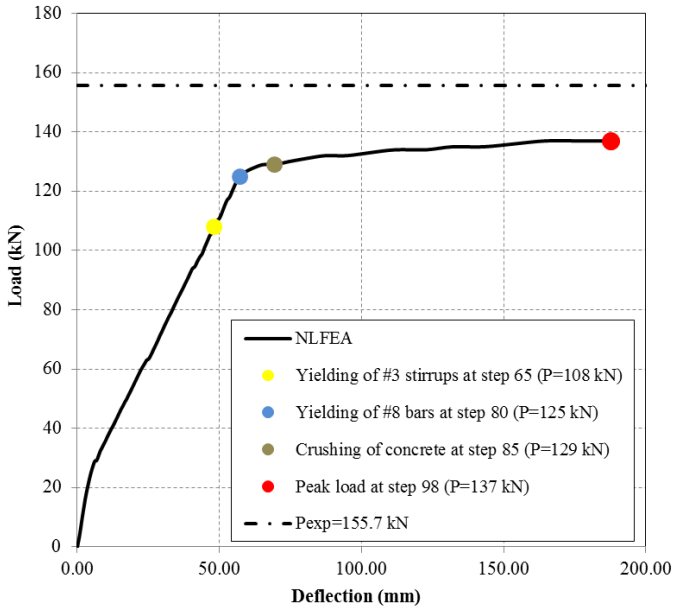

Figure 6-15: Case RB3A. Load-deflection curves

Convergence behavior

For most steps convergence was reached on the basis of the energy criterion, Figure 6-16 and Figure 6-17. For the load case 2, the peak load was defined as the highest load step where the energy norm ratio satisfied the fixed tolerance of 1×10^{-3} (step 98) and it is marked with a red dot. After the step 98, there were other steps where the energy norm ratio satisfied the fixed tolerance of 1×10^{-3}. These step however were not considered because the ultimate strain of #8 bars, assumed equal to of 5×10^{-2}, was already reached.

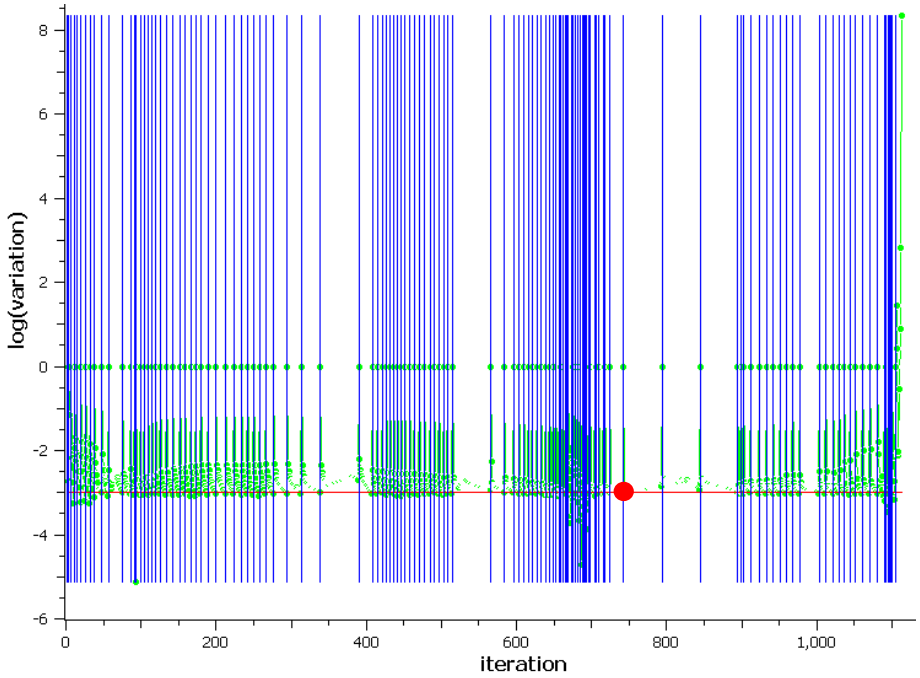

Figure 6-16: Case RB3A. Evolution of the energy norm (blue lines indicate steps, red line indicates tolerance, green points indicate iterative results)

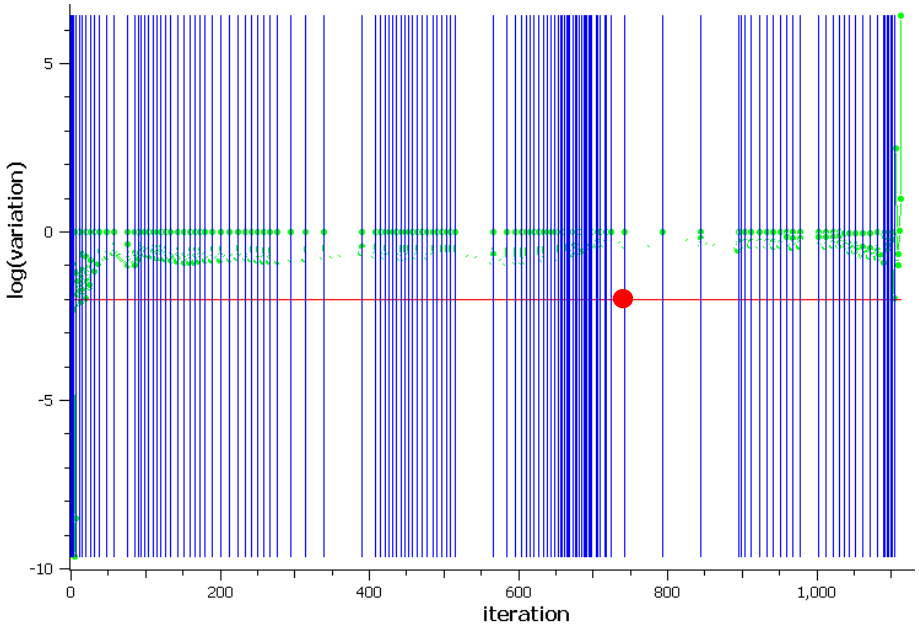

Figure 6-17: Case RB3A. Evolution of the force norm (blue lines indicate steps, red line indicates tolerance, green points indicate iterative results)

Strains

Figure 6-18 shows the crack strain values at step 98 $P = 137kN$ obtained with NLFEA. The first crack strain value plotted in Figure 6-18, equals to 7.86×10^{-4}, corresponds to the ultimate crack strain value calculated as $\varepsilon_{t,u} = \frac{G_F}{h \times f_{ctm}}$. The third crack strain value, equal to 3.62×10^{-3}, is the crack strain value corresponding to a stress value equal to 1% of f_{ctm}. An intermediate crack strain value was added in the contour plot.

The vertical crack pattern, which can be observed in the contour of the crack strain, indicates that the failure is due to shear. When compared with the experimental crack pattern shown in Figure 6-1, it can be seen that the presented crack pattern from NLFEA is a satisfactory reproduction of the experimental observations.

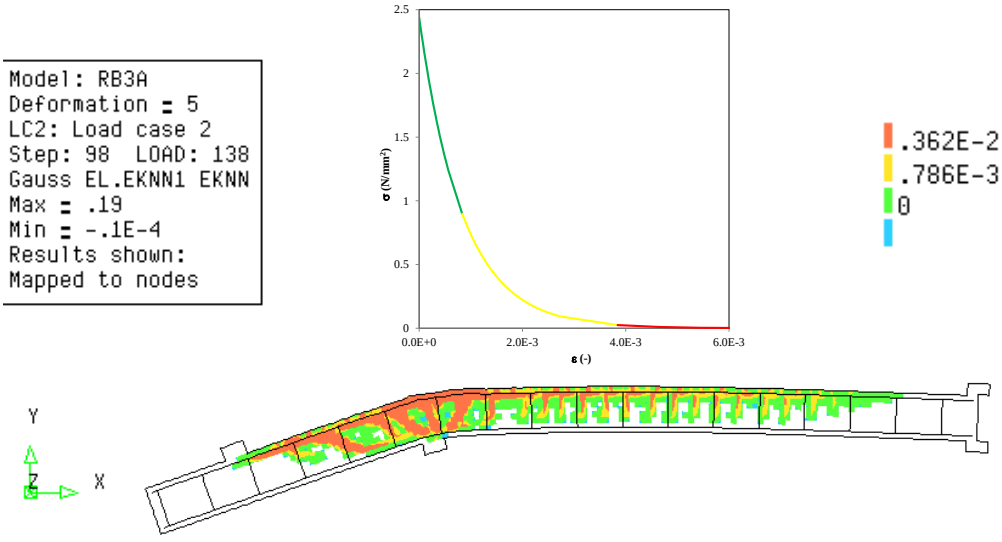

Figure 6-18: Case RB3A. Crack strain values at step 98 ($P = 137kN$)

Figure 6-19 shows the minimum values of the principal strain at the peak load; step 98. Because of the fact that the beam fails in a mix-mode due to shear and bending after yielding of the #8 reinforcing bars and stirrups, the beam displays a ductile behavior. Consequently, crushing of concrete is insignificant as it occurs in a small area due to geometrical discontinuity in proximity of the supporting steel plate.

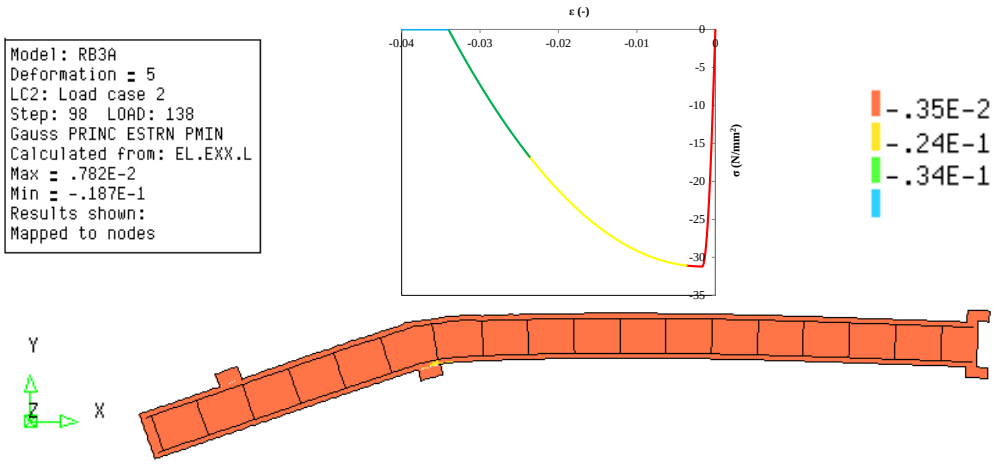

Figure 6-19: Case RB3A. Minimum principal strain values at step 98 ($P = 137kN$)

The yielding strain of the #8 reinforcing bars is equal to $414MPa/200000GPa = 2.07\times10^{-3}$. The longitudinal #8 reinforcing bars start to yield in tension at a load equal to 125 kN (step 80). In Figure 6-20, yielding of the longitudinal reinforcement at the peak load is presented.

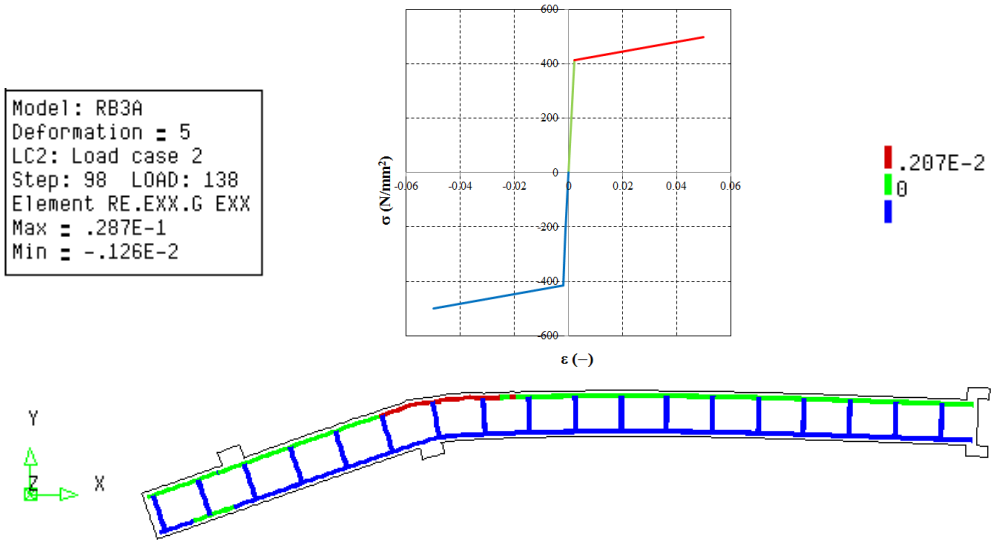

Figure 6-20: Case RB3A. Strain values of the #8 reinforcing bars at step 98 (P = 137 kN)

The yielding strain of stirrups is equal to $\frac{414MPa}{200GPa} = 2.07\times10^{-3}$. The onset of yielding of stirrups occurs at step 70 which is equivalent to the load of $P = 108kN$.

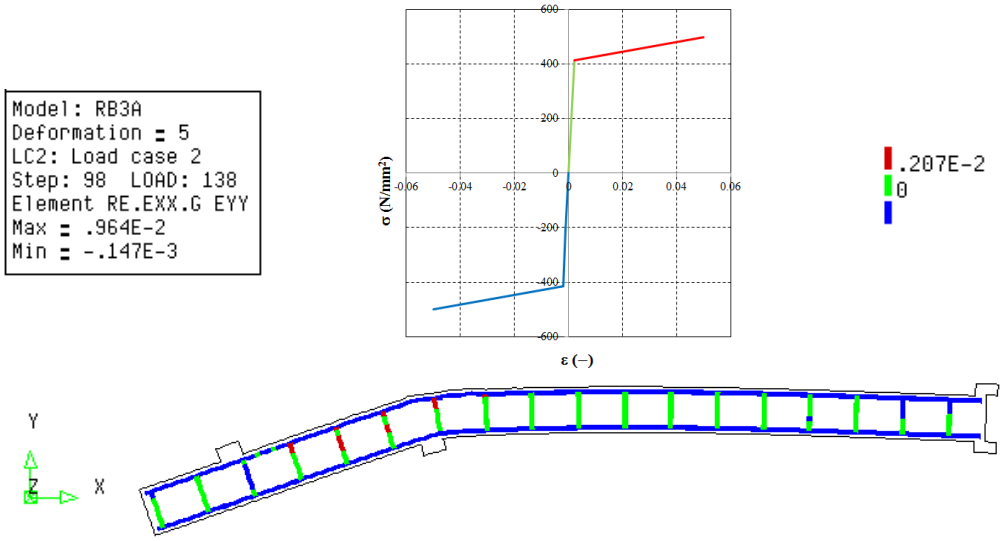

Figure 6-21: Case RB3A. Strain values of the stirrups at the peak load ($P = 137kN$)

Gauss point statistics

Table 6-3 lists the number of cracking points, crushing points and yield points at step 70 (beginning of yielding of #3 stirrups), at step 80 (beginning of yielding of #8 reinforcing bars), at step 88 (when the first element reaches minimum principal strains lower than -3.5×10^{-3}) and at step 88 5 (the peak value of applied load).

Table 6-3: Case RB3. Number of cracking points, crushing points, and yield points

YIELDING OF #3 STIRRUPS						
STEP	**70**	**ITERATIONS**		5		
GROUP NAME	**PLAST**	**PRV. PL**	**CRITIC**	**PLAST NEW**	**PRV.PL NEW**	**CRITIC NEW**
BEAM	16	0	0	5	0	0
STIRRUPS	2	0	0	2	0	0
CRUSHING	12	0	0	4	0	0
TOTAL MODEL	18	0	0	7	0	0
CRACKING LOGGING SUMMARY						
GROUP NAME	**CRACK**	**OPEN**	**CLOSED**	**ACTIVE**	**INACTI**	**ARISES**
BEAM	4060	4058	2	2576	1484	30
CRUSHING	165	165	0	128	37	0
SHEAR	561	561	0	344	217	5
TOTAL MODEL	4060	4058	2	2576	1484	30
CUMULATIVE REACTION:						
FORCE X			**FORCE Y**			
-0.47414D-09			-0.13111D+06			
STARTING OF YIELDING OF #8 REINFORCING BARS						
STEP	**80**	**ITERATIONS**		1		
GROUP NAME	**PLAST**	**PRV. PL**	**CRITIC**	**PLAST NEW**	**PRV.PL NEW**	**CRITIC NEW**
BEAM	43	0	0	4	0	0
REBAR	5	0	0	5	0	0
STIRRUPS	8	0	0	0	0	0
CRUSHING	36	0	0	3	0	0
TOTAL MODEL	56	0	0	9	0	0

CRACKING LOGGING SUMMARY						
GROUP NAME	**CRACK**	**OPEN**	**CLOSED**	**ACTIVE**	**INACTI**	**ARISES**
BEAM	4308	4306	2	2957	1351	19
CRUSHING	182	182	0	153	29	1
SHEAR	610	610	0	420	190	4
TOTAL MODEL	4308	4306	2	2957	1351	19
CUMULATIVE REACTION:						
FORCE X			**FORCE Y**			
0.39439D-09			-0.14844D+06			
CRUSHING OF CONCRETE						
STEP	**88**	**ITERATIONS**		1		
GROUP NAME	**PLAST**	**PRV. PL**	**CRITIC**	**PLAST NEW**	**PRV.PL NEW**	**CRITIC NEW**
BEAM	84	0	0	6	0	0
REBAR	34	0	0	1	0	0
STIRRUPS	11	0	0	0	0	0
CRUSHING	74	0	0	6	0	0
TOTAL MODEL	129	0	0	7	0	0
CRACKING LOGGING SUMMARY						
GROUP NAME	**CRACK**	**OPEN**	**CLOSED**	**ACTIVE**	**INACTI**	**ARISES**
BEAM	4572	4570	2	3037	1535	42
CRUSHING	266	266	0	210	56	15
SHEAR	642	642	0	394	248	3
TOTAL MODEL	4572	4570	2	3037	1535	42
CUMULATIVE REACTION:						
FORCE X			**FORCE Y**			
-0.91938D-09			-0.15468D+06			
PEAK LOAD						
STEP	**98**	**ITERATIONS**		17		
GROUP NAME	**PLAST**	**PRV. PL**	**CRITIC**	**PLAST NEW**	**PRV.PL NEW**	**CRITIC NEW**
BEAM	59	60	0	2	46	0
REBAR	40	1	0	1	1	0
STIRRUPS	16	3	0	0	3	0
CRUSHING	43	59	0	0	46	0
TOTAL MODEL	115	64	0	3	50	0
CRACKING LOGGING SUMMARY						
GROUP NAME	**CRACK**	**OPEN**	**CLOSED**	**ACTIVE**	**INACTI**	**ARISES**
BEAM	5051	5048	3	2923	2128	72
CRUSHING	428	427	1	302	126	23
SHEAR	708	708	3	399	309	8
TOTAL MODEL	5051	5048	3	2923	2128	72
CUMULATIVE REACTION:						
FORCE X			**FORCE Y**			
0.43315D-09			-0.16023D+06			

6.5 Application of safety formats Model Code 2010 (fib, 2013)

As proposed by the Model Code 2010 (fib, 2013), safety formats for non-linear finite element analyses include three numerical methods denoted as GRF (Global Resistance Factor method), PF (Partial Factor method) and ECOV (Method of Estimation of a

Coefficient of Variation of resistance). Application of safety formats requires a total of 4 non-linear analyses. In Table 6-4 till Table 6-6 mechanical properties applied in the non-linear analyses are summarized.

Table 6-4: Case RB3A. Constitutive model parameters for concrete

	f_c (N/mm^2)	f_{ct} (N/mm^2)	E_c (N/mm^2)	ν	G_F (Nmm/mm^2)	G_C (Nmm/mm^2)
Mean measured	31.20	2.44	31297.49	Var.	0.095	33.901
Characteristic	23.20	1.71	28382.42	Var.	0.090	32.140
Mean GRF	19.72	2.19	26900.34	Var.	0.088	31.214
Design	15.47	1.14	26602.86	Var.	0.084	29.878

Table 6-5: Case RB3A. Constitutive model parameters for reinforcing bars #8

	Φ (mm)	A_s (mm^2)	f_y (N/mm^2)	f_t (N/mm^2)	E_s (N/mm^2)	ε_{sy}
Mean measured	25.4	471	414.00	500.00	200000	0.00207
Characteristic	25.4	471	374.98	452.87	200000	0.00187
Mean GRF	25.4	471	412.48	498.16	200000	0.00206
Design	25.4	471	326.07	393.80	200000	0.00163

Table 6-6: Case RB3A. Constitutive model parameters for reinforcing bars #3

	Φ (mm)	A_s (mm^2)	f_y (N/mm^2)	f_t (N/mm^2)	E_s (N/mm^2)	ε_{sy}
Mean measured	9.5	71	414.00	500.00	200000	0.00207
Characteristic	9.5	71	374.98	452.87	200000	0.00187
Mean GRF	9.5	71	412.48	498.16	200000	0.00206
Design	9.5	71	326.07	393.80	200000	0.00163

In Figure 6-22 the load-deflection curves obtained with the mean measured, characteristic, mean (GRF) and design values of material strengths, calculated according to Model Code 2010 (fib, 2013) are shown. The peak loads are defined as the load values for which the ultimate strain of #8 rebars, assumed to be 5×10^{-2}, is reached.

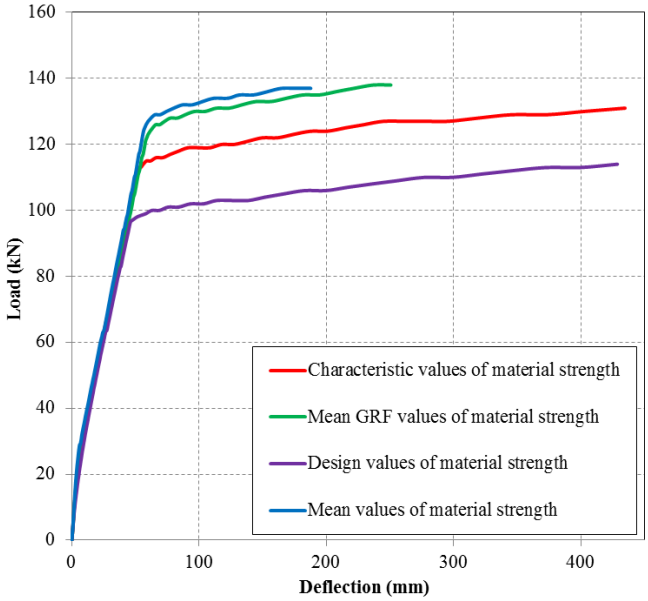

Figure 6-22: Case RB3A. Load-deflection curves obtained with mean measured, characteristic, mean (GRF) and design values of material strengths

The RB3A beam was analyzed with a use of the analytical methods for sectional analysis and numerical procedures proposed for NLFE analysis. The results of the analyses are shown in Figure 6-23. In this comparison, the design values of the beam resistance are expressed in terms of a percentage of the experimental ultimate value of applied load.

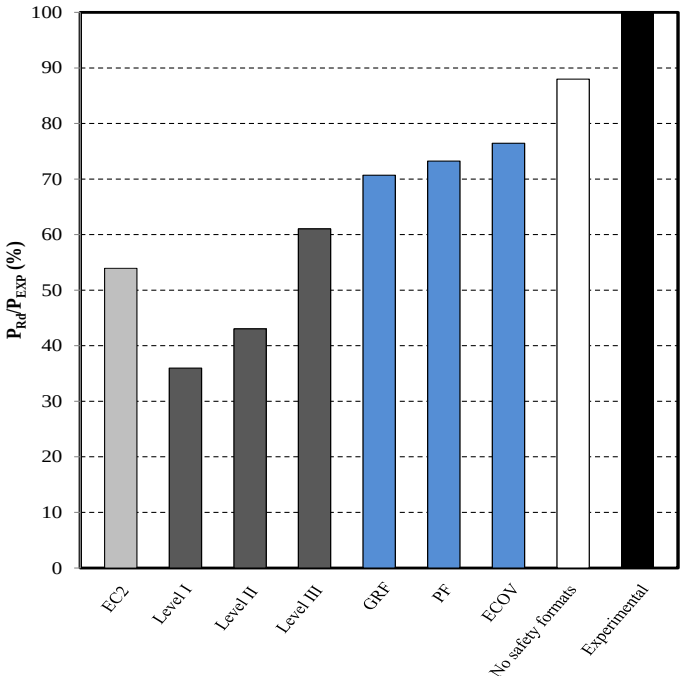

Figure 6-23: Case RB3A. Analytical and numerical design values of beam resistance expressed in terms of a percentage of the experimental ultimate value of applied load, $P_{Exp} = 155.7kN$

In Table 6-7, the design values of beam resistance, expressed in terms of applied load P_{Rd}, obtained from numerical and analytical procedures are summarized.

Table 6-7: Case RB3A. Values of design beam resistance, expressed in terms of applied load P_{Rd}

Exp. (kN)	P_{Rd} (EC2) (kN)	P_{Rd} (MC2010 - LoA I) (kN)	P_{Rd} (MC2010 - LoA II) (kN)	P_{Rd} (MC2010 - LoA III) (kN)	P_{Rd} GRF (kN)	P_{Rd} PF (kN)	P_{Rd} ECOV (kN)	No Safety Formats (kN)
155	85.88	57.67	69.15	97.65	110	114	119	137

6.6 Parametric study on crack models

A parametric study, with different values of parameters of the concrete constitutive model, such as the crack model and fracture energy of concrete in tension, was conducted. In Table 6-8 the material parameters used in NLFE analyses performed for the parametric study are listed. Analyses 1 to 3 refer to the analyses with varying values of material parameters. All the analyses were carried out with the mean measured values of material strengths. Parabolic law in compression and exponential law in tension were used for concrete, whereas steel was modelled with the elasto-plastic law with hardening.

The analyses were carried out in load-control with arc-length control. A variable Poisson ratio was adopted for all analyses.

For all analyses a limit value of the reduction of the compressive strength of concrete due to lateral cracking was adopted as:

$$\beta_{\sigma,\min} = \frac{f_{c,red}}{f_{cm}} = 0.6$$

The effect of the applied values of the fracture energy of concrete in tension on the beam response was investigated by considering the formulation proposed by Model Code 1990 (CEB-FIP, 1993) and the Model Code 2010 (fib, 2013).The fracture energy of concrete in compression was considered for all analyses equal to $250G_F$ (Nakamura et al. 2001).

For the Total Strain fixed crack model, the aggregate size based shear retention was defined. According to this model, the shear stiffness of a crack diminishes together with opening of the crack until the value of the normal crack strain reaches the size of half the mean aggregate size. This implies loss of contact between crack planes. The linear decay of shear stiffness further depends on the crack bandwidth value h. The complete formulation is:

$$\beta = 1 - \left(\frac{2}{d_{aggr}} \right) \varepsilon_n h$$

In Figure 6-24 the load-deflection curves resulting from the parametric study are plotted. The peak load values are reported in Table 6-8.

Table 6-8: Case RB3A. Data used for the parametric study

Analysis	Total strain crack model	Limit to β_σ	G_F	G_C	Peak load value (kN)
Analysis 1	rotating	0.6	MC2010	250 G_F	137
Analysis 2	rotating	0.6	MC1990	250 G_F	133
Analysis 3	fixed	0.6	MC2010	250 G_F	151

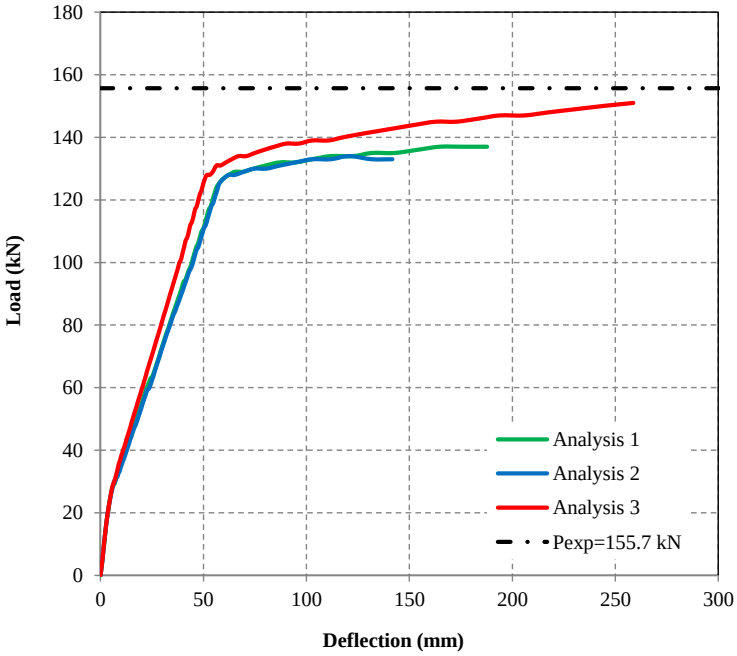

Figure 6-24: Case RB3A. Load-deflection curves (Analysis 1 to 3)

The crack model and the mechanical properties used in Analysis 1 were chosen for the safety formats to predict the design value of beam resistance from NLFE analyses.
As expected, since the beam fails in a mix mode due to shear and bending after the yielding of the #8 reinforcing bars and stirrups, the peak loads and the failure modes observed from NLFE analyses are not heavily dependent on the values of the fracture energy of concrete in tension. The fixed crack model provide a stiffer response after the yielding of #8 bars as well as after the crushing of concrete than the analyses with the applied rotating crack orientation.

6.7 Concluding remarks

The beam RB3A tested by Grace has the same overall dimensions as the previous beam RB3. The only difference consists of wider spacing of stirrups of 457mm in the present case. The beam was also subjected to the same loading scheme. The tested beam exhibited a shear failure mode with the experimental ultimate value of applied load equal to $P_{Exp} = 155.7kN$.

Experimental ultimate value of beam RB3A, having a lower ratio of transversal reinforcement than beam RB3, is higher than the experimental ultimate value of beam RB3. It is in conflict with the results of NLFEA and seems to be physically unrealistic because the material properties of concrete and steel as given in the reference (Grace, 2001) are the same for both beams.
From the analytical calculations based on sectional analysis it was concluded that beam RB3A fails due to shear after yielding of stirrups. The design resistance of the beam is evaluated using expression from Eurocode 2 (CEN, 2005) and the Model Code 2010 through the Levels of approximation approach (fib, 2013). The highest value of design shear resistance from the analytical solution is computed with the most refined level III of approximation and equals to $P_{Rd} = 97.65kN$. The design value of shear resistance calculated with LoA III is close, yet marginally lower than the load the would have otherwise led to failure in flexure.
The peak value of the applied load obtained with NLFEA, carried out with the mean measured value of material strengths, is equal to 137 kN. The beam failed in a mix

failure mode due to shear and bending after yielding of the #8 reinforcing bars and stirrup. The peak loads are defined as the load values for which the ultimate strain of #8 rebars, assumed to be 5×10^{-2} ,is reached.

The Model Code 2010 (fib, 2013) safety formats for non-linear finite element analyses were employed to determine the design value of the beam resistance. The design value of the beam resistance obtained with the safety formats methods is higher than the design value of the beam resistance calculated with analytical approach. The maximum value resulting from the ECOV method equals to $P_{Rd} = 119kN$.

Because of the fact that the beam failed after yielding of #8 bars and stirrups, the failure mode is not highly dependent on the crack model, the concrete tensile strength and the fracture energy of concrete in tension.

References

Bresler, B. & Scordelis, A.C. (1963), "Shear strength of reinforced concrete beams", *J. Am. Concr. Inst.* 60(1), 51–72.

CEB-FIP Model Code 1990. (1993), *Bullettin d'Information n° 213/214*. Thomas Telford.

CEB Bulletin No. 237 (1997), "Concrete Tension and Size Effects - Utilisation of concrete tension in structural concrete design and relevance of size effect - Contributions from CEB Task Group 2.7", Comite Euro-International du Beton (CEB), Lausanne, Switzerland.

CEN (2005), Eurocode 2 - Design of concrete structures - Part 1-1: General rules and rules for buildings, EN 1992-1-1, Brussels: CEN.

Collins, M.P. & Kuchma D. (1999), "How Safe Are Our Large, Lightly Reinforced Concrete Beams, Slabs, and Footings?" *ACI Struct. Journal* 96(4), 482-490.

fib (2013), fib Model Code for Concrete Structures 2010, Ernst & Sohn.

Grace, N.F. (2001), "Strengthening of Negative Moment Region of Reinforced Concrete Beams Using Carbon Fiber-Reinforced Polymer Strips", *ACI Struct. Journal* 98(3), 347-358.

Muttoni, A. & Ruiz, M.F. (2012), "Levels-of-Approximation Approach in Codes of Practice", *Structural Engineering International*, 22, 190-194.

Nakamura, H. & Higai T. (2001), "Compressive Fracture Energy and Fracture Zone Length of Concrete" in "Modeling of Inelastic Behavior of RC Structures under Seismic Loads", Benson P. Shing (editor), *ASCE J. Str. Eng.*, 471-487, Benson P. Shing.

Oliver, J. (1989), "A consistent characteristic length for smeared cracking models", *International Journal for numerical Methods in Engineering*, 28, 461- 474

Selby R.G., Vecchio F.J. (1993). "Three-dimensional Constitutive Relations for Reinforced Concrete", Tech. Rep. 93-02, Univ. Toronto, dept. Civil Eng., Toronto, Canada.

Vecchio, F.J. & Shim W. (2004), "Experimental and Analytical Reexamination of Classic Concrete Beam Tests", *J. Struct. Engrg.* ASCE 130(3), 460-469.

Vecchio F. J. & Collins M. P. (1986), "The modified compression-field theory for reinforced concrete elements subjected to shear", *ACI Journal* 83, 219-231

Vervuurt, A.H.J.M. & Leegwater, G.A. (2008), "Workshop on the assessment of the shear strength of concrete structures", TNO report 2008-D-R0010.